SECOND SOUND SHOCK WAVES AND CRITICAL VELOCITIES IN LIQUID HELIUM II

Thesis by

Timothy Neal Turner

In Partial Fulfillment of the Requirements

for the Degree of

Doctor of Philosophy

California Institute of Technology

Pasadena, California

1980

(Submitted October 12, 1979)

ACKNOWLEDGMENTS

Many individuals have been instrumental in the successful completion of this thesis. Past members of GALCIT's liquid helium group and Dr. Harris Notarys of Low Temperature Physics have generously enlightened the author about the mysteries that persist in modern cryogenic technology.

Special thanks are extended to my father, Aldin F. Turner, whose expertise was frequently called upon to solve difficult engineering problems encountered during the design and construction of the experimental apparatus.

I would like to thank my adviser, Professor Hans W. Liepmann, for many valuable discussions and for the freedom to proceed in the direction I thought would best accomplish our research goals. The inevitable mistakes have become valuable lessons.

Most importantly, I would like to thank my wife, Marla, for her patience, concern, and encouragement, which endured through the long years of graduate study; also, for her enthusiastic ability to create unusual money-making ventures when funds were short, while ever caring for our two children; and finally, for typing this manuscript.

This research was supported by a NASA grant (NSG-7508).

To my son Darrell,

for his love and concern

for "Daddy's machine"

ABSTRACT

Large amplitude second-sound shock waves have been generated and the experimental results compared to the theory of nonlinear second-sound. The structure and thickness of second-sound shock fronts is calculated and compared to experimental data. Theoretically it is shown that at $T = 1.88^{o}K$, where the nonlinear wave steepening vanishes, the thickness of a very weak shock must diverge. In a region near this temperature, a finite-amplitude shock pulse will evolve into an unusual double-shock configuration consisting of a front steepened, temperature raising shock followed by a temperature lowering shock. Double-shocks are experimentally verified. The theoretical dependence of the shock-induced temperature jump on the Mach number is successfully verified for large amplitudes ($\Delta w/a \leq .15$) after the response of a thin-film superconducting temperature sensor is analyzed.

The ability of second-sound shock waves to simultaneously produce and measure very large relative velocities in regions away from the disruptive influence of walls makes them an invaluable tool in the study of critical velocities intrinsic to the fluid. It was experimentally discovered that very large second-sound shock waves initiate a breakdown in the superfluidity of helium II, which is dramatically displayed as a limit to the maximum attainable shock strength. Although the observed breakdown could not be definitely attributed to a critical velocity, the value of the maximum shock-induced relative velocity represents a significant lower bound to the intrinsic critical velocity of helium II. The observed limits within which

superfluidity was still maintained ($w = 3.67$ m/sec at $T = 1.45^{o}K$, and $w = 3.20$ m/sec at $T = 1.85^{o}K$) are the largest counterflow velocities ever obtained outside of restricted geometries.

TABLE OF CONTENTS

LIST OF TABLES

LIST OF FIGURES

LIST OF SYMBOLS

a	second-sound speed
b	second-sound steepening coefficient
c	first-sound speed
d	channel diameter or width
e	specific internal energy
f	second-sound convection coefficient
h	Planck's constant
h^*	dissipative stress acting on the superfluid
j	mass flux
k_B	Boltzman constant
ℓ_{pr}	mean free path of phonons scattered by rotons
m	mass of He^4 atom
p	pressure; momentum of an elementary excitation
q	heat flux
t	time
u	characteristic wave velocity
v	bulk or barocentric fluid velocity
v_s	superfluid velocity
v_n	normal fluid velocity
w	relative velocity $(v_n - v_s)$
C_p, C_v	specific heats
D	damping coefficient of second-sound
K	quantum of circulation
L	propagation length
M_S	shock Mach number

Q	total energy flux
Q^*	dissipative energy flux
R_+, R_-	Riemann invariants for second-sound
R_C	contact resistance
R_K	Kapitza resistance
S	specific entropy
T	temperature
U_S	shock velocity
α	second-sound attenuation coefficient
β	thermal expansion coefficient
δ	shock thickness
ε	energy density; energy of an elementary excitation
$\zeta_1, \zeta_2, \zeta_3, \zeta_4$	second viscosity coefficients
η	shear viscosity coefficient
θ	dimensionless temperature $(T/T_0 - 1)$
$\Delta\theta$	shock strength $(\Delta T/T_0)$
κ	thermal conductivity coefficient
μ	chemical potential
ρ	total mass density
ρ_n	normal fluid mass density
ρ_s	superfluid mass density
τ	time constant
τ^*	dissipative stress tensor
χ	thermal diffusivity $(\kappa/\rho C_p)$
ω	angular frequency
Ψ	quantum mechanical wave function

Subscripts and superscripts:

$( )_n$	normal fluid
$( )_s$	superfluid
$( )'$	perturbation quantity
$\Delta( )$	shock jump quantity
$(\tilde{})$	function of w
$(\vec{})$	vector quantity
$( )_0$	flow state $w = 0$
$\langle( )\rangle$	average quantity

Chapter 1. INTRODUCTION

Amongst a host of peculiar phenomena, the reversible transfer of heat by temperature or entropy waves, known as second-sound, can certainly be singled out as one of the most scientifically interesting and technologically useful properties of liquid helium II. The current exploitation of helium II as a refrigerant for superconducting technologies alone warrants a thorough study into the generation and propagation of nonlinear second-sound. However the properties of second-sound can be put to an even more important task: that of probing the nonlinear aspects of two-fluid mechanics.

Landau's version of the two-fluid model has led to a very good understanding of many diverse phenomena exhibited by helium II; for example, second-sound was actually predicted by the theory. Using this theory it becomes clear that the fluid mechanical phenomena unique to helium II are most apparent when there exists a relative velocity between the two fluid components. When the components move together liquid helium formally behaves like an ordinary fluid. Thus, the ability of second-sound to produce large relative velocities is of singular importance when used as a probe of two-fluid mechanics.

The most important unsolved problem in two-fluid mechanics is the mechanism of critical velocities. At flow velocities less than the critical velocity, helium II exhibits "superfluidity" in a wide variety of ways -- that is, under a certain set of conditions, the superfluid component can flow without viscosity as a perfect potential fluid. The reversible transfer of heat via second-sound and the existence of persistent currents in toroidal geometries are two

important examples of superfluidity.

There are actually many critical velocities in liquid helium which signal the breakdown of superfluidity as a sudden onset of extra dissipation in the flow. Interactions between the normal fluid and walls, between the superfluid and walls, and between the normal and superfluid components can all trigger transitions describable in terms of critical velocities. Of these the mutual interaction between the normal fluid and superfluid, which should be expressed in terms of a relative critical velocity, is the most fundamental to the two-fluid model. Mutual interactions will destroy the superfluidity* of the liquid even in the absence of walls or viscous interactions. These interactions are not recognized by the present two-fluid model, and thus they represent the limit of its validity.

The "fundamental critical velocity" describing the mutual interactions between the two fluids has been long sought. However, in all previous experiments, large critical velocities have only been realized in highly restricted geometries -- capillary tubes or powder packed containers. The walls containing the fluid restrict the types of possible flow states of helium II; thus they allow superfluidity to be expressed at the expense of inducing fluid-wall interactions. In fact, all of the critical velocities observed have been manifestations of fluid-wall interactions except for possibly one: the

*Destruction of superfluidity does not imply that the helium II phase is transformed to helium I; rather, the normal and superfluid components both exist, but they no longer move independent of one another. Thus the manifestations of superfluidity -- persistent currents, second-sound, etc. -- are inhibited or obliterated by the preponderance of dissipative interactions occurring in the flowing liquid.

"intrinsic" critical velocity, which is independent of channel size. Unfortunately, this critical velocity is observed only in the smallest geometries -- submicron pores and intersticies between particles.

Since second-sound induces large relative velocities in the fluid independent of walls, it should be a very useful tool for investigating the fundamental critical velocity in helium II due to mutual interactions. In particular, the dual role of shock waves to both produce and measure a flow state is invaluable: second-sound shock waves can be used to generate large regions of high relative velocity away from the walls, and simultaneously, they can unobtrusively measure the shock-induced flow state. This measurement is accomplished by accurately determining one parameter -- either the shock Mach number or the shock temperature jump.

Of course, the above procedure relies on the accuracy of the theory describing second-sound which was originally given by Temperley (1951), who derived a theory of reversible nonlinear second-sound, and Khalatnikov (1952b), who solved the shock jump conditions for first- and second-sound. Both these theories are only second-order approximations which are valid only for "weak" shocks; therefore the validity of the theory must be tested experimentally.

The generation of nonlinear second-sound including shock waves has been accomplished several times in the past thirty years. Osborne (1951) was the first to experimentally observe the nonsteady propagation of second-sound brought about by nonlinearity. He noticed that a positive temperature pulse would either steepen in the front or the back depending on the initial equilibrium temperature of the

fluid. These observations were qualitatively explained by the second-order theories. Further experimental verification of the predicted phenomena was obtained by Dessler and Fairbank (1956), who measured the increment in characteristic velocity produced by large amplitude second-sound pulses.

The preliminary work conducted for this thesis showed a dramatic departure of the experimental results from second-order theory and a breakdown in the superfluidity of helium II. It was found that as the heater power which generated the shock pulse was increased, the amplitude of the shock increased, but only to a limit. Any further increase in heater power would not increase the amplitude of the shock front, and in many cases, it tended to decrease it.

The same type of "shock-limited" second-sound pulses were observed contemporaneously by Wise (1979), who produced both first- and second-sound shock waves by reflecting a gasdynamic shock off a helium II liquid-vapor interface. Cummings, Schmidt, and Wagner (1978) observed that over the temperature range from $1.61^{o}K$ to $2.09^{o}K$ the Mach number of large amplitude second-sound shocks was limited by some unknown process, and the profile of such a limited shock was substantially modified from the rectangle heat pulse input by the heater. Similar "wave modification" was observed earlier with Schlieren photography by Gulyaev (1970) who also reported boiling at the heater for large input heat pulses.

Although observed by many experimentalists, the breakdown of superfluidity with large amplitude second-sound has not been thorougly investigated nor has the mechanism responsible been

illuminated. The main goal of the present thesis is to fill this gap and to determine whether or not the observed breakdown is a manifestation of the "fundamental critical velocity". In order to accomplish this task it will also be necessary to determine the validity of second-order theory for the large amplitude second-sound shock waves generated experimentally.

Chapter 2. CONCEPTS OF THE TWO-FLUID MODEL

The two-fluid model conceives of liquid helium II as consisting of two independent fluids -- the normal fluid and the superfluid. Each fluid has associated with it a momentum density which can be described quantitatively by a fluid velocity and a mass density. In an ordinary fluid, like air, water, or liquid helium I, all three quantities -- momentum density, fluid velocity, and mass density -- can be measured independently and therefore have real physical significance. For helium II much of the physical significance of the velocities and mass densities of the two separate components is lost. The reason for this is that individual helium molecules cannot at any instant be classified as being part of a superfluid or normal fluid phase, but instead each helium molecule simultaneously participates in two types of motion, separately classified as superfluid or normal fluid motion. With this idea in mind, the mass densities can be understood as a quantification of the extent to which helium molecules partake in each motion, rather than being the number of molecules that participate. The fact that helium II can be accurately described by a two-fluid model is a consequence of the fact that these two collective motions are qualitatively different and independent of one another.

The difference between the super and normal fluid motions can be understood by first viewing helium II as its temperature approaches absolute zero. At temperatures above absolute zero every macroscopic system continually proceeds through a range of accessible microscopic*

---

*microscopic in the sense that the motion of the individual atoms is quantified.

states; the thermodynamic state is a macroscopic average of these states, and the thermodynamic fluctuations are the deviations that occur from the average. At absolute zero, thermal fluctuations in all substances must cease, which means that the thermodynamic macrostate of a system is equivalent to a single microstate -- the ground state. Another way of saying this is embodied by the Nernst postulate which states that the entropy of a system vanishes at absolute zero.

Liquid helium is the only substance that does not solidify under its own vapor pressure. The reason for this is quantum mechanical in that the zero point energy is sufficient to overcome the weak binding potential between helium atoms. Thus, as absolute zero is approached, helium II remains a liquid, but at the same time it possesses thermodynamic features similar to dielectric solids. Specifically the specific heat of helium II approaches the temperature cubed Debye law, and the entropy of the liquid similarly decreases until it vanishes at absolute zero.

At this limiting temperature helium II is totally superfluid, that is, only superfluid motions are present. This motion is one devoid of thermal fluctuations, and can be described as a single microscopic state. This ground state can be altered into another, that is liquid helium can be made to flow by changing the boundary conditions. However, no matter what the macroscopic flow state of the liquid, there will always be only one microscopic state associated with it.

Compare this behavior to an ordinary fluid. On the macroscopic scale, a fluid moves with some definite velocity which varies

continuously from point-to-point. Going beyond this scale of observation into the microscopic domain reveals molecules moving randomly with velocities distributed over a wide range. Only the average of all the molecular velocities constitutes the fluid velocity observed macroscopically. The microscopic deviations from the mean flow show up as viscosity and thermal conductivity, and thus their effect is to make the fluid imperfect.*

In contrast to ordinary fluids, a superfluid flows like a perfect fluid at both the macroscopic and microscopic levels. There is an apparent coherence between the molecular motions which inhibits the degrees of freedom in the superfluid that are ordinarily expressed as random molecular motion. Although the cause of this coherence is unclear, it is certainly due to the quantum mechanical nature of the fluid.

Consider the de Broglie wavelength of a free particle having energy, $\varepsilon = k_B T$:

$$\lambda = \frac{h}{p} = \frac{h}{\sqrt{2mk_B T}} \tag{2.1}$$

where h = Planck's constant

p = particle momentum

m = particle mass

k_B = Boltzmann constant

This length is a measure of the physical extent of the quantum mechanical wavefunction, $\psi(\vec{x})$, which describes the motion of the particle.

*A perfect fluid is one having no viscosity or thermal conductivity.

A system of particles must be described quantum mechanically if the natural length scale -- the average interparticle distance -- is small compared to the de Broglie wavelength (see Landau and Lifshitz, 1977, chapter 7). This occurs when the thermal momentum or temperature is low and the density of particles is large. Ordinary liquids at room temperature behave classically even though their particle density is large, because their thermal de Broglie wavelength is very small (for H_2O at 300^oK, $\lambda = .28$ Å). At the temperatures where liquid helium II exists, the low thermal energy gives rise to single particle wavefunctions which would extend over many molecules in a many particle system (for He^4 at 2.0^oK, $\lambda = 11$ Å). Therefore liquid helium is properly a quantum fluid.

The wavefunction of a quantum liquid having N particles must in general be a function of N vector coordinates and time-- $\Psi(\vec{x}_1, \vec{x}_2, \ldots \vec{x}_N, t)$. This wavefunction completely describes the microscopic state of the fluid as a probability amplitude in configuration space. Now it has been expressed that the superfluid has essentially one degree of freedom since the other degrees of freedom are in effect inhibited or are expressed only in the normal fluid component, which vanishes anyway at absolute zero. Therefore it is reasonable to formulate a pseudo-wavefunction describing the coherent motion of the superfluid, which is a function of a single vector coordinate-- $\psi_s(\vec{r},t)$. If this function is normalized so that

$$\int_V \psi_s^* \psi_s \, d\vec{r} = M \qquad \text{as } T \to 0 \qquad (2.2)$$

where M and V are the mass and volume of the system, then $\psi_s(\vec{r},t)$ can in general be written as the following complex function:

$$\psi_s(\vec{r},t) = \sqrt{\rho_s(\vec{r},t)}\ e^{i\phi(\vec{r},t)} \tag{2.3}$$

where the superfluid density, ρ_s, can be identified as:

$$\rho_s = \psi_s^* \psi_s \tag{2.4}$$

The phase, $\phi(\vec{r},t)$, has special significance which can be elucidated by calculating the quantum mechanical current density of $\psi_s^* \psi_s$:

$$\vec{J}_s = \frac{i\hbar}{2m}\left(\psi_s \nabla\psi_s^* - \psi_s^* \nabla\psi_s\right) \tag{2.5}$$

When $\rho_s(r,t)$ is a slowly varying function of $\vec{r}$, the superfluid velocity can be ascertained by identifying $\vec{J}_s$ as $\rho_s\vec{v}_s$:

$$\vec{v}_s = \frac{\hbar}{m}\nabla\phi \tag{2.6}$$

From this result it is evident that the superfluid is a potential or irrotational fluid, and the phase of the wavefunction is the velocity potential. If $\vec{v}_s$ is integrated on a closed contour, in order to calculate the circulation, the result will always be zero in a simply connected domain. If the domain is multiply connected, the circulation need not be zero. For example:

$$\Gamma_s = \oint \vec{v}_s \cdot d\vec{\ell} = \frac{\hbar}{m}\oint(\nabla\phi)\cdot d\vec{\ell} = \frac{\hbar}{m}\,2\pi n \tag{2.7}$$

where n is an integer. Since the wave function must be continuous, the phase change around a closed path must be a multiple of 2π. This condition translates into quantization of circulation in units of K.

$$K = \frac{h}{m} = 0.997 \times 10^{-3} \text{ cm}^2/\text{sec} \qquad (2.8)$$

Although vorticity in the superfluid is forbidden, this interestingly enough does not rule out the existence of superfluid vortex lines. First imagined by Onsager, a superfluid vortex can form around a singularity where $|\psi_s| \to 0$ as long as the circulation is quantized. These peculiar quantized vorticies have been experimentally verified in the form of vortex rings (Rayfield and Reif, 1963 and 1964) and vortex lines trapped on a minute wire (Vinen, 1961; Whitmore and Zimmermann, 1965 and 1968).

At temperatures exceeding absolute zero, liquid helium deviates from a purely microscopic ground state and begins to possess thermal fluctuations. It was shown by Landau that the excited states of Helium II can be represented by a system of basically non-interacting excitations superimposed on a background sea of molecules collectively participating in the ground state. The excitation gas comprises the normal fluid and the collective ground state is the superfluid. This separation of thermodynamically excited helium II into two distinguishable parts leads to some interesting consequences. The excited or normal fluid obviously has entropy, and it also interacts viscously with itself and the vessel which contains it. The superfluid, on the other hand, has zero entropy because it is the manifestation of a single microscope state, which is maintained even at nonzero temperatures.

The excitations which comprise the normal fluid are described by the dispersion curve of energy versus momentum presented in Figure

2.1. There are two regions of specific interest on this curve: 1) the low momentum range, where the curve is linear, represents phonons; and 2) the high momentum valley in the energy spectrum represents

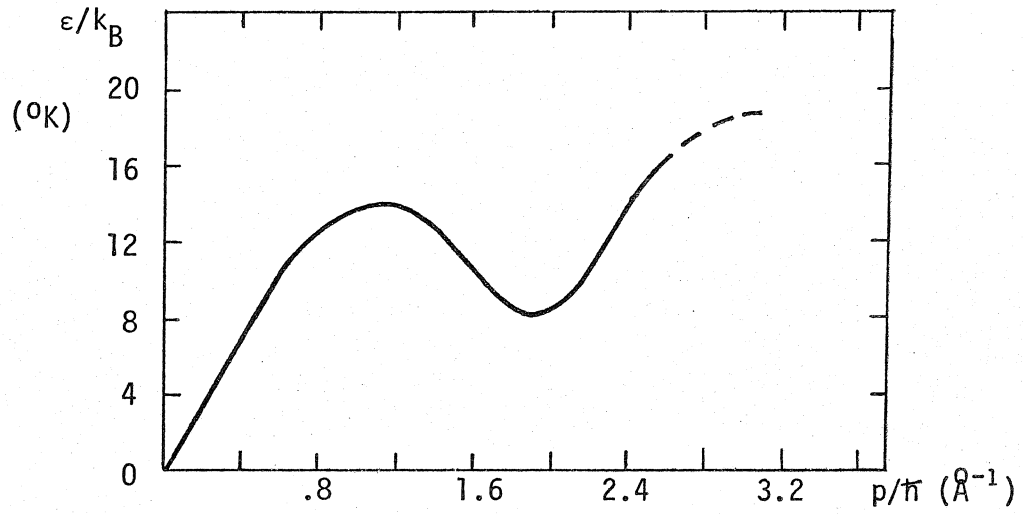

Figure 2.1. EXCITATION ENERGY SPECTRUM FOR HELIUM II

excitations called rotons. The energy spectra of these two groups of excitations are usually expressed by the following simple analytical expressions:

$$\text{PHONONS:} \quad \varepsilon = cp \tag{2.9}$$

$$\text{ROTONS:} \quad \varepsilon = \Delta_r + \frac{(p - p_r)}{2\mu_r} \tag{2.10}$$

where ε and p are the energy and momentum of the excitation, c is the speed of first-sound, and Δ_r, p_r and μ_r are parameters.

At fairly low temperatures -- $T < 0.6^{\circ}K$ -- phonons, which are simply sound waves of quantized amplitude, are excited almost to the exclusion of all the other higher energy excitations. Phonons, as their name

signifies, are analogous to excitations occurring in solids. Thus their exclusive presence is why helium II characteristically exhibits solid-like thermodynamic behavior at low temperatures. At warmer temperatures the liquid begins to be inhabited by rotons, which may be vortex rings whose diameter has been shrunk to atomic dimensions (Feynman, 1955); or they may be simply an extension of the phonon branch to half wave lengths shorter than the average interatomic spacing (Dimotakis, 1979). Plane-wave excitations at these wavelengths are allowable in a liquid, because it lacks the long range periodicity which generates the Brillouin zones found in crystalline solids (see Kittel, 1971, Chapter 5).

As the temperature increases the population of rotons increases very rapidly -- due to its large density of states -- so that above $1.2^{o}K$ the thermodynamics of helium II is completely dominated by them. This is illustrated by the change in behavior of the specific heat, which goes from a Debye-like temperature dependence to an exponential temperature dependence, characterisitic of a thermodynamic system with essentially one excited energy level of large degeneracy.

Since the density of excitations in helium II changes dramatically with temperature, the character of the normal fluid is highly temperature dependent. At low temperatures the excitation gas is so tenuous that the normal fluid behaves like a rarefied gas. For example, below $0.6^{o}K$, the flow of heat in helium II is very similar to low temperature heat transport in a pure dielectric crystal; experiments by Fairbank and Wilks (1955) verified that phonons can behave like molecules in a rarefied gas: their mean free path, and hence thermal conductivity,

limited only by collisions with the container walls. Also, the shear viscosity derived from Poiseuille flow in round capillaries was found to depend on the capillary diameter (d = 52 μm and 107.6 μm) for temperatures below 1.3°K (Brewer and Edwards, 1959). This behavior is indicative of slip between the fluid and capillary walls which occurs when the mean free path between collisions is the same order as the capillary diameter.

At higher temperatures the irreversible thermal conductivity and shear viscosity decrease as the phonon mean free path is limited by the exponentially increasing population of rotons. This mean free path, ℓ_{pr}, which has been evaluated by Khalatnikov (see Table 2.1 and Wilks, 1967, p. 176), is equal to the mean time between collisions of phonons with rotons, multiplied by the phonon velocity, c. There are many other collisional processes in the normal fluid -- roton-roton, phonon-phonon, and various inelastic scattering processes; therefore, more than one mean free path can be defined. However, the slowest collisional frequency is due to elastic scattering of phonons by rotons; thus ℓ_{pr} is the longest mean free path and is the one that determines the viscosity and irreversible thermal conductivity of the liquid (Khalatnikov and Chernikova, 1966a).

At temperatures exceeding 1.9°K the excitations are so numerous that interactions between them cannot be treated as collisions. When the lifetimes of phonons and rotons, become shorter than the mean time between collisions, the concept of an elementary excitation interacting only via collisions is invalid. Thus, the normal fluid in this temperature regime can only be viewed as a dense gas or

Table 2.1. MEAN FREE PATH OF PHONONS SCATTERED BY ROTONS

T	ℓ_{pr}
.94°K	1 mm
1.16	100 μm
1.48	10 μm
1.89	1 μm
2.0	0.6 μm

liquid.*

* It is remarkable that the shear viscosity increases with temperature for $1.9^{\circ}K \lesssim T \lesssim T_{\lambda}$. This behavior is similar to ordinary liquids.

THE TWO-FLUID EQUATIONS

Once the concepts or postulates of a two-fluid model are set down, a consistent mathematical formalism can then be derived with an appeal to the conservation laws of mass, momentum, and energy, and to the invariance of these laws under a Galilean transformation*. The principle of Galilean invariance is of special significance in a two-fluid model since there is in general no frame of reference that can follow a small volume of fluid having two simultaneous velocities. Because of this, the thermodynamics of helium II can never be separated from the fluid velocity dependence as is done with an ordinary isotropic fluid. In other words, the thermodynamic description of helium II depends on two ordinary variables, like pressure, p, and temperature, T, and the magnitude of the relative velocity between the normal and superfluid, w. Ramifications of this intrinsic velocity dependence in the thermodynamics are elucidated in Appendix A.

The postulates sufficient to derive a self-consistent two-fluid model in the approximation of no dissipation are:

1. The two fluid proposition:

$$\rho \equiv \rho_n + \rho_s \tag{2.11}$$

$$\vec{j} \equiv \rho_n \vec{v}_n + \rho_s \vec{v}_s \tag{2.12}$$

Where ρ, $\vec{j}$ are the mass density and flux of the fluid, and ρ_n, $\vec{v}_n$, ρ_s, $\vec{v}_s$ are the mass densities and velocities of the normal and superfluid

*A transformation between two frames of reference is called Galilean if the two frames differ only by a non-relativistic velocity, uniform in space and time.

components respectively;

2. Entropy is associated only with the normal fluid:

$$\frac{\partial}{\partial t} \rho S + \nabla \cdot (\rho S \vec{v}_n) = 0 \tag{2.13}$$

where S is the specific entropy of the fluid;

3. Superfluid is irrotational and can be described by a velocity potential, μ, such that:

$$\frac{\partial}{\partial t} \vec{v}_s + \nabla(\mu + \tfrac{1}{2} v_s^2) = 0 \tag{2.14}$$

The results of the derivation, originally accomplished by Landau, show that the velocity potential driving the superfluid can be identified with the chemical potential of the liquid.

The derived two-fluid equations, listed in Table 2.2 are written in terms of the bulk fluid velocity, $\vec{v}$, and the relative velocity, $\vec{w}$:

$$\vec{v} \equiv \frac{\vec{j}}{\rho} = \frac{\rho_n}{\rho} \vec{v}_n + \frac{\rho_s}{\rho} \vec{v}_s \tag{2.15}$$

$$\vec{w} \equiv \vec{v}_n - \vec{v}_s \tag{2.16}$$

Formulating the equations in this manner reveals similarities and differences between the two-fluid equations and those for an ordinary fluid, since $\vec{v}$ is analogous to the ordinary fluid velocity, and $\vec{w}$, which represents an internal countercurrent, is not present at all in an ordinary fluid. It should be noted that when either w or ρ_s vanish, the two-fluid equations are equivalent to the equations describing an ordinary fluid. Thus, the remarkable properties attributed uniquely to helium II will manifest themselves with a non-zero relative velocity.

Table 2.2 THE TWO-FLUID EQUATIONS

MASS CONSERVATION:

$$\frac{\partial}{\partial t}\rho + \nabla \cdot \rho\vec{v} = 0$$

MOMENTUM CONSERVATION:

$$\frac{\partial}{\partial t}\rho\vec{v} + \nabla \cdot \left[\rho\vec{v}\vec{v} + \frac{\rho_n\rho_s}{\rho}\vec{w}\vec{w} + pI + \tau^*\right] = 0$$

ENERGY CONSERVATION:

$$\frac{\partial}{\partial t}\left[\rho e + \tfrac{1}{2}\rho v^2 + \tfrac{1}{2}\frac{\rho_n\rho_s}{\rho}w^2\right]$$

$$+ \nabla \cdot \left[\vec{v}\left(\rho e + p + \tfrac{1}{2}\rho v^2 + \tfrac{1}{2}\frac{\rho_n\rho_s}{\rho}w^2\right)\right.$$

$$\left. + \frac{\rho_s}{\rho}\vec{w}\left(\rho_n\vec{w}\cdot\vec{v}_n - \rho ST\right) + \vec{Q}^*\right] = 0$$

SUPERFLUID EQUATION:

$$\frac{\partial}{\partial t}\vec{v}_s + \nabla\left[\mu + \tfrac{1}{2}v_s^2 + h^*\right] = 0$$

where

I = identity tensor

$\tau^*, \vec{Q}^*, h^*$ are the dissipative fluxes

$$e = ST - \frac{p}{\rho} + \mu + \tfrac{1}{2}\frac{\rho_n}{\rho}w^2$$

NOTE: All thermodynamic variables have an intrinsic dependence on w^2

Table 2.3 DISSIPATIVE TERMS OF THE TWO-FLUID EQUATIONS

$$\tau^*_{ik} = -\eta \left[\frac{\partial v_{ni}}{\partial x_k} + \frac{\partial v_{nk}}{\partial x_i} - \frac{2}{3}\delta_{ik} \nabla \cdot \vec{v}_n \right]$$

$$- \delta_{ik} \left(\zeta_1 \nabla \cdot (\vec{j} - \rho \vec{v}_n) + \zeta_2 \nabla \cdot \vec{v}_n \right)$$

$$h^* = -\zeta_3 \nabla \cdot (\vec{j} - \rho \vec{v}_n) - \zeta_4 \nabla \cdot \vec{v}_n$$

$$\vec{Q}^* = -\kappa \nabla T + h^* (\vec{j} - \rho \vec{v}_n) + \tau^* \cdot \vec{v}_n$$

From the Onsager symmetry principle $\zeta_4 = \zeta_1$; also the requirement that entropy production be positive-definite ensures that η, ζ_2, ζ_3, and κ are positive and $\zeta_1^2 < \zeta_2 \zeta_3$.

With this set of equations in hand, the complete equations including dissipation can be determined by initially inserting arbitrary terms representing the kinectic fluxes with the one restriction -- the superfluid equation contains no shear viscosity. The form of these terms is self-consistently determined by forming the energy equation (which is conservative), from the mass, momentum, and superfluid equations, and by noting that the left over terms in the entropy equation must represent positive-definite entropy production (Khalatnikov, 1965). The results of these calculations are given in Table 2.3.

It is remarkable that even though shear viscosity is absent in the superfluid, second viscosities are not. These second viscosities are a result of the fluid relaxing to its equilibrium state after sudden expansions or contractions of the normal fluid (div $\vec{v}_n$ large) or of the normal fluid with respect to the superfluid (div $\vec{w}$ large). When such changes are made in the fluid they instantaneously shift the equilibrium pressure and temperature which requires a redistribution of excitations among the phonon and roton energy levels. Redistribution cannot occur infinitely fast, and therefore there is a relaxation into the equilibrium state on a time scale proportional to the coefficients of second viscosity.

The presence of second viscosity terms in the superfluid equation means that the superfluid can be perturbed by thermodynamic relaxation processes occurring exclusively in the normal fluid. In addition, thermodynamic fluctuations of pressure and temperature also perturb the superfluid through its velocity potential, which has been identified as the chemical potential of the fluid. These perturbations do

not alter the concept that the superfluid is a manifestation of the ground state, which in itself can have no thermal fluctuations. Instead, fluctuations in the normal fluid perturb the superfluid flow state in the same manner that time-dependent boundary conditions change the state: at all times the superfluid retains its coherence and flows as a potential or irrotational fluid.

BOUNDARY CONDITIONS

In order to solve any problem in two-fluid mechanics the equations of motion must be supplemented by the appropriate boundary conditions. Some of these conditions are obvious, while others are still unclear.

First, since mass cannot flow into or out of a solid wall, the component of bulk velocity perpendicular to the wall, $v_\perp$, must be zero at the wall. Second, excitations comprising the normal fluid behave analogously to molecules in a viscous fluid; colliding with the wall, excitations will exchange momentum and end up travelling with the wall. Thus the tangential component of $\vec{v}_n$ must equal the wall velocity. Third, there can be no similar restriction on the tangential component of $\vec{v}_s$, because imposing one might violate the irrotationality condition.

An ordinary fluid requires two boundary conditions -- one for each component perpendicular and tangential to a wall. In a two-fluid, four boundary conditions must be necessary, but traditionally only three conditions on the velocity components $v_\perp$, $v_{n\|}$, and $v_{s\|}$ are given. Obviously one more boundary condition on a velocity component perpendicular to the wall is needed. As will be shown, one can be derived from the boundary condition imposed on the superfluid mass fraction, ρ_s/ρ.

Recall that the superfluid density is best pictured as the square modulus of the wave function describing the superfluid state. Since this state cannot penetrate the wall, it is logical to assume that the wavefunction, and hence ρ_s/ρ, both vanish at the wall. This

boundary condition, first proposed by Ginzburg and Pitaevskii (1958), has been justified by many experimental observations. For example, the speed of third sound -- surface waves on helium II films -- is highly dependent on boundary conditions imposed on ρ_s at the wall and the free surface of the film (Putterman, 1974, p. 222). Comparison of the experimentally determined velocities with the theoretical analysis shows that the superfluid component of the liquid must begin to decrease within a few angstroms of the film boundaries.

The boundary layer in which ρ_s/ρ vanishes, theoretically of the form $\tanh^2(x/\lambda_{heal})$ -- (Ginzburg and Pitaevskii, 1958), has a temperature dependent "healing length", λ_{heal}, which becomes macroscopically large near T_λ. Accurate values of this length have been obtained using gyroscopic techniques to measure the angular momentum of persistent superfluid currents set up in thin helium II films (Henkel, Smith, and Reppy, 1969). The experimentally determined temperature dependence is in agreement with the phenomenological theory as extended by Mamaladze (1967), although the theoretical layer thickness is half the experimental value:

$$\lambda_{heal} \simeq 4 \frac{(T/T_\lambda)}{(\rho_s/\rho)_{bulk}} \quad 10^{-8} \text{ cm}$$

The boundary condition imposed on the fluid velocities at a wall can be determined by examining the velocity identity for $\vec{v}_n$, which follows directly from equations (2.15) and (2.16):

$$\vec{v}_n = \vec{v} + \frac{\rho_s}{\rho} \vec{w} \qquad (2.17)$$

As the wall is approached ρ_s/ρ vanishes, and the normal fluid and bulk velocities become identical -- as long as $\vec{w}$, or equivalently $\vec{v}_s$, remains finite:

$$\vec{v}_n = \vec{v} \quad \text{at the wall} \tag{2.18}$$

Condition (2.18) summarizes all the boundary conditions in helium II which are the same as those for an ordinary fluid; at a wall -- or any other interface where the superfluid state disappears -- the fluid is entirely normal, and therefore it interacts with the boundary just as any ordinary fluid would.

Attempting to find a boundary condition on the superfluid velocity (or w) using condition (2.18) always results in the indeterminate form 0/0. This simply reinforces the fact that the superfluid cannot be constrained by boundary conditions typical of ordinary fluids.

CONSEQUENCES OF THE TWO-FLUID MODEL

The major phenomenon which inspired the two-fluid approach was the observed superconductivity of heat, which manifests itself most obviously as a sudden cessation of boiling when initially passing through the λ-transition into the helium II state. According to two-fluid mechanics, heat can be reversibly transported by internal counterflow. If an object in helium II is hot, heat is convected away from it by the normal fluid, while superfluid flows in the opposite direction balancing the net mass flux. Near the surface, incoming zero-entropy superfluid is transformed into normal fluid excitations. This counterflow process is so effective that temperature gradients are as difficult to achieve in helium II as pressure gradients in an ordinary fluid.

Steady temperature gradients do not appear in the bulk fluid, but only in nozzles where the counterflow is being accelerated, or in steady pipe flow where a temperature gradient is required to balance the retarding viscous forces. This latter case is important experimentally, and it is easily analyzed if the flow is laminar and therefore one-dimensional. In that case the steady superfluid equation yields:

$$\nabla(\mu + \tfrac{1}{2}v_s^2) = 0 \tag{2.19}$$

If the velocities are small enough that terms involving their square can be neglected, the "London relation" results:

$$\nabla T = \frac{1}{\rho S} \nabla p \tag{2.20}$$

The pressure gradient is of course balanced by the shear stress acting on the channel wall.

Another method of producing temperature or pressure gradients is by nonsteady motion, or waves. Nonsteady flow in ordinary fluids is initiated by pressure or sound waves. Similarily, counterflow in helium II is initiated by temperature waves, which are called second-sound (first-sound in helium II terminology refers to ordinary pressure waves familiar to all substances.) Second-sound waves were one of the major predictions offered by Tisza as a test of the two-fluid theory. When Peshkov, in 1944, first attempted to verify this prediction, he obtained a negative result because he tried to generate second-sound with a vibrating piezo-electric crystal. This motion generates pressure disturbances which propagate chiefly as first-sound. Although there are pressure fluctuations in second-sound waves, they are very weak when compared to the temperature fluctuations (these pressure fluctuations are proportional to the coefficient of thermal expansion, which is exceedingly small in liquid helium). When this was realized, a second successful attempt was made to excite second-sound by periodically heating an electrically resistive wire.

First- and second-sound waves can be derived from the two-fluid model by linearizing the equations with respect to the rest state of the fluid. This has been done in detail and is included for reference as Appendix B. The results show that second-sound is a temperature wave, accompanied by variations of the same order in relative velocity, normal mass fraction (ρ_n/ρ), and entropy. Variations of pressure,

density, and bulk fluid velocity are significantly smaller and vanish to first order as the coefficient of thermal expansion goes to zero. For first-sound the situation is reversed -- the first order variations being in p, ρ, and v.

One of the most dramatic consequences of the two-fluid model and the one which best illustrates the reversible nature of flowing superfluid is the phenomenon of persistent currents established in annular geometries. Persistent currents have been achieved in thin helium films adhering to glass cylinders as well as in the bulk fluid. In the latter case the container holding the liquid is typically packed with fine powder or closely spaced mica disks; these act to clamp the normal fluid component and therefore inhibit dissipation interactions between it and the walls. The persistent current is set up by rotating the container while it is above the λ-temperature; after the container is cooled to the desired temperature, its rotation is halted. The superfluid, however, does not stop, but retains the initial velocity imparted to the fluid above the λ-transition. The magnitude of this current can be measured by doppler-shifted fourth sound* or gyroscopic precession.

When this was originally done, it was found that the angular momentum attributed to the superfluid was not constant, but varied as the temperature was changed in such a way that the superfluid velocity remained unaltered. For example, decreasing the temperature requires that some normal fluid, initially having zero angular momentum, be

*Fourth sound is wave propagation occurring in helium II when the normal fluid is held stationary.

converted into superfluid, which is coherently participating in a state of quantized circulation. This state is not changed by the addition of extra superfluid; thus, the total angular momentum of the superfluid is increased at the expense of the container and normal fluid. Increasing the temperature exactly reverses this process as long as the λ-temperature is not exceeded.

A SHORT REVIEW OF CRITICAL VELOCITIES

The phenomena of counterflow, persistent currents, as well as other consequences of the two-fluid model, are manifestations of superfluidity -- defined as the reversible and irrotational flow of the superfluid component. This means that the superfluid can flow through the normal fluid and next to boundaries without suffering dissipative interactions which would otherwise change the superfluid state. Unfortunately, all the manifestations of superfluidity occur only within a limited range of flow velocities. As long as the fluid velocities are smaller than some unspecified critical velocity, the two-fluid model can very accurately describe the mechanics of helium II. Beyond this critical velocity, there appear additional interactions between the two fluids and their boundaries which lead to extra dissipation in the flow, and signal the end of superfluidity.

Critical velocities are not unique to liquid helium; they are, in fact, a ubiquitous phenomenon common to all fluids. Solving the equations of motion for a fluid constrained by steady boundary conditions generally results in a time independent flow which is physically valid only for low enough velocities. If the flow velocity is increased beyond some critical velocity -- for Newtonian fluids some critical Reynolds number -- this steady solution develops instabilities making the flow nonsteady. The laminar-to-turbulent transition and initiation of secondary flows (e.g., Taylor vortices in rotating Couette flow) are two general examples of transitional phenomena characterized by critical velocities.

Since helium II is a fluid, it must exhibit the transitional

phenomena common to all fluids, but, because this liquid is essentially two fluids in one, it should be no surprise that additional critical velocities appear which are unique to liquid helium. A simple experiment that illustrates this behavior considered the damping of fluid mechanical oscillations induced in a U-tube (Donnelly and Penrose, 1956). If the logarithmic decrement of the oscillations (the logarithm of the ratio of two successive maxima) is plotted against the oscillation amplitude, the result for helium I is a constant curve independent of amplitude, h, from h = 0 to h = h_t. Amplitudes exceeding h_t show a gradual but steady increase in logarithmic decrement. This excessive damping was attributed to a laminar-turbulent transition which occurs at the critical velocity associated with h_t. When this experiment was repeated below T_λ, the transition at h_t was accompanied by two additional transitions, identified as breakpoints in the logarithmic decrement plot, occurring at lower amplitudes. The three critical velocities associated with these transitions all show different temperature dependences and are presumably initiated by different mechanisms, some of which do not occur in ordinary fluids, like helium I.

There are two points to be made by examining this experiment and others like it that show qualitatively the same behavior (for example, oscillating disks and spheres). First, the fact that helium II exhibits a variety of transitions between flow states is obvious, but also, it should be apparent that the sum of these transitions adds a complexity to critical velocity experiments making interpretation unusually difficult.

For example, consider the transition found in the U-tube experiment at the amplitude h_t. Attempting to turn pipe flow through an 180^o angle is a very efficient way to generate secondary flows, which are unrelated to turbulence, but which would nevertheless manifest themselves as extra resistance to the oscillatory flow. There is definite evidence of this occurring in a different type of critical velocity experiment having the same U-tube configuration, which showed that the onset of secondary flow is directly related to the severity of the bend and can occur at velocities considerably below the actual laminar-to-turbulent transition (Staas, Taconis, and Van Alphen, 1962).

With this in mind, it is useful to set a primary criterion when examining and designing critical velocity experiments: an experiment should be sufficiently simple in configuration that undesirable fluid mechanical effects will not be excited or at least be separable from the effect under study. Even though the generalization of this principle is one of the basic tenets of the scientific method, its application to critical velocity experiments has often been ignored, because it is usually very difficult to realize in practice.

The use of persistent currents to investigate critical velocities in the superfluid has become a very valuable technique which for the most part satisfies the above criterion. As explained in the last section, persistent currents can be set up and then measured unobtrusively by precessing the container and measuring the gyroscopic torque which results (Clow, Weaver, Depatie, and Reppy, 1964). This directly yields the total angular momentum of the superfluid state, which together with the initial angular velocity of the container, determines

both the mean velocity and mass density of the superfluid flowing within the pores of the superleak packed container. The persistent superfluid velocity at a particular temperature is linearly proportional to the initial angular velocity of the container as long as the critical velocity is not exceeded. The final steady state of the superfluid is always limited by this velocity since if it is initially exceeded dissipative interactions will cause the superfluid velocity to decay to the critical velocity limit.

Measuring the critical velocity in this way is much more straightforward than trying to ascertain the onset of extra dissipation encountered when driving helium II through a small channel. The ambiguity of not knowing the exact velocity of the normal fluid during a measurement is also removed by using the persistent velocity technique.

Even with all these advantages there are a couple of problems associated with this technique, which also plague many other experiments. First, the velocity measured is only an average of the fluid velocities actually occurring within the irregular interstices of the superleak packed container. Second, one may question whether the critical velocity measured is actually a superfluid critical velocity or a relative critical velocity. Since the normal fluid in this experiment is immobile, and therefore $-v_s = w$, it may not seem worthwhile to try to distinguish one from the other. However, there is a significant, although subtle, difference between the two which requires elaboration.

Fluid velocities such as v_s and v_n are not absolute but are fixed

only with respect to a chosen reference frame. This reference frame is nearly always fixed with respect to the experiment or in this instance the persistent current container. This means the velocities v_n and v_s are measured with respect to the walls bounding the fluid. On the other hand, the relative velocity, w, is always the velocity of the normal fluid relative with respect to the superfluid, and it is independent of reference frame.

When the normal fluid is clamped there are two fundamental modes of interaction which could cause the observed critical velocity transitions: 1) a direct interaction between the walls and the superfluid; or 2) an interaction between the normal and superfluid components of the liquid. In both modes of interaction momentum and energy are eventually transferred from the superfluid to the container, but in the latter case this transfer is mediated by the normal fluid.

There is always a causal relationship between the critical velocity and the resulting transition mediated by the responsible interaction; therefore, a description of the direct interaction between the superfluid and its boundaries must involve the superfluid velocity, whereas the interaction between the two individual fluid components of helium II necessarily involves the relative velocity. A logic diagram illustrating the causal relations for three interactions that occur in helium II is presented as Figure 2.2.

The interaction of the normal fluid flowing next to a wall is analogous to similar boundary layer interactions occurring in an ordinary fluid. The parameter which determines the resulting critical transition in an ordinary incompressible fluid is the Reynolds

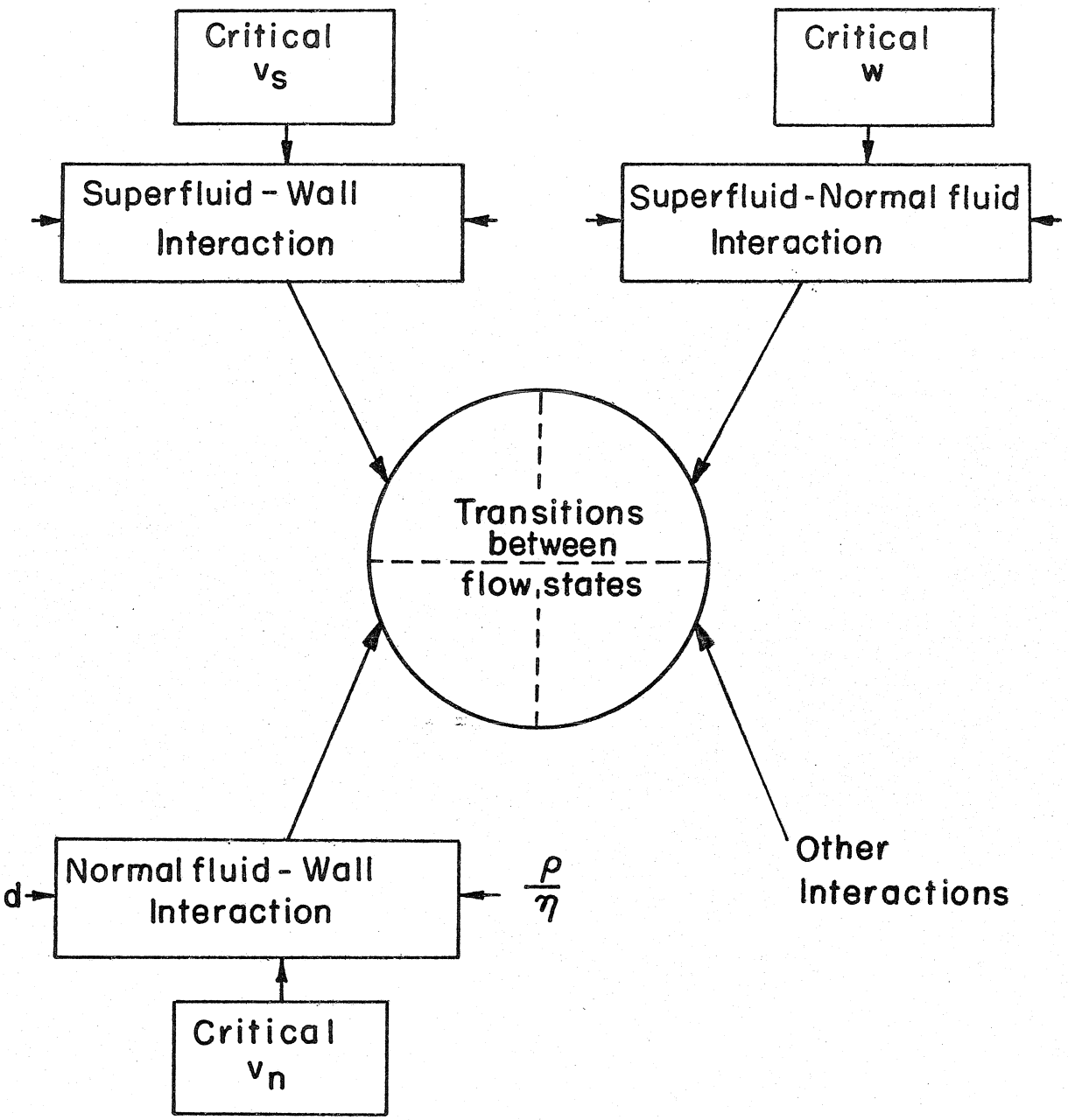

Figure 2.2 CAUSAL RELATIONS BETWEEN CRITICAL VELOCITIES AND TRANSITIONS

number, which involves not only the fluid velocity, but also the kinematic viscosity of the liquid, as well as a natural length scale. Similarly, the interactions in helium II must involve other unknown parameters besides the associated velocity. Furthermore, the three interactions shown are not necessarily independent nor do they form a complete set. The aforementioned diagram is therefore adequate only to illustrate the following simple point: a fluid mechanical interaction occurring in helium II is reciprocally associated with a particular fluid velocity.

Thus, if a critical transition is found to depend on w instead of v_s the responsible interaction must be operative between the two fluids. Conversely, if an interaction between the superfluid and its boundaries is supposed, the proper critical velocity must be in terms of v_s and not w.

Having completed the discussion presenting the philosophies of critical velocities, attention can now be directed towards the few specific triumphs, in theory and experiment, achieved over the last forty years.

In the monumental paper advancing the theory of superfluidity (Landau, 1941), the reversible flow of the superfluid was attributed to the impossibility of exciting thermal excitations in a particular velocity range. Landau's analysis considered helium II at absolute zero (so interactions due to the normal fluid could be ignored) as it flowed past a wall or physical object of mass, M. A detailed balance of momentum and energy during an interaction showed that an excitation of energy, ε, and momentum, p, could only be generated if:

$$\vec{p} \cdot \vec{v}_s = \varepsilon + p^2/2M \tag{2.21}$$

For a massive object ($M \to \infty$) this means that excitation generating interactions occur only if the superfluid velocity is larger than the minimum value of (ε/p). This result, known as Landau's criterion, yields a superfluid critical velocity of:

$$v_{sc} = \left(\frac{\varepsilon}{p}\right)_{minimum} \tag{2.22}$$

From the excitation spectrum of helium II, (see Figure 2.1), a minimum in ε/p around the roton valley is apparent which yields a very large critical velocity approaching 60 m/sec. This was several orders of magnitude larger than critical flow velocities in channels experimentally observed in Landau's time; although more modern experiments, utilizing accelerated ions to probe the superfluid at rest, display an upper velocity apparently limited by the excitation of single rotons (Reif and Meyer, 1960; Meyer and Reif, 1961). Another problem with Landau's critical velocity was its independence of a fundamental length scale; even the earliest experiments noted that critical velocities depended dramatically on the width of the channel -- the smaller the channel, the larger the velocity.

Inspired by Onsager's suggestion of quantized circulation, Feynman (1955) proposed that another type of excitation was possible in liquid helium -- the quantized superfluid vortex ring. Such an excitation would not participate significantly in the thermodynamics (their population is very scarce compared to the phonon and roton populations), but it would be effective in reducing the critical

velocity of superfluid flow. Feynman deduced that the critical velocity required to produce free vortex rings in the superfluid having a single quantum of circulation is:

$$v_{sc} \simeq \frac{K}{2\pi d} \log \frac{2d}{r} \tag{2.23}$$

where r is the vortex core radius. This result not only predicted the correct order of magnitude of the observed critical velocities, but it also included a dependence on the channel size, d, which closely matched the experimental data of the time.

Generation of thermal excitations and superfluid vortexes represent the two modes in which superfluidity of helium II can be destroyed. Creation of excitations destroys the reversibility of the flow, while the creation and multiplication of vortex lines impairs the irrotationality of the fluid (although on the microscopic level the superfluid is always irrotation, a macroscopic view, averaging over many vortexes, leads to an "average vorticity" in the superfluid).

Although the generation of quantum superfluid vortexes in itself absorbs energy from the flow, an additional source of dissipation arises from the interaction of the normal fluid excitations with the superfluid vortex cores. This occurs because the energy of phonon and roton excitations depends on the velocity of the background superfluid:

$$E = \varepsilon(p) + \vec{p} \cdot \vec{v}_s \tag{2.24}$$

Here $\varepsilon(p)$ and p are the energy and momentum of an excitation viewed in the superfluid rest frame (the function $\varepsilon(p)$ is the energy spectrum

presented as Figure 2.1). The rapid superfluid motion near a vortex core produces a central energy potential effective in scattering the normal fluid excitations. Since quantum vortexes move with the superfluid, this interaction produces a momentum exchange between the two fluids, which to lowest order is proportional to the relative velocity (see Goodman, 1971). Thus, when quantum vortexes are present a mutual interaction arises whenever there is an average relative velocity between the two fluids.* The energy dissipated by the mutual interactions is converted into thermally generated normal fluid excitations.

Although well received at first, Feynman's theory eventually found disfavor as additional experiments yielded critical velocities whose dependence on channel size was at variance with the concept of "free" vortex ring generation. As pointed out initially by Feynmann himself, the image vortices caused by the ever present channel walls will greatly affect the generation process; so in order to better fit the experimental data, various authors have included these complications into the model as well as those arising from the vortex

*Scattering of excitations by quantum vortexes is believed to be the mechanism responsible for the Gorter-Mellink force of mutual friction. This body force, appended to the superfluid equation, was originally proposed by Gorter and Mellink (1949) to explain the details of supercritical counterflow. Taking the curl of the modified superfluid equations shows that the presence of the Gorter-Mellink term is enough to invalidate the irrotationality of the superfluid. However, on the microscopic level the superfluid motion is always irrotational; therefore the superfluid velocity described by this modified equation is interpreted as a macroscopic average over many quantum vortexes.

The presence of the Gorter-Mellink term always implies the existence of superfluid vortexes; therefore it is reasonable to assume that the G-M force is "switched-on" when quantum vortexes appear, and it is inoperative when no quantum vortexes are present. Notice that if the G-M force were always present persistent currents would not exist: the G-M force would dissipate energy from the flow until the relative velocity and superfluid velocity vanished.

core. The extra theoretical complexities, however, have not produced a decisively favorable result, possibly because the irregularities in the channel walls, which are usually on the order of the mean channel width, add mathematically intractable complications to the real life process.

Eventually as the complications inherent to the critical velocity problem were recognized, careful experiments were constructed which attempted to isolate the various interactions from one another. An experiment by Staas, Taconis, and Van Alphen (1962), which allowed only the normal fluid to flow through round capillaries (d = 173 μm and 255 μm), conclusively identified a laminar-turbulent transition at a Reynold's number, Re ≃ 1200:

$$\mathrm{Re} \equiv \frac{\rho \langle v_n \rangle d}{\eta} \qquad (2.25)^*$$

In the turbulent region the pressure drop followed the ordinary Blasius law: $\Delta p \propto \langle v_n \rangle^{1.75}$

This identification was able to clear up many previous critical velocity measurements. Van Alphen, Van Haasteren, Ouboter, and Taconis (1966) found that many of the transitions in channels larger than d ∿ 10 μm, which were attributed to a superfluid critical velocity, were actually caused by normal fluid turbulence. Elimination of these data showed that the superfluid critical velocity has only a weak dependence on channel size:

---

*It is interesting that although Re is a function of the normal fluid velocity, the mass density involved includes both the normal fluid and superfluid components.

$$v_{sc} \propto d^{-\frac{1}{4}} \tag{2.26}$$

and is independent of temperature (this last feature is consistent with a theoretical explanation based on the creation of superfluid vortices).

Experiments with persistent currents (Clow and Reppy, 1967) revealed a new superfluid critical velocity which was temperature dependent -- near T_λ it was proportional to the superfluid mass fraction -- but was independent of channel size. This critical velocity has been named the "intrinsic superfluid critical velocity", due to its independence of channel size, in contrast to the "extrinsic superfluid critical velocity" which has a length scale dependence given by equation (2.26). In order to see the intrinsic critical velocity the channel size had to be made very small -- less than 1 μm. Otherwise the extrinsic critical velocity dominated the flow.

Inspired by these experiments, Langer and Fisher (1967) proposed that the intrinsic superfluid critical velocity is caused by homogeneous nucleation of superfluid vortex rings. These rings are supposed to occur spontaneously within the fluid, generated by normal fluid thermal fluctuations. Depending on the velocity of the superfluid, there is a critical ring size which determines the critical velocity of the fluid. If a vortex ring is created which is larger than the critical size it will tend to expand and in the process absorb energy from the flow. Smaller rings tend to collapse and therefore will not cause the flow to decay.

According to the Langer-Fisher theory the temperature dependence

of the intrinsic critical velocity should be given by:

$$v_{sc} \propto \frac{\rho_s}{\rho T} \tag{2.27}$$

This dependence was observed by Clow and Reppy and has been further verified by pressure driven superflow through microscopic pores ($d \sim 100$ to 800 Å), etched in thin mica sheets (Notarys, 1969). The constant of proportionality, making (2.27) an equation, was determined by Notarys to be 4.6 m/sec which is ten times smaller than the theoretical value. This slight embarrassment to the theory is consistently obtained in all experiments designed to observe the intrinsic critical velocity.

Ignoring the large discrepancy in the predicted magnitude of the critical velocity, there are two criticisms that can be made about the thermal-fluctuation theory. First, if the critical velocity is truly intrinsic to the fluid -- that is, if it is due to mutual interactions instead of superfluid-wall interactions -- then it must be a relative critical velocity. Changing the v_{sc} to a w_c is not a problem in either experiment or theory since the normal fluid is always clamped by viscous interactions with the walls. Thus, it will be assumed that the thermal-fluctuation theory yields a critical relative velocity.

Second, the fact that the intrinsic critical velocity is observed in only the smallest available channels is more than ironic. If a large relative velocity is produced in helium II far away from the walls containing the fluid, then its magnitude should be limited only by the intrinsic critical velocity, since all other critical

velocities discovered experimentally are fundamentally related to fluid-wall interactions. The fact that these latter critical velocities always dominate large geometries has led experimentalists into smaller and smaller geometries until the flow is so confined that the extrinsic critical velocities are inhibited. The hope is that the true intrinsic critical velocity, due only to mutual interactions between the two fluids, can still be observed even in these confined geometries. However, when the fluid is so confined that transitions due to wall interactions are inhibited, it is difficult to believe that the two fluid components are still allowed to freely interact one with the other. As a case in point, Notarys has shown that the ring vortices, hypothesized by Langer and Fisher to be the agents mediating the mutual interaction, are actually larger than the channels in which the intrinsic critical velocity has been observed.

This inconsistency cannot be resolved by more work in restricted geometries. Instead the mutual interaction must be identified in the fluid away from all walls. As proposed in the introduction, second-sound shock waves are the ideal tool to produce and observe mutual interactions. Since the plane shocks produced are not infinite in extent, there certainly will be wall interactions. However, during the time interval necessary to generate and observe second-sound shock waves these effects will be confined to a thin layer near the shock tube sidewall.

Chapter 3. APPARATUS FOR THE GENERATION AND DETECTION OF SECOND-SOUND SHOCK WAVES

The present study concentrated exclusively on large-amplitude second-sound waves in one-dimension. Unfortunately, perfect plane waves, unencumbered by three-dimensional secondary wave fields, can only be approached in finite geometries. Edge effects due to a finite source are traditionally negated by propagating the wave down a tube having cylindrical geometry. Propagating perpendicular to the shock tube walls, the wave fronts are inhibited from three-dimensional spreading, but at the same time wall-induced boundary layers extract momentum from the flow and eventually destroy the unadulterated one-dimensional motion on the interior. Since the normal viscosity is remarkably small in liquid helium, laminar boundary layers are very thin compared to the shock tube diameter, and thus wall-induced three-dimensional effects are insignificant.

Second-sound is primarily a temperature wave; therefore, heat extracted through the shock tube walls will lead to three-dimensional effects similar to those generated by the viscous boundary layers. Fortunately this effect is also very small due to the negligible heat capacity of common materials at cryogenic temperatures compared to liquid helium (see Table 3.1); also, heat transfer to or from helium II is severely limited by temperature discontinuities proportional to the penetrating heat flux appearing at all liquid-solid interfaces (the constant of proportionality is known as the Kapitza resistance).

TABLE 3.1. HEAT CAPACITIES OF COMMON MATERIALS

	(10^{-3} J/cm^3 - ^{o}K)	
Material	@1.2^{o}K	@2.0^{o}K
Helium II @ 1 bar	46.2	748.5
Steel	.8	1.4
Copper	.13	.25
Aluminum	.16	.29
Teflon	.07	.33

The non-steady evolution of a second-sound shock pulse is most clearly observed when the generating heat pulse possesses a rectangular power-versus-time profile. To approach a step response a very fast rise time heating element is required. A thin-film heater, 1000 Å thick nichrome vacuum deposited on a quartz or glass substrate, has adequate response and has proven very durable. Electrical contact is made with either pressed or soldered indium to 2000 Å thick copper leads which extend over part of the nichrome film.

The only significant problem attributed to the heater was the inability to perfectly seal the heater face to the end of the shock tube. The superfluidity of liquid helium makes leak proof or "super-leak" proof seals very difficult to obtain since traditional cryogenic seals of metallic indium could not be used as they would electrically short-circuit the heater. To date, the best seal has been made against a teflon collar having sharp edges machined in a circular pattern (see Figure D.5); but even this seal was never perfect, as evident

from the existence of small secondary waves, originating at the heater and generated by heat leaks through the seal.

Due to imperfectly sealed heaters, three-dimensional waves always accompanied the main one-dimensional pulse. Since these secondary waves could not be successfully eliminated, it was essential to accurately predict their arrival so that they could be identified separately from features germane to the one-dimension pulse. Accurate prediction was accomplished and is discussed in detail in Appendix D.

To accurately determine the arrival of shock waves having small temperature amplitudes requires very fast rise time sensors with high sensitivity. Both of these requirements are met by superconducting thin-films vacuum deposited on glass substrates. Layered films of superconducting tin on normal conducting gold were constructed following procedures developed by Notarys (1964), who used them to detect high frequency second-sound up to 25 MHz, and Laguna (1975 and 1976). The sensor is operated in the middle of its superconducting transition where the resistance changes appreciably with temperature. Sensor resistance is monitored by passing a fixed current, usually 1 mA, through the sensor and observing the voltage drop. The overall sensitivity of a typical sensor usually can be made to exceed 1 $V/^{o}K$.

Different operating temperatures were achieved by two methods: 1) magnetic fields were used to depress the transition temperature of the sensor; and 2) the zero-field transition temperature was set by varying the tin-gold composition. The zero-field transition temperature for these layered films can be calculated with the following formula (see Joynson, 1970):

$$T_c = (T_c)_{Sn} \sqrt{\frac{1 - \nu z}{1 + \nu z}} \qquad (3.1)$$

where $$z = \frac{M_{Au}}{M_{Sn}} = \frac{\rho_{Au}}{\rho_{Sn}} \frac{d_{Au}}{d_{Sn}}$$

$\nu \simeq .8 - .9$ $\qquad (T_c)_{Sn} = 3.72^{o}K$

d = film thickness

The thickness of the gold layer was always between 200 to 250 Å, and the entire sensor was about 1000 Å thick.

Electrical contact was made to the sensing element with vacuum deposited copper leads 1000 to 2000 Å thick, and the electrical circuit was completed with thin copper wires indium soldered to the copper films. The copper film leads were a significant improvement over the superconducting tin leads used by previous investigators since wires could be directly soldered to the copper films -- a procedure which greatly increased the reliability of the sensor.

In addition to the intrinsic sensor response, the observable rise time depends on the orientation of the sensor with respect to the approaching wave front, because the finite size of the temperature sensing element precludes a point measurement. The resistance of the element material is about .5 Ω/square (at $4^{o}K$); therefore, to achieve a suitable sensor resistance of one or two hundred ohms, a long, narrow sensing element is manditory. The two sensor configurations employed, endwall and sidewall, are shown in Figure 3.1. The sidewall sensor consists of a single long strip aligned parallel to the approaching

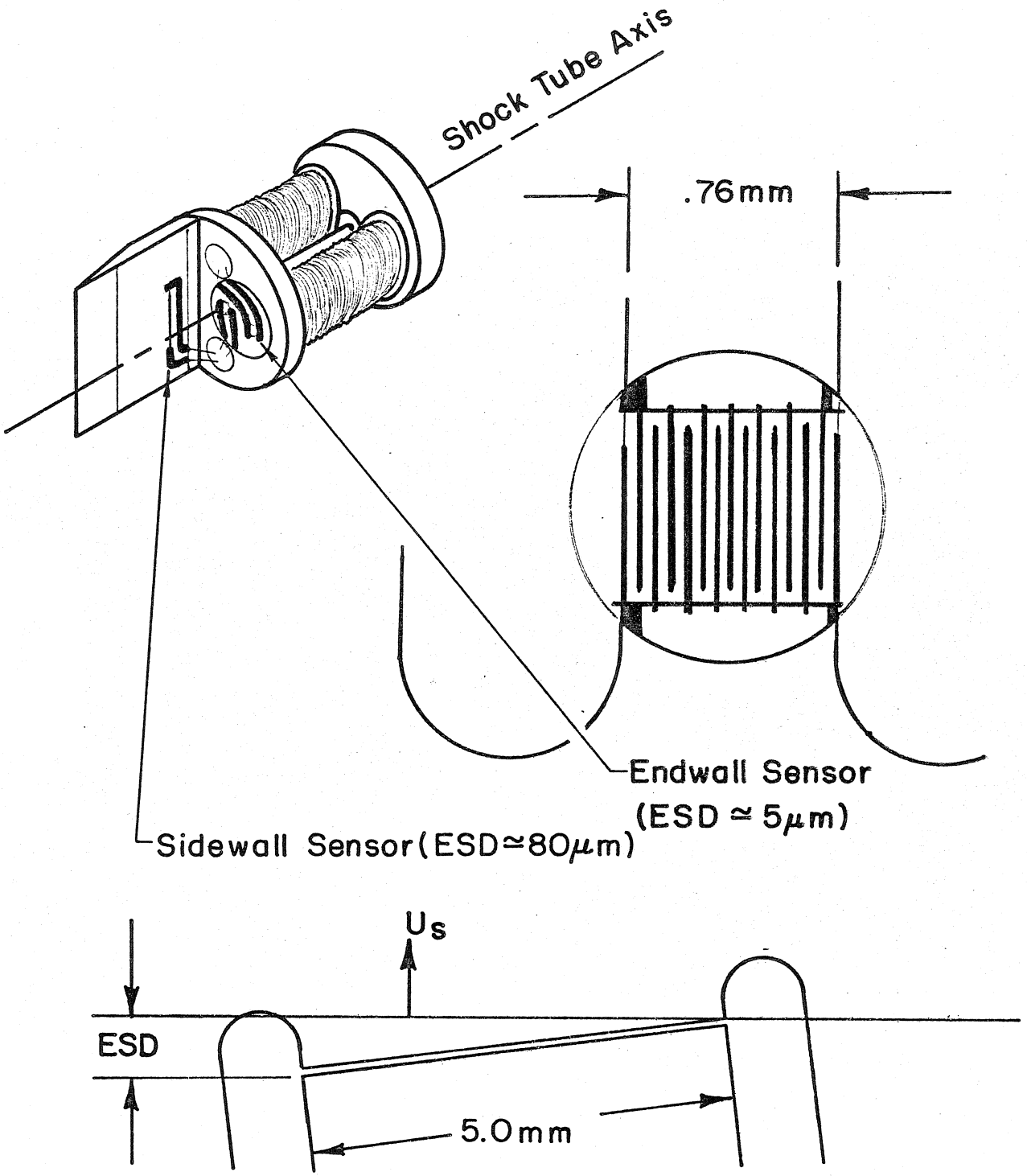

Figure 3.1 INSTRUMENTED ENDWALL OF THE VARIABLE LENGTH SHOCK TUBE

wavefronts, while the endwall sensing strip is folded back-and-forth into a pattern which minimizes the overall projected length.

The rise time of a sensor due to geometric constraints is the distance traversed by a wave front until the entire sensor is activated, divided by the propagation speed of the wave. This geometric distance, referred to as the "equivalent sensor depth" (ESD), can be made much smaller for an endwall mounted sensor than for a sidewall sensor; hence, the former is preferred in most applications.

The endwall sensor pattern was scratched into the film with a razor blade mounted on a three-axis micrometer. With this technique a square sensing element as small as .60 mm on a side and having a normal resistance of 75 ohms (at $4^{o}K$) was achieved. Its estimated ESD due to unavoidable misalignment was only 3 μm.

The basic parts of a one-dimensional shock tube -- the heater, a parallel-sided tube, and the detecting sensors -- can be configured in an infinite variety of ways. The present study utilized five separate and distinct shock tubes whose pertinent dimensions and specifications are compared in Table 3.2. The shock tubes in which the shock limit was first discovered (I and II) were made out of plexiglass and had rectangular cross sections. From these initial experiments an advanced shock tube was designed which incorporated variable length and a circular cross section -- a change desirable to eliminate the possibility of secondary flow originating in the corners.

Table 3.2 SHOCK TUBE SPECIFICATIONS

	I	II	III[a]	IV	V[b]
Side wall material	Plexiglass	Plexiglass	Brass	Plexiglass	Glass and Teflon
Tube Cross Section	Square 2.54 cm wide	Rectangular .64 cm x 1.91 cm	Round 2.21 cm dia	Round 1.91 cm dia	Square 2.54 cm wide
Length (heater to endwall)	10.05 cm	7.62 cm (open ended)	2 to 20 cm	1.93 cm	1.50 cm
Sensor Configuration	2 Sidewall 1 Endwall	2 Sidewall	1 Sidewall 2 Endwall	1 Endwall	1 Endwall
Designed for pressurization	No	No	Yes	No	Yes
Heater seal	Open	Silicone Rubber Gasket	Teflon	Plexiglass flat overlapping the heater	Teflon and indium

[a]Variable Length Shock Tube

[b]Optical Shock Tube

VARIABLE LENGTH SHOCK TUBE

Nonlinear second-sound waves are nonsteady -- that is they change shape as they propagate; therefore, it is useful to observe them at various distances from the heater. Instead of aligning a plethora of sensors along the entire length of the shock tube, which exceeds 20 cm, it seemed more reasonable to place a few sensors on a movable endwall. Besides the obvious advantage of simplicity offered by this configuration, it also allowed the use of endwall sensors whose superiority was previously noted.

Temperature sensors instrumenting the movable endwall are depicted in Figure 3.1; they include one sidewall and two endwall versions. Two iron-core magnets, wound with superconducting Nb-Ti wire, were provided to bias and align the transition temperatures of the three sensors in pairs; this enabled temperature measurements to be obtained simultaneously at two distinct locations.

The instrumented endwall can be positioned anywhere along the shock tube axis via external commands, even in cryogenic environments (immersed in liquid helium or liquid nitrogen) as well as at room temperature. The components comprising the positioning system are fourfold: 1) an A.C. driving motor; 2) a mechanical transmission; 3) a linear position indicator; and 4) a wire feed mechanism, which keeps the signal cables from tangling (see Figure 3.2).

An A.C. motor was chosen over a D.C. one, because the former does not require commutating brushes for operation. Brushed commutation, besides being dirty, produces a lot of electrical arcing which would

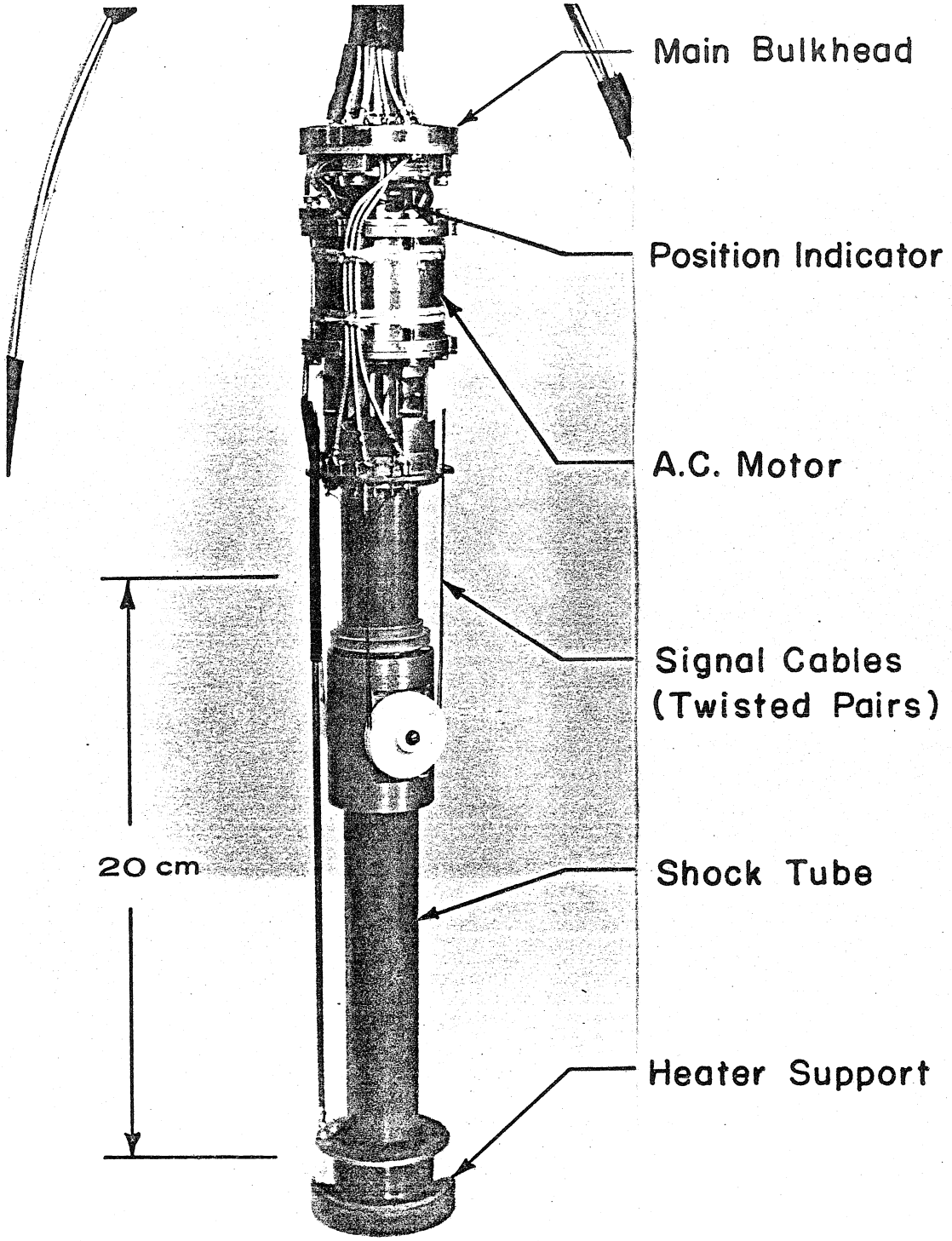

Figure 3.2 THE VARIABLE LENGTH SHOCK TUBE

be greatly enhanced in a helium environment (the arcing potential in helium gas or liquid is much lower than in air at STP). A two phase, split-series field, 400 Hz motor was readily available (General Design, Inc.; Sun Valley, Calif.), and was placed in a housing machined from 430F stainless steel. The thermal expansions of this material and the motor shaft material, 420F, very closely match that of the bearing material, 440C. This choice of materials minimizes the differential contraction at cryogenic temperatures that would otherwise jam the bearings.

The motor shaft is hollow and threaded at one end to accommodate a 35 cm long screw (6-32 thread). As the motor shaft rotates, the screw, which is constrained against rotation, executes linear motion and ultimately positions the instrumented endwall attached at the lower end. The screw was prevented from rotating by two tiny wheels, free to roll up or down in a rectangular track located in the tube extending vertically from the main bulkhead. All the moving parts were dry lubricated by a thin layer of tungsten disulfide permanently bounded to the metallic surfaces (Dicronite DL-5; Rotary Component, Inc.; Covina, Calif.). Since all foreign substances freeze solid in liquid helium, the exclusive use of dry lubricants is essential. The bearings employed--also dry lubricated--were designed for high temperatures but work equally well at absolute zero as long as care is taken to preclude the presence of water vapor that would form ice particles during cool down (Bartemp bearings, Barden).

Driving the screw directly by the motor greatly simplified the mechanical transmission, but it also caused the mechanism to be driven

ten times faster than was practical. This problem was solved by electronically controlling the motor speed with pulse length modulation. A block diagram illustrating the electronic control and position sensing mechanism is presented in Figure 3.3. The speed controller turns the motor on or off depending on its speed, which is derived from the position indicator tachometer signal.

The position sensing system, which must operate at any motor speed and all accessible temperatures, consists of two pairs of coils separated by a slotted aluminum disk. A 1.3 MHz frequency is input to the coils below the disk and the output, modulated by the disk rotation, is picked up by the two upper coils. These signals, when demodulated, represent two overlapping position signals which specify the rate and direction of the shaft rotation. An electronic up/down counter keeps track of the net number of shaft rotations in 45^{o} increments. This number corresponds to the linear position of the instrumented endwall (one count equalling .0099 cm at 2.0^{o}K).

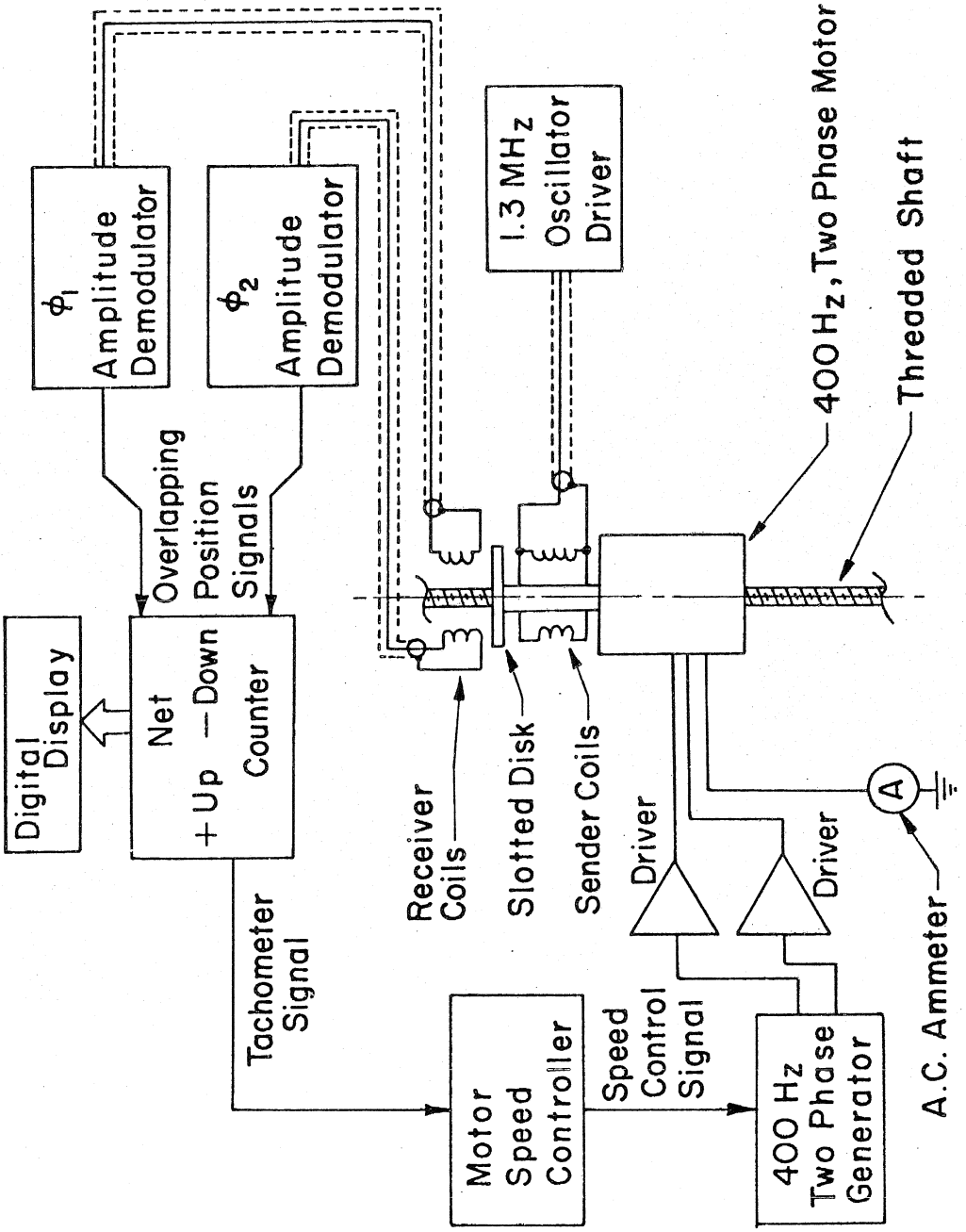

Figure 3.3 ENDWALL POSITIONING SYSTEM

SETTING THE EQUILIBRIUM PRESSURE AND TEMPERATURE

The equilibrium pressure and temperature of liquid helium filling the test section is controlled by the system illustrated in Figure 3.4. Constant temperature is maintained by a pressure-regulated external bath of liquid helium in equilibrium with its vapor; the saturated vapor pressure is monitored by a sensitive Barocel, and subsequently converted into absolute temperature with the 1958 He^4 temperature scale.

In order to set the test section pressure significantly above the saturated vapor pressure it was necessary to enclose the variable length shock tube in a 50 mm diameter copper tube. A radial indium seal was provided between this tube and the main bulkhead into which twenty-four electrical feedthru terminals (Hermmetic Seal Corp.; Rosemead, Calif.) had been soldered. This pressure vessel was filled and pressurized through a 3 mm diameter, thin wall, stainless steel tube, which extended out of the dewar to a helium gas cylinder and associated plumbing. Maintaining the pressure at liquid helium temperatures was not an easy task since the absence of viscosity allows the superfluid to quickly flow through any hole no matter how small; this was a problem that plagued the radially sealed pressure vessel and is at the moment unresolved.

After a shock wave is fired, a significant length of time is required before the fluid in the test section regains equilibrium. In order to moniter this recovery time, as well as any constant temperature differential between the test section and the outside bath (due to

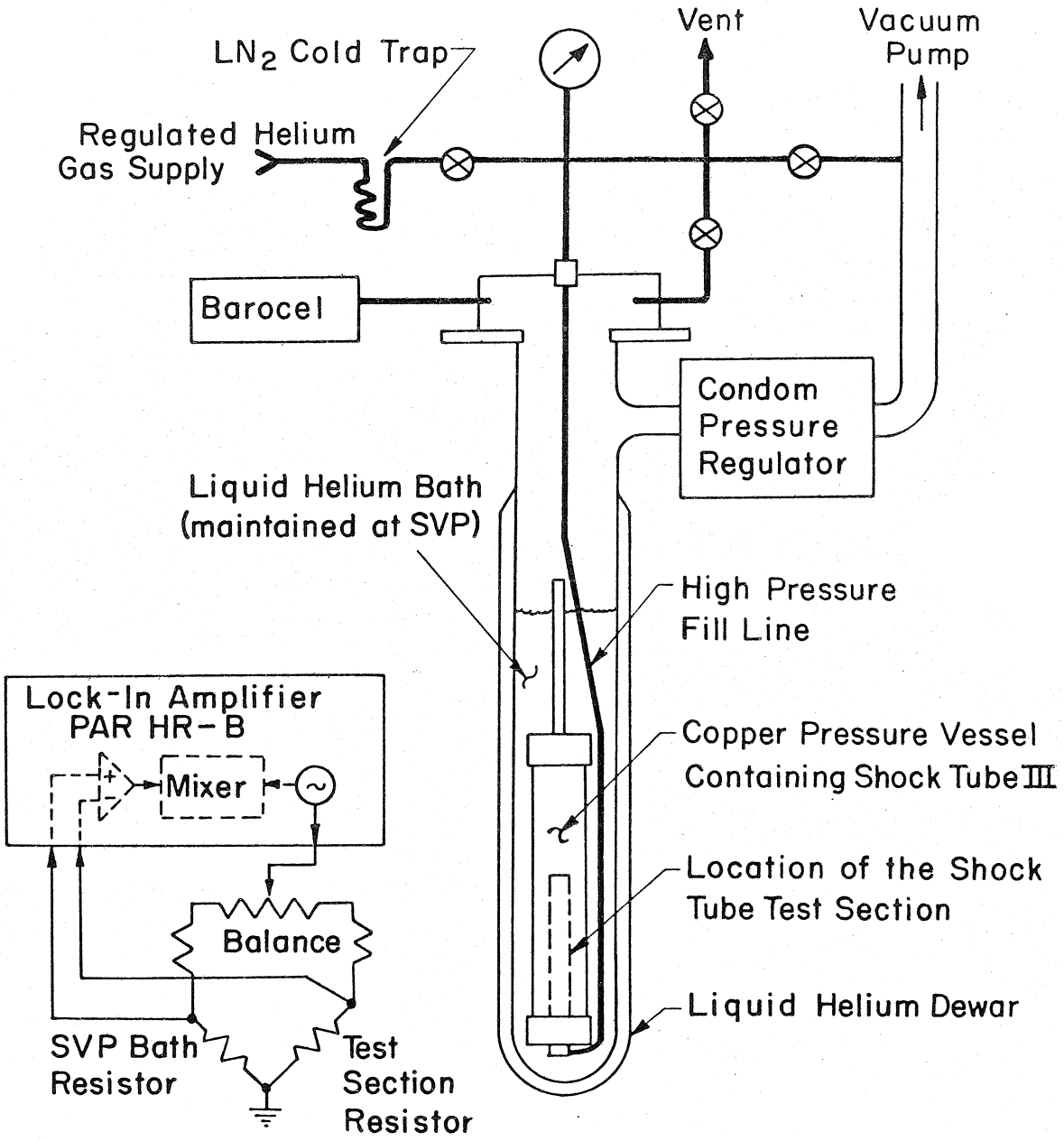

Figure 3.4 SYSTEM FOR MAINTAINING THE TEST SECTION EQUILIBRIUM PRESSURE AND TEMPERATURE

internal electrical dissipation or very small superleaks), two calibrated carbon resistors, connected in a bridge circuit, were monitored by a sensitive lock-in amplifier. Using this system the temperature recovery time constant at $T = 1.60^{o}K$ was determined to be 1.5 seconds.

THE OPTICAL SHOCK TUBE

Boiling in a region near the heater was found to accompany the breakdown of superfluidity. This encouraged the construction of an optical shock tube in which shock generation could be visually observed. Figure 3.5 is a photograph of this device.

Two quartz windows were sealed to a brass housing with axial indium seals, each spring loaded by two 400 lb thrust Belleville washers. These axial seals have proven reliable in helium II up to 5 bar, which is over twice the critical pressure of liquid helium.

Shock waves, generated by a thin-film heater on the bottom, are detected by an endwall sensor at the top of the cavity. No magnet is employed to bias the superconducitng transition, because its proximity to the heater would enable the magnetic field to distort the heater current distribution, resulting in a spatially nonuniform heat pulse. The walls of the shock tube are formed by the windows and two teflon spacers, also used to hold the sensor and heater slides in place. The resulting test section has a 25.4 mm square cross section and is 15.0 mm long.

Pressure and temperature were maintained by the same system developed for the variable length shock tube and adapted for use with a Janis research dewar having an optical tail.

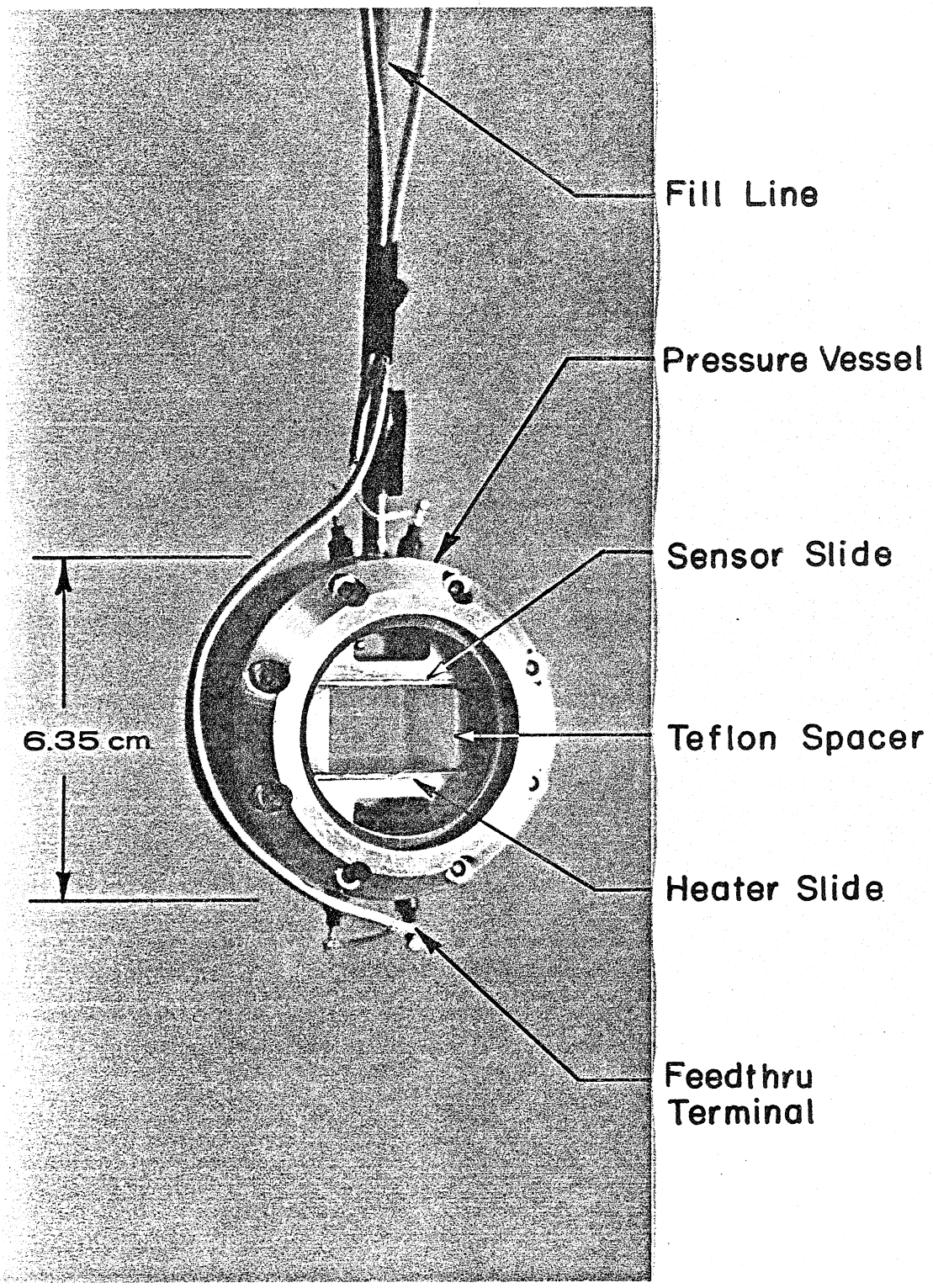

Figure 3.5 THE OPTICAL SHOCK TUBE

AUXILIARY EQUIPMENT

The primary measurements taken in a typical shock wave experiment include: 1) shock front time of flight; 2) the shock temperature amplitude; 3) the temperature profile of the shock pulse; and 4) the power delivered to the heater. Figure 3.6 is a schematic representation of the electronic system responsible for obtaining these data. Most of the setup is self-explanatory except for a few points.

The pulse power driver generates the high-power voltage pulse used to produce the shock pulses. The output of this device rises quickly (rise time ≃ 1 μsec) to an internal voltage level (monitored by an external digital voltmeter) and is held there for a time interval determined by the H.P. pulse generator. This results in voltage and power pulses having nearly rectangle profiles.

The signals from the superconducting sensors are amplified by a low noise, broad band amplifier: usually a Princeton Applied Research Model 113; when shock structure is being recorded a high frequency preamp is included. This preamp, which employed a common base input stage, was optimally designed for high sensitivity, low noise, and a sufficient frequency range. Its input impedance was set to 50Ω to achieve optimal high frequency coupling with miniature coaxial cables. The clean oscillograph traces of second-sound shock waves are a result of improved electronics and increased sensor sensitivity (achieved by increasing the overall sensor resistance).

The temperature amplitude of the shock front is measured by a fast 12-bit analog-to-digital converter. The measured voltage is

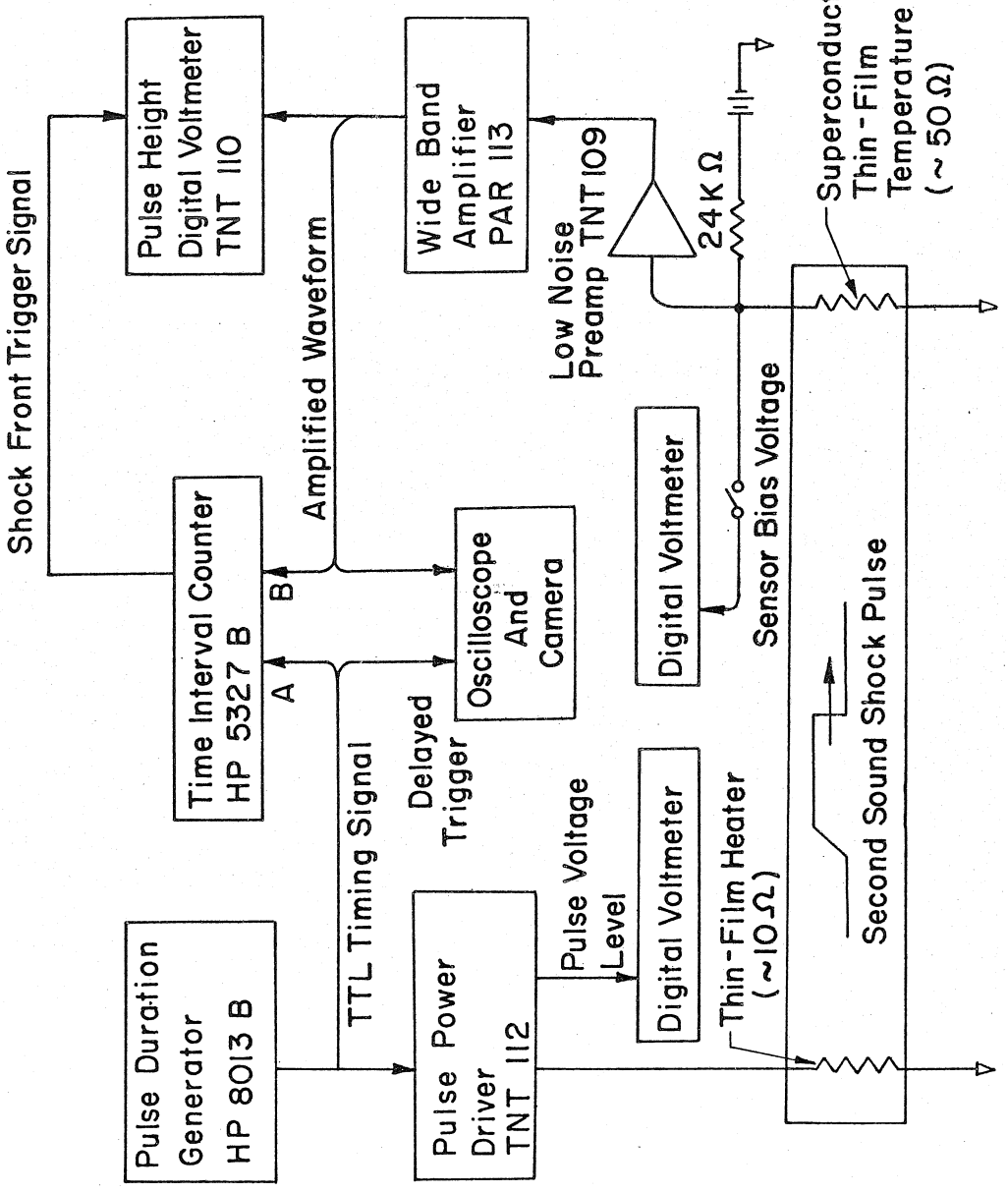

Figure 3.6 DATA ACQUISITION SYSTEM

maintained during conversion by a track-and-hold circuit triggered, after a suitable delay (usually 5 μsec), by the Hewlett-Packard time interval counter.

In order to accurately deduce the temperature amplitude it is necessary to record the nonlinear temperature-resistance transfer function of each sensor. Computer analysis can later invert resistance changes to temperature jumps if the bias voltage of the sensor prior to each shock wave firing is known. This measurement is made with a DMV and recorded just prior to each run.

Chapter 4. NONLINEAR SECOND-SOUND

A wave supporting medium in motion convects any wave field which is impressed upon it. Consider, for instance, an ordinary fluid flowing with velocity, $\vec{v}$, in which sound waves have been excited. When the fluid is at rest, waves propagate at velocity $\vec{c}$, whose magnitude is a function of direction only if the fluid is anisotropic. In a moving fluid this velocity must be supplemented by the convection velocity, which according to the principle of Galilean relativity equals the fluid velocity. Of course, use of a Galilean transformation presupposes that all velocities under consideration, including the wave velocity, are non-relativistic. Thus, the convection of light cannot be so simply ascertained, but must be calculated using the relativistic Lorentz transformation. In any case the principle is the same: waves are convected by the medium in which they propagate. For the present example, the propagation velocity of sound in a moving fluid denoted $\vec{u}_c$, may be written as:

$$\vec{u}_c = \vec{c} + \vec{v} \tag{4.1}$$

The principle of convection may be applied to second-sound in helium II, but in this case a problem arises due to the two-fluid nature of the medium. The convection due to the independent velocity fields, $\vec{v}_n$ and $\vec{v}_s$, cannot be deduced from simple arguments using Galilean relativity; however, the convection due to the bulk velocity, $\vec{v}$, can be so determined. For example, take any combination of $\vec{v}_n$ and $\vec{v}_s$ and increment both velocities by the same vector amount. Then

Galilean relativity ensures that the wave velocity is incremented by the same amount. Since this increment corresponds to a change in $\vec{v}$ while $\vec{w}$ remains unaltered, one can deduce that wave velocities in helium II are always convected with velocity $\vec{v}$. The convection due to the relative velocity must be calculated from the two-fluid model, but in general the velocity of second-sound in moving helium II can be written as:

$$\vec{u}_a = \vec{a} + \vec{v} + f(\vec{w})\vec{w} \tag{4.2}$$

where a is the speed of second-sound in the liquid at rest and $f(\vec{w})$ is a convection coefficient to be determined. In order to differentiate between the two wave velocities, $\vec{u}_a$ and $\vec{a}$, the former will be called the "characteristic velocity" -- in reference to the formulation of hyperbolic equations in terms of characteristic curves -- while the latter will be simply termed "second-sound velocity".

Second-sound is akin to ordinary sound in that they both consist of nondispersive, longitudinal, nonlinear waves. The longitudinal character of these waves -- that is, the induced wave motion lying parallel to the direction of propagation -- leads to their essential nonlinearity; as a wavefront advances into the fluid it induces a fluid velocity which in turn convects the wavefront and alters its speed. Since the magnitude of the induced velocity increases with the wave amplitude, the propagation velocity or characteristic velocity of the wave must also depend on the wave amplitude -- a feature essential to nonlinear waves.

Wave convection is not the only process leading to an amplitude-

dependent characteristic velocity: pressure and temperature dependency of the wave speed are also important and may add to or detract from the overall magnitude of the amplitude dependence.

In contrast to nonlinear waves, the characteristic velocities of linear waves are always independent of the wave amplitude. When deriving the expressions for linear first- and second-sound (see Appendix B), all terms quadratic or higher in the wave-induced or perturbation quantities, that might lead to an amplitude-dependent velocity, are assumed so small that they can properly be neglected. The resulting linear wave equations are known to possess very simple solutions. In the one-dimensional or plane-wave case, any disturbance can be described by a linear superposition of four simple waves -- two for first-sound and two for second-sound -- travelling in opposite directions. Each simple wave has a single profile in space and time which totally specifies the wave-induced quantities: changes in pressure temperature, velocity, etc. Finally, as a consequence of the amplitude independence of the characteristic velocity, this profile propagates without changing size or shape -- it is steady in the reference frame moving with the wave.

Since v and w are linearly proportional to the temperature perturbation, the convection present in a second-sound wave will always produce an amplitude-dependent propagation velocity except in the limit of vanishing amplitude. Only in this limit do second-sound waves behave linearly.

SECOND-ORDER THEORY

The theory of nonlinear waves in helium II can be developed using the method of characteristics originally invented by Riemann for application to nonlinear sound waves in ordinary substances (see Courant and Friedrichs, 1948 or Whitham, 1974). In the development which follows three assumptions are prerequisite: 1) the wave-induced motion is one-dimensional; 2) the resulting flow is thermodynamically reversible; and 3) the relative velocity is small, but nevertheless significant.

The final assumption is somewhat contradictory to a fully nonlinear theory of waves, since as has been pointed out, a full accounting of wave convection is a primary criterion in a nonlinear theory. The small velocity restriction is required in an analytic theory, since the functional form of the thermodynamics of helium II with respect to w^2 is unknown except for a linear expansion around the state $w = 0$. This expansion is valid only when w^2 is small. Thus from the beginning, it is apparent that an exact analytic theory is unobtainable. Instead a second-order theory will be advanced which is one step beyond the linear limit: it is applicable to second-sound waves having small, but finite, amplitude. It will be shown that this theory, which ignores all terms in the wave-induced perturbations higher than second order, accurately describes the nonlinear behavior of second-sound.

Four variables are required to specify the state of a fluid particle in liquid helium II: two velocities, $\vec{v}$ and $\vec{w}$, and two thermodynamic variables, of which p and T will be used. The four equations necessary to determine these variables are presented as Table 4.1. First, the continuity equation is a simple restatement of conservation

Table 4.1 THE EXACT TWO-FLUID EQUATIONS FOR ONE-DIMENSIONAL REVERSIBLE FLOW

CONTINUITY EQUATION:

$$\frac{\partial \tilde{\rho}}{\partial t} + \tilde{\rho}\frac{\partial v}{\partial x} + v\frac{\partial \tilde{\rho}}{\partial x} = 0$$

BULK VELOCITY EQUATION:

$$\frac{\partial v}{\partial t} + \frac{1}{\tilde{\rho}}\frac{\partial p}{\partial x} + v\frac{\partial v}{\partial x} + \left(2\frac{\tilde{\rho}_n\tilde{\rho}_s}{\tilde{\rho}^2}\right)w\frac{\partial w}{\partial x} + \left(\frac{\tilde{\rho}_n\tilde{\rho}_s}{\tilde{\rho}^2}\, w^2\right)\frac{1}{\tilde{\rho}}\frac{\partial \tilde{\rho}}{\partial x} + \left(\frac{\tilde{\rho}_s - \tilde{\rho}_n}{\tilde{\rho}}\right) w^2 \frac{\partial}{\partial x}\left(\frac{\tilde{\rho}_n}{\tilde{\rho}}\right) = 0$$

RELATIVE VELOCITY EQUATION:

$$\frac{\partial w}{\partial t} + w\left(\frac{\tilde{\rho}}{\tilde{\rho}_n}\right)\frac{\partial}{\partial t}\left(\frac{\tilde{\rho}_n}{\tilde{\rho}}\right) + \frac{\tilde{\rho}\tilde{S}}{\tilde{\rho}_n}\frac{\partial T}{\partial x} + 3\frac{\tilde{\rho}_s}{\tilde{\rho}}w\frac{\partial w}{\partial x} + \left[\left(1 - 3\frac{\tilde{\rho}_n}{\tilde{\rho}}\right)w^2 + vw\right]\left(\frac{\tilde{\rho}}{\tilde{\rho}_n}\right)\frac{\partial}{\partial x}\left(\frac{\tilde{\rho}_n}{\tilde{\rho}}\right) + v\frac{\partial w}{\partial x} + w\frac{\partial v}{\partial x} + \left(\frac{\tilde{\rho}_s}{\tilde{\rho}}w^2\right)\frac{1}{\tilde{\rho}}\frac{\partial \tilde{\rho}}{\partial x} = 0$$

ENTROPY CONSERVATION:

$$\frac{\partial \tilde{S}}{\partial t} + \left(v + \frac{\tilde{\rho}_s}{\tilde{\rho}}w\right)\frac{\partial \tilde{S}}{\partial x} + \frac{\tilde{\rho}_s}{\tilde{\rho}}\tilde{S}\frac{\partial w}{\partial x} - \tilde{S}w\frac{\partial}{\partial x}\left(\frac{\tilde{\rho}_n}{\tilde{\rho}}\right) + \left(\frac{\tilde{\rho}_s}{\tilde{\rho}}\right)\tilde{S}w\frac{1}{\tilde{\rho}}\frac{\partial \tilde{\rho}}{\partial x} = 0$$

Table 4.2 SECOND-ORDER TWO-FLUID EQUATIONS FOR ONE-DIMENSIONAL, REVERSIBLE FLOW

CONTINUITY EQUATION:

$$\frac{\partial \rho}{\partial t} + \rho^2 \xi_p \, w \frac{\partial w}{\partial t} + \rho \frac{\partial v}{\partial x} + v \frac{\partial \rho}{\partial x} = 0$$

BULK VELOCITY EQUATION:

$$\frac{\partial v}{\partial t} + \frac{1}{\rho} \frac{\partial p}{\partial x} + v \frac{\partial v}{\partial x} + 2 \frac{\rho_n \rho_s}{\rho^2} w \frac{\partial w}{\partial x} = 0$$

RELATIVE VELOCITY EQUATION:

$$\frac{\partial w}{\partial t} + w \left(\frac{\rho}{\rho_n} \xi_T \frac{\partial T}{\partial t} + \frac{\rho}{\rho_n} \xi_p \frac{\partial p}{\partial t} \right) + \frac{\rho S}{\rho_n} \frac{\partial T}{\partial x} + 3 \frac{\rho_s}{\rho} w \frac{\partial w}{\partial x}$$

$$+ v \frac{\partial w}{\partial x} + w \frac{\partial v}{\partial x} = 0$$

ENTROPY CONSERVATION:

$$\frac{\partial S}{\partial t} + \xi_T w \frac{\partial w}{\partial t} + \left(v + \frac{\rho_s}{\rho} w \right) \frac{\partial S}{\partial x} + \frac{\rho_s}{\rho} S \frac{\partial w}{\partial x}$$

$$- Sw \left(\xi_T \frac{\partial T}{\partial x} + \xi_p \frac{\partial p}{\partial x} \right) + \frac{\rho_s S}{\rho^2} w \frac{\partial \rho}{\partial x} = 0$$

of mass. The next two, the bulk velocity and relative velocity equations, are forms of two-fluid momentum conservation with the superfluid equation or continuity equation or both substrated out; the thermodynamic identity has also been employed to simplify the relative velocity equation. The final equation, which replaces energy conservation, is a statement of entropy conservation, which is valid since the flow is assumed reversible. All four equations are written in only one spatial dimension, but they are otherwise exact.

These equations are rewritten in Table 4.2 as expansions from the $w = 0$ state using thermodynamic relations for entropy and density in terms of w^2, which are derived in Appendix A. Only terms up to second-order in the perturbations are now included.

In principle, these four equations can be put in characteristic form to yield four coupled ordinary differential equations, occurring along four separate sets of characteristics. These characteristics represent first- and second-sound, each propagating in both directions as in the linear plane wave case presented in Appendix B. However, in the nonlinear case the algebra is so overwhelming -- a quartic equation would have to be solved -- that a simplified analytic approach is more valuable. Fortunately, the coefficient of thermal expansion of liquid helium II, β, is very small. Thus the temperature and pressure variations that actually occur in both first- and second-sound will uncouple in the limit of vanishing β and small w; the result is that second-sound will appear to cause perturbations in T and w, but not p or v, while the opposite will occur for first-sound.

For thermodynamics having no dependence on the relative velocity,

the differentials of density and entropy can always be written in terms of pressure and temperature:

$$d\rho = \frac{\gamma}{c^2} dp - \rho\beta\, dT \tag{4.3}$$

$$dS = \frac{C_p}{T} dT - \frac{\beta}{\rho} dp \tag{4.4}$$

where $\gamma \equiv C_p/C_v$

Note that as the coefficient of thermal expansion goes to zero, density becomes only a function of pressure and entropy only a function of temperature. This totally uncouples pressure and temperature perturbations occurring in linear waves (see Appendix B). Finite-amplitude waves, on the other hand, can still be coupled through the relative velocity dependence implicit in two-fluid thermodynamics. Thus second-sound waves produce p and v variations proportional to w^2 in addition to those proportional to βw. However with this understanding, if terms higher than second-order are neglected, then the continuity and bulk velocity equations conveniently uncouple from the relative velocity and entropy equations. The latter two, written presuming only second-sound waves are present, are:

$$\frac{\rho_n}{\rho} \frac{\partial w}{\partial t} + w\xi_T \frac{\partial T}{\partial t} + S \frac{\partial T}{\partial x} + 3 \frac{\rho_n \rho_s}{\rho^2} w \frac{\partial w}{\partial x} = 0 \tag{4.5}$$

$$\frac{C_p}{T} \frac{\partial T}{\partial t} + \xi_T w \frac{\partial w}{\partial T} + \left(\frac{\rho_s}{\rho} \frac{C_p}{T} - S\xi_T \right) w \frac{\partial T}{\partial x} + \frac{\rho_s}{\rho} S \frac{\partial w}{\partial x} \tag{4.6}$$

These two equations can be put in characteristic form by multiplying the first by an arbitrary constant, λ, and then adding it to the second

(it is convenient first to divide (4.5) by S and multiply (4.6) by T/C_p so that λ will be in units of velocity):

$$\left(\lambda \frac{\rho_n}{\rho S} + T\xi_T \frac{w}{C_p}\right)\frac{\partial w}{\partial t} + \left(3\lambda \frac{\rho_n \rho_s}{\rho^2}\frac{w}{S} + \frac{\rho_s}{\rho}\frac{TS}{C_p}\right)\frac{\partial w}{\partial x}$$

$$+ \left(\lambda \frac{w}{S}\xi_T + 1\right)\frac{\partial T}{\partial t} + \left(\lambda + \frac{\rho_s}{\rho} w - T\xi_T \frac{S}{C_p} w\right)\frac{\partial T}{\partial x} = 0 \qquad (4.7)$$

To be in characteristic form the derivatives of w and T must lie in the same direction in the x-t plane. That is, there must be a characteristic velocity, u, which is real and identical for variations of w and T:

$$u = \frac{\lambda + \frac{\rho_s}{\rho} w - T\xi_T \frac{S}{C_p} w}{\lambda \frac{w}{S}\xi_T + 1} = \frac{3\lambda \frac{\rho_n \rho_s}{\rho^2}\frac{w}{S} + \frac{\rho_s}{\rho}\frac{TS}{C_p}}{\lambda \frac{\rho_n}{\rho S} + T\xi_T \frac{w}{C_p}} \qquad (4.8)$$

Solving (4.8) for λ leads to a quadratic equation:

$$\left(\frac{\rho_n}{\rho S} - 3\frac{\rho_n \rho_s}{\rho^2}\frac{w^2}{S^2}\xi_T\right)\lambda^2 - \left(2\frac{\rho_n \rho_s}{\rho^2}\frac{w}{S}\right)\lambda - \frac{\rho_s}{\rho}\frac{TS}{C_p}$$

$$+ \left(\frac{\rho_s}{\rho} - T\xi_T \frac{S}{C_p}\right) T\xi_T \frac{w^2}{C_p} = 0 \qquad (4.9)$$

To be consistent with the procedure of neglecting terms higher than order w^2, it will only be necessary to find the characteristic velocities, and hence λ, to order w. The solution of (4.9) is therefore:

$$\lambda_{\pm} = \pm a + \frac{\rho_s}{\rho} w + O(w^2) \qquad (4.10)$$

where $a^2 = \frac{\rho_s}{\rho_n}\frac{S^2 T}{C_p}$

Substituting this into the equation for u we have:

$$u_{\pm} = \pm a + \left[2 \frac{\rho_s}{\rho} - \left(\frac{\rho}{\rho_n} T\xi_T \right) \frac{S}{C_p} \right] w + O(w^2) \qquad (4.11)$$

This equation contains the sought-after coefficient for the convection of second-sound by $\vec{w}$ -- $f(\vec{w})$ in equation (4.2). To lowest order, $f(\vec{w})$ is independent of w:

$$f = 2 \frac{\rho_s}{\rho} - \left(\frac{\rho}{\rho_n} T\xi_T \right) \frac{S}{C_p} \qquad (4.12)$$

It is interesting to note that in the temperature range where the roton population dominates the thermodynamics -- above $1.2^{o}K$ -- the groups $\frac{\rho}{\rho_n} T\xi_T$ and C_p/S are both almost independent of temperature and numerically equal. Thus the convection coefficient is very nearly:

$$f \simeq \frac{\rho_s - \rho_n}{\rho} \quad \text{for } T > 1.2^{o}K$$

This is the result obtained by Temperley (1951) in his analysis of finite-amplitude second-sound which parallels the present theory. However, Temperley based his analysis on a set of two-fluid equations which differ slightly from the set derived by Landau. Interestingly enough, it is apparently not the difference in equations which results in the discrepancy, but the thermodynamic "Tisza approximation" used by Temperley, namely:

$$S = \frac{\rho_n}{\rho} S_n$$

where S_n is assumed constant. Invoking this assumption implies that:

$$\frac{C_p}{S} = \frac{\rho}{\rho_n} \xi_T T$$

which is all that is required to recover Temperley's result.

At the pressure and temperature where ρ_n equals ρ_s -- T = 1.97°K for p = SVP -- second-sound is not convected by the relative velocity. At lower temperatures convection occurs in the direction of w, while at higher temperatures it is oppositely directed. This temperature dependent convection coefficient has profound effects on the behavior of nonlinear second-sound as will be shown in succeeding sections.

The convection coefficient derived in the present analysis (equation 4.12) was obtained originally by Khalatnikov (1956), who solved the full set of linear equations for first- and second-sound propagating in a moving medium. Experimental verification of his result has been obtained over the temperature range from 1.3°K to 1.95°K by measuring the time of flight of a second-sound pulse propagating through a steady-state counterflow (Johnson and Hildebrandt, 1969). Earlier experiments by Dessler and Fairbank (1956), using second-sound shock waves, confirmed Khalatnikov's form of the convection coefficient for temperatures as low as 1.0°K.

The results obtained so far can be used to rewrite the equations for w and T in a more transparent form:

$$\left[\frac{\partial w}{\partial t} + u_{\pm} \frac{\partial w}{\partial x}\right] \pm \left(\frac{\rho S}{\rho_n a}\right) \left[\frac{\partial T}{\partial t} + u_{\pm} \frac{\partial T}{\partial x}\right] = 0 \qquad (4.13)$$

It is useful to introduce two new functions of w and T, known as Riemann invariants:

$$R_+ = w + \int \frac{\rho S}{\rho_n a}\, dT \tag{4.14}$$

$$R_- = w - \int \frac{\rho S}{\rho_n a}\, dT \tag{4.15}$$

The equation set (4.13) can now be written in terms of R_+ and R_-:

$$\left[\frac{\partial}{\partial t} + (v + fw + a)\frac{\partial}{\partial x}\right] R_+ = 0 \tag{4.16}$$

$$\left[\frac{\partial}{\partial t} + (v + fw - a)\frac{\partial}{\partial x}\right] R_- = 0 \tag{4.17}$$

The name Riemann invariant stems from the fact that these quantities are constant along associated characteristic curves in the x-t plane, C_+ and C_-:

$$C_+: \quad \frac{dx}{dt} = u_+ = v + fw + a \tag{4.18}$$

$$C_-: \quad \frac{dx}{dt} = u_- = v + fw - a \tag{4.19}$$

The preceding nonlinear theory of second-sound bears more than a superficial resemblance to the Riemann theory of ordinary sound. It should therefore be no surprise that the behavior of nonlinear second-sound includes nonsteady wave profiles, shock and expansion waves -- all typical of nonlinear, nondispersive wave motion in general. It should be remembered, however, that this theory of second-sound is only approximate, although it usually is a very good approximation.

SIMPLE WAVES

Even though the Riemann invariants are constant along their respective characteristics, they are not necessarily constant from characteristic to characteristic. If a particular Riemann invariant is constant throughout a region in the x-t plane then there are no waves propagating along the associated set of characteristics in that region. When all the Riemann invariants, except one, are constant everywhere -- recall there must also be two additional sets of characteristics and Riemann invariants for first sound -- wave propagation will be in the form of a "simple wave" along a single set of characteristics.

In this section we will consider a simple second-sound wave travelling along the positive x-axis. Since no first-sound is present p, v, and ρ will be uniform; also v will be taken equal to zero. By definition, the Riemann invariant, R_-, is constant everywhere, which immediately yields a relation for w in terms of T:

$$w = \int_{T_0}^{T} \frac{\rho S}{\rho_n a} \, dT \tag{4.20}$$

where $T = T_0$ has been taken as the rest state $w = 0$. When comparing this result to the case of linear second-sound --

$$w = \left(\frac{\rho S}{\rho_n a} \right)_0 (T - T_0)$$

it is obvious that the amplitudes predicted by second-order theory differ only slightly from linear theory as long as $T - T_0$ is small, which is usually the case. Large corrections are encountered only

near the λ-line where the speed of second-sound is a strong function of temperature.

The one-to-one correspondence between w and T shows that only one independent variable is required to specify fully the conditions produced by a simple wave. For example, the Riemann invariant R_+ can be written as:

$$R_+ \equiv w + \int \frac{\rho S}{\rho_n a}\, dT$$

$$= 2w = 2 \int_{T_0}^{T} \frac{\rho S}{\rho_n a}\, dT \qquad (4.21)$$

Plugging R_+ into equation (4.16) results in an equation for either w or T, the latter one being:

$$\frac{\partial T}{\partial t} + (fw + a)\frac{\partial T}{\partial x} = 0 \qquad (4.22)$$

where the characteristic velocity, $u = fw + a$, is a function only of temperature. Also note that temperature is constant along a C_+ characteristic. These two facts imply that the characteristic velocity is constant on a C_+ characteristic, or in other words, all C_+ characteristics trace out straight lines in the x-t plane.

It will be useful to calculate the characteristic velocity in terms of the fluid temperature. To do this, u will be calculated as an expansion in temperature from the rest state:

$$u = u_0 + \left(\frac{\partial u}{\partial w}\right)_0 w + \left(\frac{\partial u}{\partial T}\right)_0 (T-T_0) + \ldots$$

where $\left(\frac{\partial u}{\partial w}\right)_0 = f = 2\frac{\rho_s}{\rho} - \left(\frac{\rho}{\rho_n}\xi_T T\right)\frac{S}{C_p}$

$$\left(\frac{\partial u}{\partial T}\right)_0 = \frac{\partial a}{\partial T}$$

$$dw = \frac{\rho S}{\rho_n a}\, dT$$

The characteristic velocity to first order in the temperature perturbation can be written as:

$$u = a_0(1 + b_0\theta) \tag{4.23}$$

where $\theta \equiv (T - T_0)/T_0$

$$b = \frac{T}{a}\left(\frac{\rho S}{\rho_n a} f + \frac{\partial a}{\partial T}\right)$$

The thermodynamic function b(p,T), which will be called the steepening coefficient, can be algebraically reduced to the following form:

$$b(p,T) = T\frac{\partial}{\partial T}\left[\log\left(a^3\frac{C_p}{T}\right)\right] \tag{4.24}$$

Finally with these results, the temperature perturbation in a simple second-sound wave can be written as:

$$\frac{\partial\theta}{\partial t} + a_0(1 + b_0\theta)\frac{\partial\theta}{\partial x} = 0 \tag{4.25}$$

where it is understood that the temperature perturbation is always measured from the rest state w = 0--otherwise u_0 would not be simply a_0.

The application of (4.25) illustrates how second-sound waves evolve

as they propagate. When b_0 is positive-definite, a temperature raising wavefront -- that is $\partial\theta/\partial X > 0$ -- will steepen as it propagates because the characteristic velocity increases with θ. Similarily a temperature lowering part of the profile will unsteepen or expand.

The evolution of a positive temperature pulse -- drawn initially trapezoidal in shape for convenience -- is shown in the x-t diagram of Figure 4.1. The solid straight lines are C_+ characteristics (C_- characteristics are suppressed since they contain no information) and the dashed lines are temperature (or w) profiles at several instants in time. The front of the pulse can be seen to steepen until it is vertical, at which point the characteristics would begin to cross and produce a physically unreal, multivalued temperature profile. To eliminate this problem a shock discontinuity must be fitted in; its trajectory is shown by the heavy line. While the shock is forming at the front, the back of the pulse is expanding. Note that the leading edge of this expansion fan is propagating faster than the shock, so that the two will eventually coincide. The speed of the shock is for the moment unknown, except that it obviously is greater than the characteristic speed in the undisturbed region, a_0; that is, the Mach number, M_S, is greater than unity:

$$M_S \equiv \frac{U_S}{a_0} \tag{4.26}$$

where U_S = shock velocity.

Figure 4.1, recall, is for a positive steepening coefficient, but this function can also be negative depending on the initial temperature and pressure (see Figure 4.2). When b(p,T) is negative, a positive

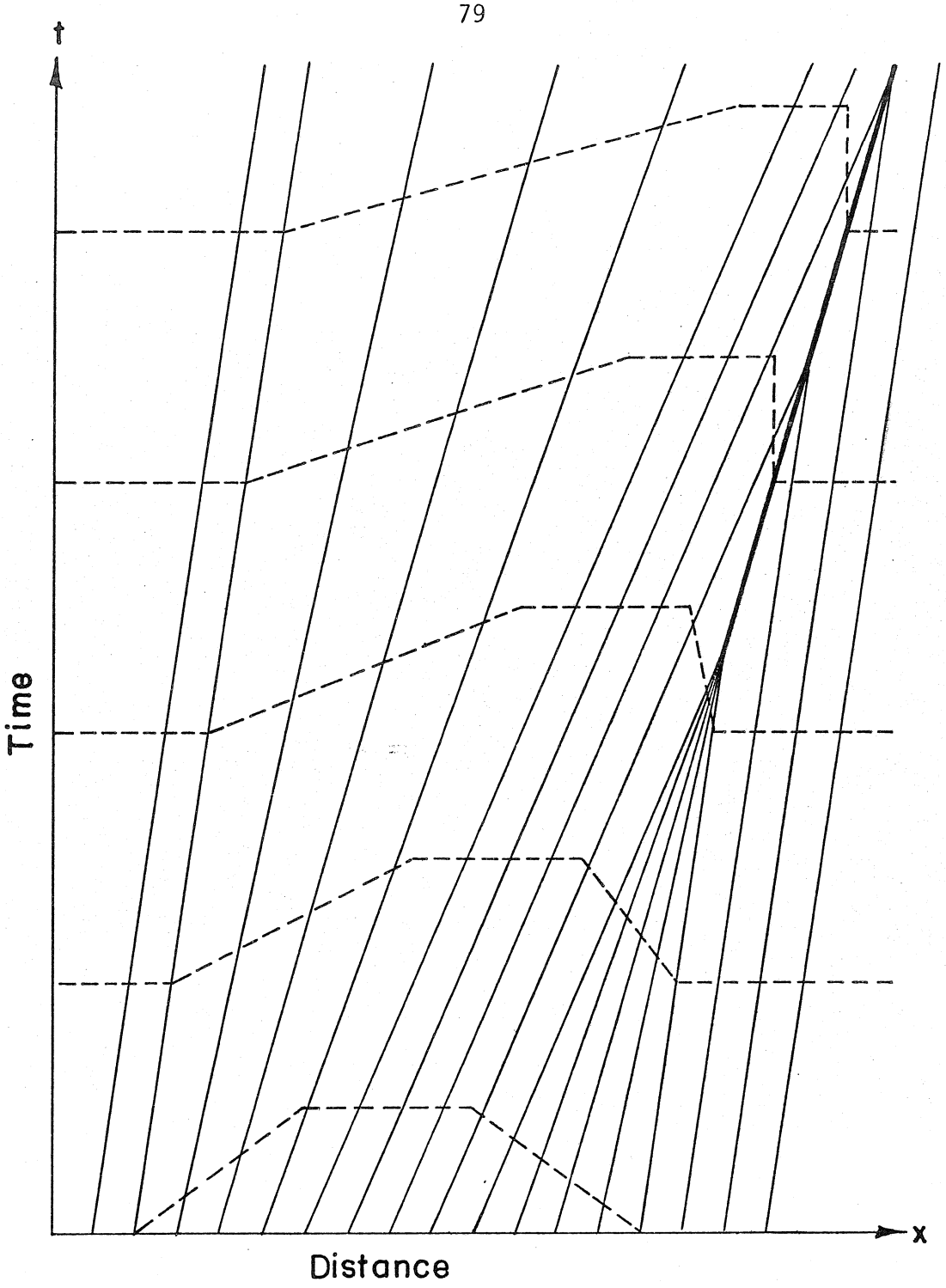

Figure 4.1 x-t DIAGRAM OF A FRONT STEEPENED SHOCK PULSE

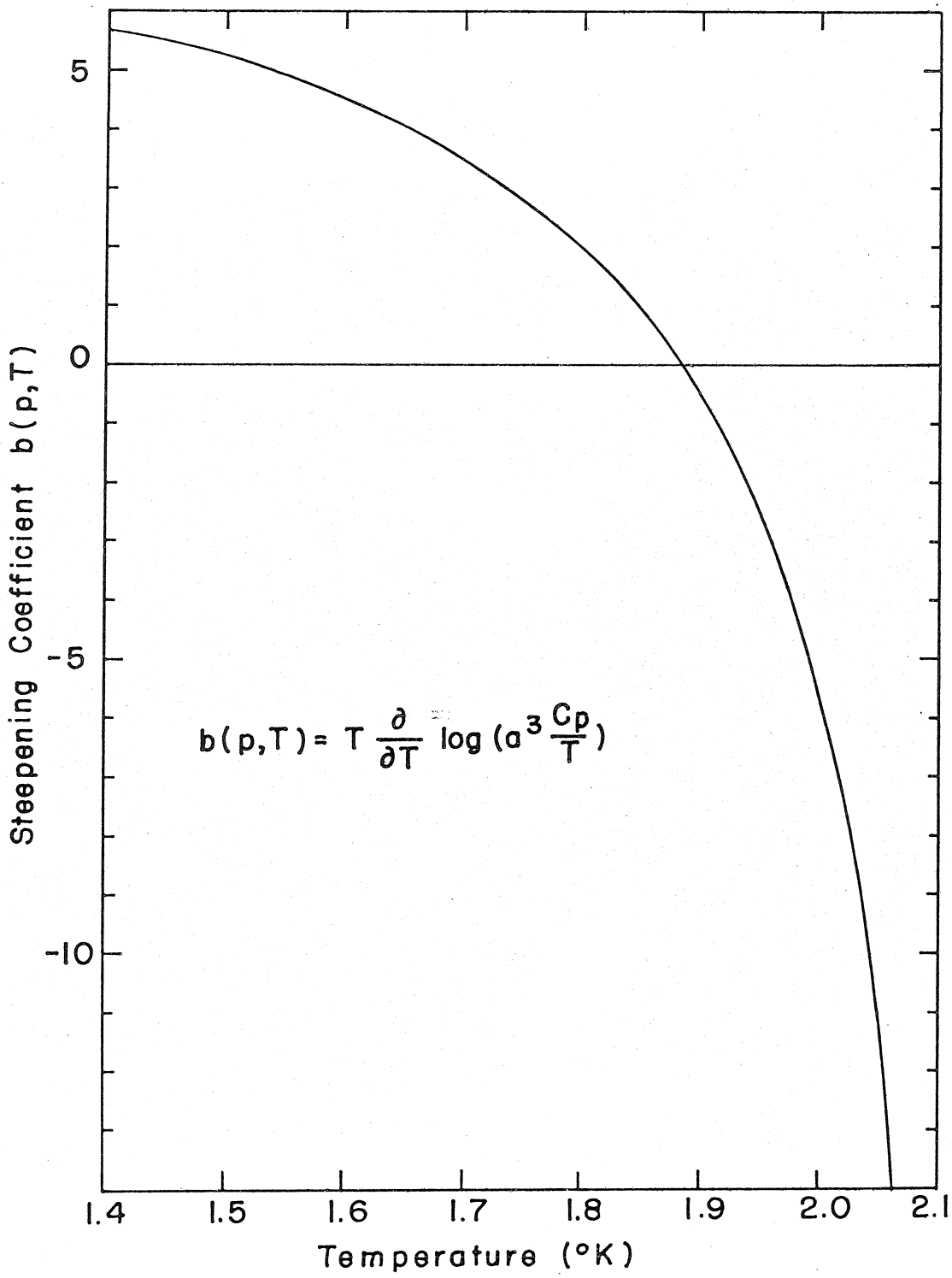

Figure 4.2 STEEPENING COEFFICIENT AT THE SATURATED VAPOR PRESSURE

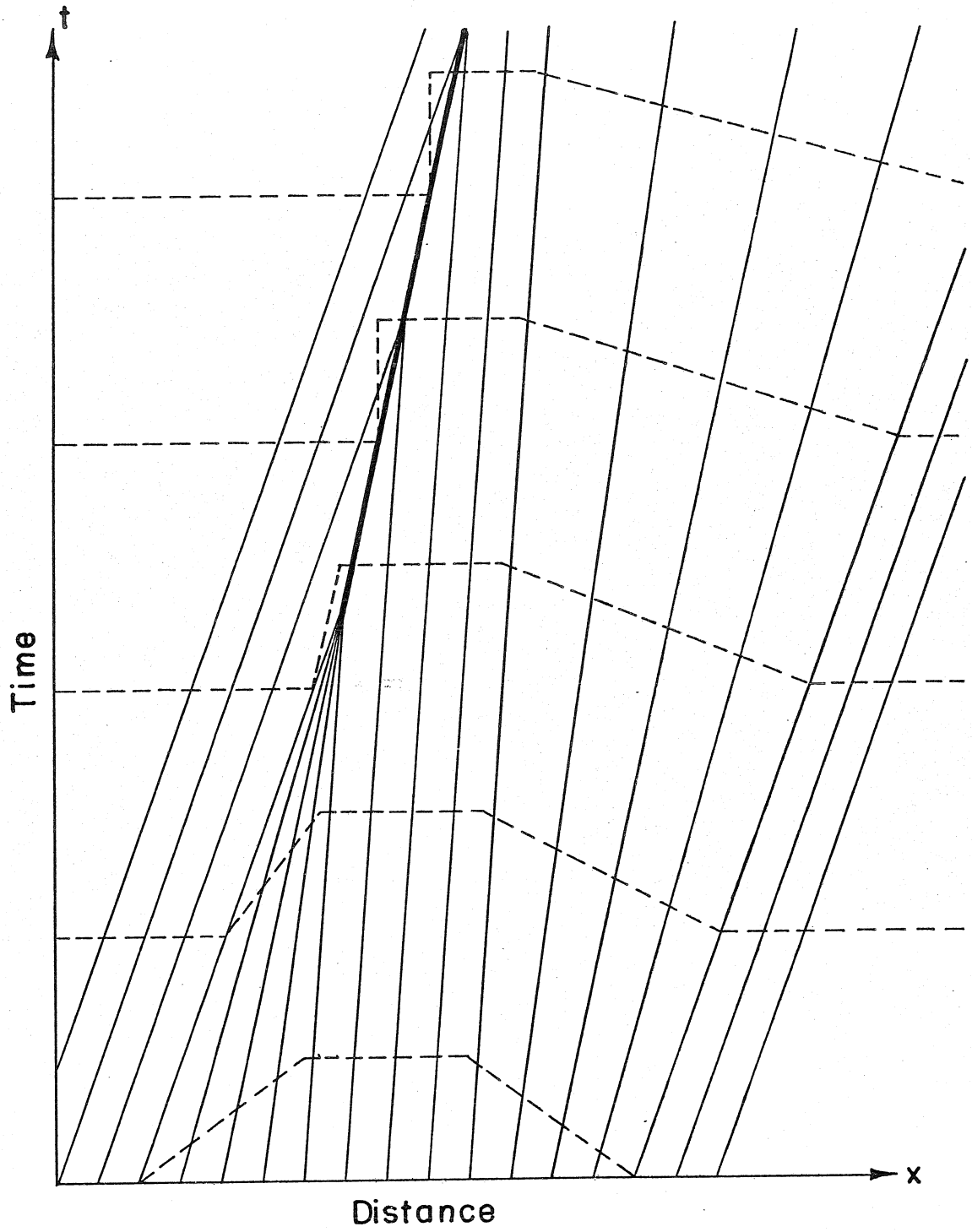

Figure 4.3 x-t DIAGRAM OF A BACK STEEPENED SHOCK PULSE

temperature pulse evolves in the reverse direction: the front expands and the back steepens into a temperature lowering shock having a Mach number less than one (see Figure 4.3). This peculiar behavior is not really extraordinary because a negative pressure pulse in an ordinary substance will also evolve a back steepened shock with $M < 1$. In helium II, however, both temperature raising and temperature lowering shocks are possible depending on the sign of $b(p,T)$, while in ordinary substances only pressure raising or compressional shocks are permissible. (Rarefaction pressure shocks can occur in exceptional substances -- fluids near their critical point and solids undergoing shock-induced phase transitions.)

An interesting property of simple waves is that the area under the wave profile is conserved even as the wave evolves. To see why this happens, consider a wave profile having a single positive hump of finite extent. Now define a length, $X(T)$, which for some fixed time is the distance between front and back edge points of the profile having temperature, T (see Figure 4.4).

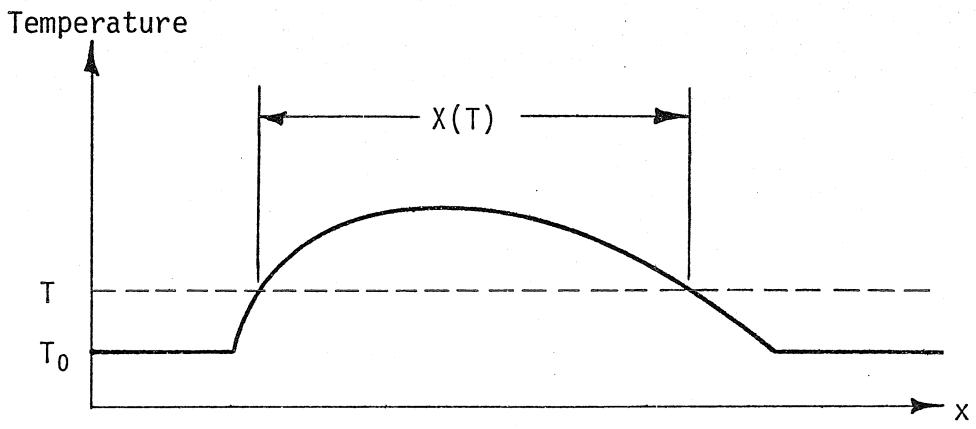

Figure 4.4 DEFINITION OF X(T)

THE SHOCK DISCONTINUITY

In the preceding two sections, one-dimensional nonlinear waves, treated as thermodynamically reversible, were examined and found to display nonsteady evolution which naturally developed discontinuities between equilibrium states. As a second-sound wavefront gradually steepens, the gradients in temperature and velocity will begin to generate appreciable entropy at the expense of some of the mechanical energy in the wave. The ever increasing dissipation in the steepening wavefront tends to smooth out the large gradients and slow the steepening process. Eventually, equilibrium between nonlinear steepening and irreversible dissipation will be attained yielding a steady profile: typically two equilibrium states, where the gradients vanish, connected by a sharp transition known as the shock front or shock layer.

The most useful property of shock waves is that the jump conditions connecting the two equilibrium states can be determined without reference to the exact nature of the transition layer, as long as it is steady. This property is significantly advantageous, because within the shock layer non-equilibrium thermodynamics are the rule rather than the exception, making shock structure very difficult to calculate in general. The conservation laws for mass, momentum, and energy always hold; therefore, they must still apply across a shock layer of unknown description. These relations, which are the only ones required to specify the jump conditions for a plane shock front in an ordinary substance, must be supplemented by the superfluid equation in liquid helium II, because the extra velocity field requires an additional connecting relation.

The temperature-area under this profile is just the following integral of X(T):

$$\int_{T_0}^{\infty} X(T)\, dT$$

As has been shown, the characteristic velocity of a particular point on a simple wave profile depends only on a single variable (T, w, or S) and not on the local shape of the profile (slope, curvature, etc). As long as this is true, X(T) will be a function only of T, unaltered by time as the wave propagates and evolves. The integral of X(T) must therefore be constant. Obviously, the concept of temperature-area invariance can easily be extended to an arbitrary wave profile having both positive and negative temperature excursions.

Since the temperature in a simple wave can be written as a function of w or S, similar velocity-areas and entropy-areas can be calculated and found to be invariant. Multiplying the latter by the area of the plane wave and the fluid density, which is constant to this approximation, yields the total excess entropy in the wave. Thus the total entropy carried by a simple wave must be conserved; this is no surprise since thermodynamic reversibility was one of the prerequisite assumptions used to derive the second-order theory.

The validity of entropy conservation only becomes a concern when the temperature and velocity gradients become very large, as in a shock discontinuity. In such a region the velocity of a point on the wave profile will depend not only on the local temperature, but also on its gradient. As a consequence of this, the lengths X(T) which intersect

a shock will not be constant in time or space, and therefore the temperature-area will not necessarily be invariant. Fortunately, the principle of profile-area invariance can be rescued after discovering the properties of the shock discontinuity in the next section.

Table 4.3 RESULTS OF SECOND-ORDER SHOCK THEORY (SECOND-SOUND)

SHOCK MACH NUMBER:

$$M_S = 1 + \tfrac{1}{2} b_0 \Delta\theta$$

RELATIVE VELOCITY JUMP:

$$\Delta w = a_0 \left(\frac{\rho}{\rho_s} \frac{C_p}{S} \right)_0 \Delta\theta \left\{ 1 + \tfrac{1}{2} \left[T \frac{\partial}{\partial T} \left(\log a \, \frac{C_p}{T} \frac{\rho^2}{\rho_s^2} \right) \right]_0 \Delta\theta \right\}$$

SHOCK STRUCTURE:

$$T(x) = T_0 + \tfrac{1}{2}(T_1 - T_0) \left(1 + \tanh \frac{2x}{\delta} \right)$$

SHOCK THICKNESS:

$$\delta = \left(\frac{4D}{a} \right)_0 \frac{1}{b_0 \Delta\theta} = \left(\frac{2D}{a} \right)_0 \frac{1}{M_S - 1}$$

IRREVERSIBLE ENTROPY JUMP:

$$(\Delta S)_{\text{irreversible}} = \frac{1}{6} \left| b(\Delta\theta)^3 \right| C_p$$

If the shock wave is viewed in the frame of reference travelling with the shock, these relations will be time-independent or steady. They may then be spatially integrated perpendicular to the shock front and evaluated in the equilibrium regions fore and aft of the shock front. The result is a set of algebraic "shock equations" solvable for the jump conditions and shock velocity. This prescription, originally carried out by Khalatnikov (1952b), is detailed in Appendix C which also contains new results including the theoretical structure of a weak second-sound shock front.

Table 4.3 summarizes the results of "second-order shock theory" discussed in the aforementioned appendix. This theory of second-sound shocks represents the same approximation to the two-fluid model as second-order theory of the preceding sections does for nonsteady, reversible second-sound waves. The distinction between the two variations is a consequence of the irreversibility of a shock front. The dissipation that must occur to make the front steady invalidates the concept of entropy conservation, which was a basic assumption in the theory as applied to nonsteady waves. Instead of using an entropy equation which allows for production, the equation for energy conservation is more conveniently employed in the shock theory.

The velocity of the shock front, U_S, can be written in terms of the characteristic velocities ahead and behind the shock. Using the definition of the shock Mach number and its relation to the shock strength, together with the equation for the characteristic velocities in a simple wave (equation 4.23), the following ensues:

$$U_S = \tfrac{1}{2}(u_0 + u_1) \tag{4.27}$$

The shock velocity is therefore the average of the characteristic velocities fore and aft -- a result in common with all weak shock waves.

It happens that this is exactly the condition required to maintain the principle of profile-area invariance in the presence of shock fronts (see Whitham, 1974, pg. 42). This principle is graphically illustrated by four temperature-time profiles of an initially rectangular heat pulse which were measured at various distances from the heater (Figure 4.5). As the shock pulse propagates down the shock tube, the shape of the wave profile changes dramatically, but its total area remains unaltered.

With this invariance principle intact, one is forced to conclude that, according to second-order theory, the entropy carried by a second-sound shock wave is conserved! Obviously, since entropy is always produced in the shock front, this last statement is not exactly correct and its validity relies on the fact that for weak shock waves, the entropy generated is proportional to the cube of the shock strength -- a quantity neglected by the present theory.

The actual entropy jump of a fluid particle processed by a second-sound shock wave is proportional to the temperature jump and may therefore be positive or negative depending on the type of shock wave. This happens because entropy can be transported reversibly in helium II. The entropy irreversibly generated within the shock front is consistently positive and must be proportional to $(\Delta\theta)^3$ as long as the shock wave is weak.

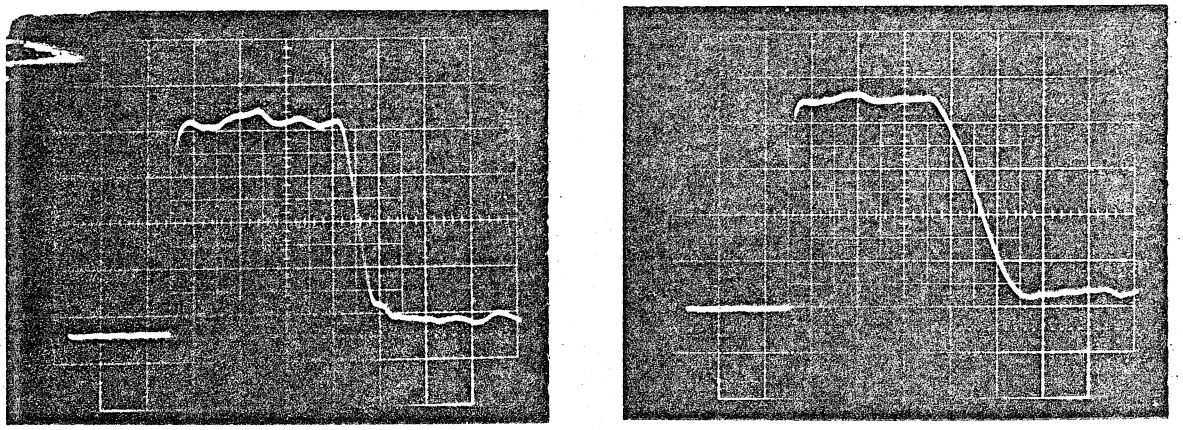

(a) L = 6.8 cm

(b) L = 16.3 cm

50 μ sec / division

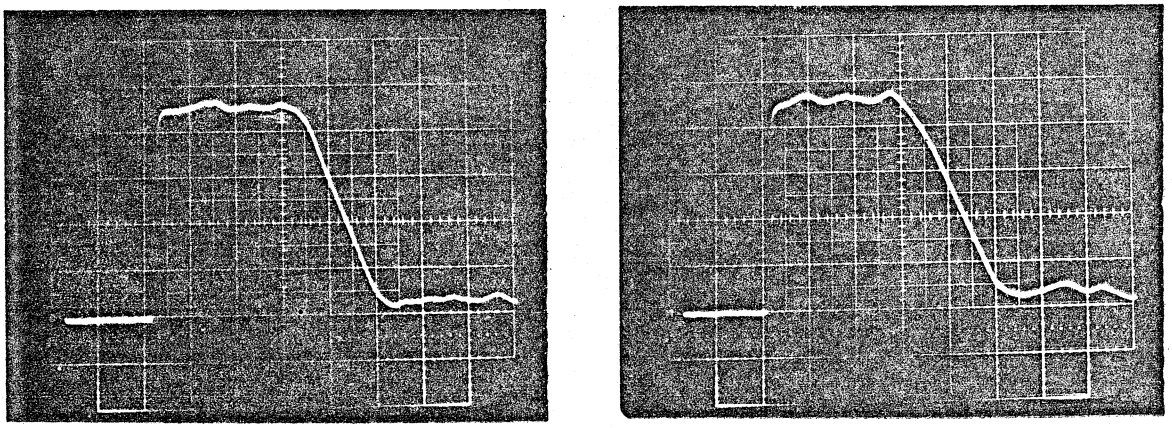

(c) L = 17.4 cm

(d) L = 20.6 cm

Figure 4.5 EVOLUTION OF AN INITIALLY RECTANGULAR SHOCK PULSE (M_s = 1.0059)

SHOCK STRUCTURE

The structure of a steady shock front, maintained by a balance of nonlinear steepening with dissipative smoothing, can be ascertained by solving the shock equations including the irreversible terms. The solution of these equations to second-order is a hyperbolic tangent profile, typical of weak shock fronts in general:

$$T(x) = T_0 + \tfrac{1}{2}(T_1 - T_0)\left(1 + \tanh 2x/\delta\right) \tag{4.28}$$

The shock layer is scaled by a thickness, δ, defined by the maximum slope of profile; its theoretical value is:

$$\delta = \left(\frac{4D}{a}\right)\frac{1}{b\Delta\theta} = \left(\frac{2D}{a}\right)\frac{1}{M_S - 1} \tag{4.29}$$

where b is the steepening coefficient and D is the damping factor of second-sound. This latter coefficient is proportional to the attenuation of second-sound per frequency squared and is defined in Appendix C where calculations leading to the above results are presented in detail.

Figure 4.6 displays some experimental results obtained with very weak second-sound shocks at 1.45^{o}K. The oscillograph shows a shock profile as detected with an endwall sensor positioned 8.89 cm away from the heater. The thickness of this weak shock ($M_S = 1.00125$) was measured to be 37 μm.

According to equation (4.29), the shock thickness is inversely proportional to the shock strength, $\Delta\theta$, or $M_S - 1$, which is a result generally true for weak shocks in any substance. Experimental values of δ and $(M_S - 1)^{-1}$, plotted in Figure 4.6, verify this relation and

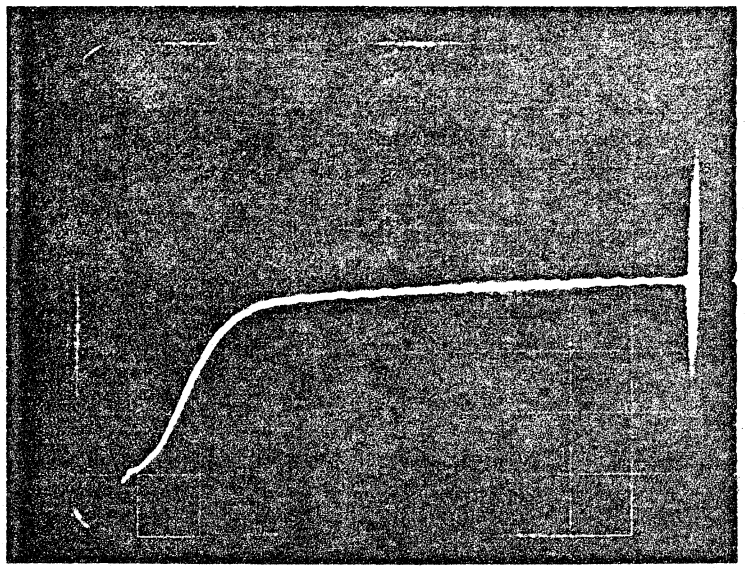

(a) L = 8.89 cm

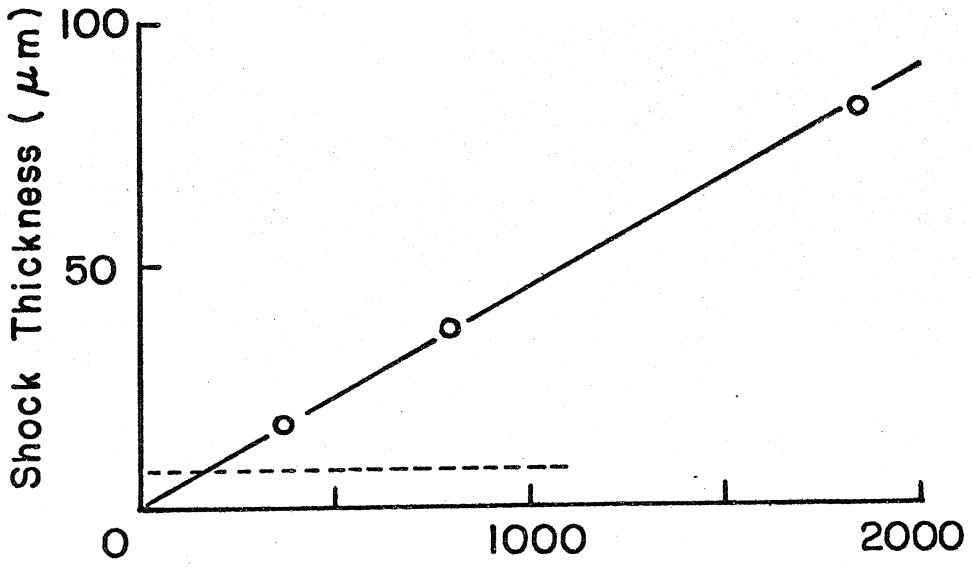

(b) $(M_s-1)^{-1}$

Figure 4.6 SECOND SOUND SHOCK STRUCTURE
(T = 1.45° K)

yield an experimental damping factor of 4.5×10^{-3} cm^2/sec. This is about thirty-five percent smaller than the value of D obtained by measuring the attenuation of second-sound directly (Hanson and Pellam, 1954). Although in this particular instance the shock data have a relative accuracy of no more than ±15%, this is not a fundamental limit of the method. Ultimately, the attenuation coefficient can be measured much more easily and accurately with shock fronts compared to more conventional methods.

The dotted line on the graph (Figure 4.6b) at $\delta = 8$ μm represents an experimentally determined limit obtained with stronger shock waves. Shock thicknesses smaller than 8 μm were not observed. There are two possible explanations of this result. First, since geometric constraints ultimately determine the sensor response, an equivalent sensor depth of 8 μm, instead of the estimated 5 μm, would produce the observed artifact. However, it is possible that the result is genuine. Recall that at this low temperature, the excitations are so scarce that the phonon mean free path is about 10 μm (Table 2.1). Since dispersion of second-sound should begin when the wavelength is on the order of the phonon mean free path (Khalatnikov and Chernikova, 1966a and 1966b), a limit to the shock thickness of this order should be expected. It appears that low temperature second-sound provides a unique opportunity to observe non-equilibrium kinetics with relatively weak shock waves.

None of the second-sound shock fronts observed in the present study have displayed any peculiarity in the profile attributable to relaxation effects. Thus it can be concluded that relaxation effects

longer than one microsecond are not significant, if present at all.

When the shock thickness, normalized by the relative velocity jump, is plotted against temperature a very interesting result is obtained (this normalization is a natural choice since a shock is generated by controlling the heat flux or equivalently Δw). At $T = 1.88^{o}K$, where the steepening coefficient goes to zero, the relative thickness diverges (Figure 4.7). The meaning of this divergence is simple: when $b = 0$, any wave front no matter how weak will be nonsteady until it has unsteepened to the point where the gradients vanish. Thus at $T = 1.88^{o}K$, an infinitesimally weak shock front will have an infinite thickness. Finite-amplitude shock waves which span this divergence display more extraordinary behavior to be examined in the next section.

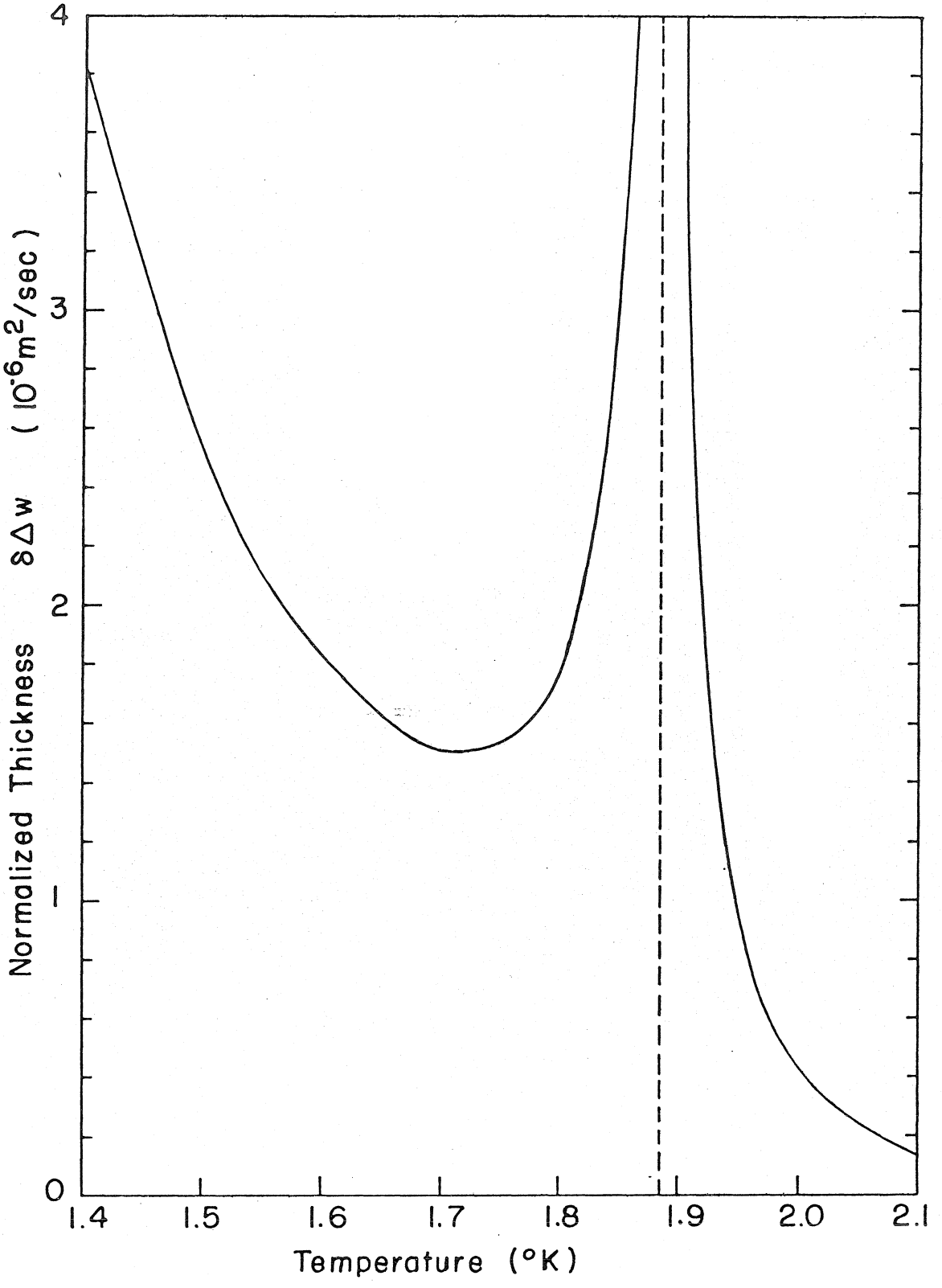

Figure 4.7 THEORETICAL THICKNESS OF A WEAK SECOND SOUND SHOCK WAVE (P_0= SVP)

DOUBLE-SHOCKS

Denote the temperature where the steepening coefficient passes through zero as T_b. Near this point b(p,T) can be approximated by a linear function:

$$b(p,T) = -B(T - T_b)/T_b \tag{4.30}$$

where the slope, B, is a nondimensional function only of pressure. If this expansion is substituted into the equation for the characteristic velocity of a simple wave:

$$\frac{u}{a} = 1 + b\theta \tag{4.31}$$

then in the region near $T = T_b$, the characteristic velocity is a quadratic function of T:

$$\frac{u}{a_0} = 1 - B\left(\frac{T - T_b}{T_b}\right)\left(\frac{T - T_0}{T_0}\right) \tag{4.32}$$

This function is illustrated by Figure 4.8 for a positive temperature pulse spanning the shock thickness divergence at $T = T_b$.

For temperatures where $(\partial u/\partial T) > 0$ the front edge will steepen to form a temperature raising shock. For slightly larger temperatures the wave front would tend to unsteepen except that the characteristic velocity is still larger than the shock velocity, U_S. When the temperature has increased to the point where $u < U_S$ the expansion wave will begin. The result is a shock front and an expansion fan both originating from the leading edge of the heat pulse! The trailing edge of the heat pulse similarly evolves a temperature lowering

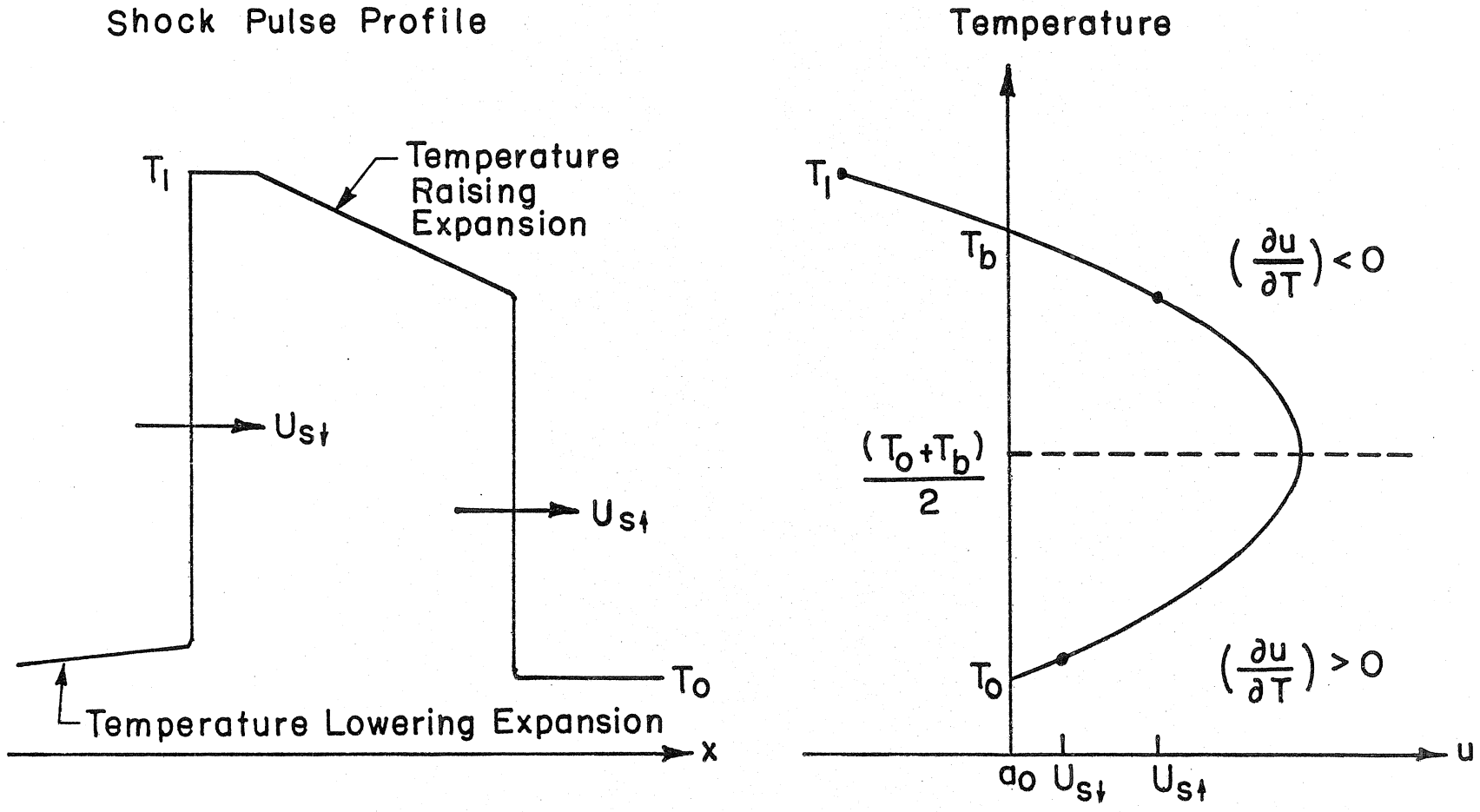

Figure 4.8 DOUBLE-SHOCK

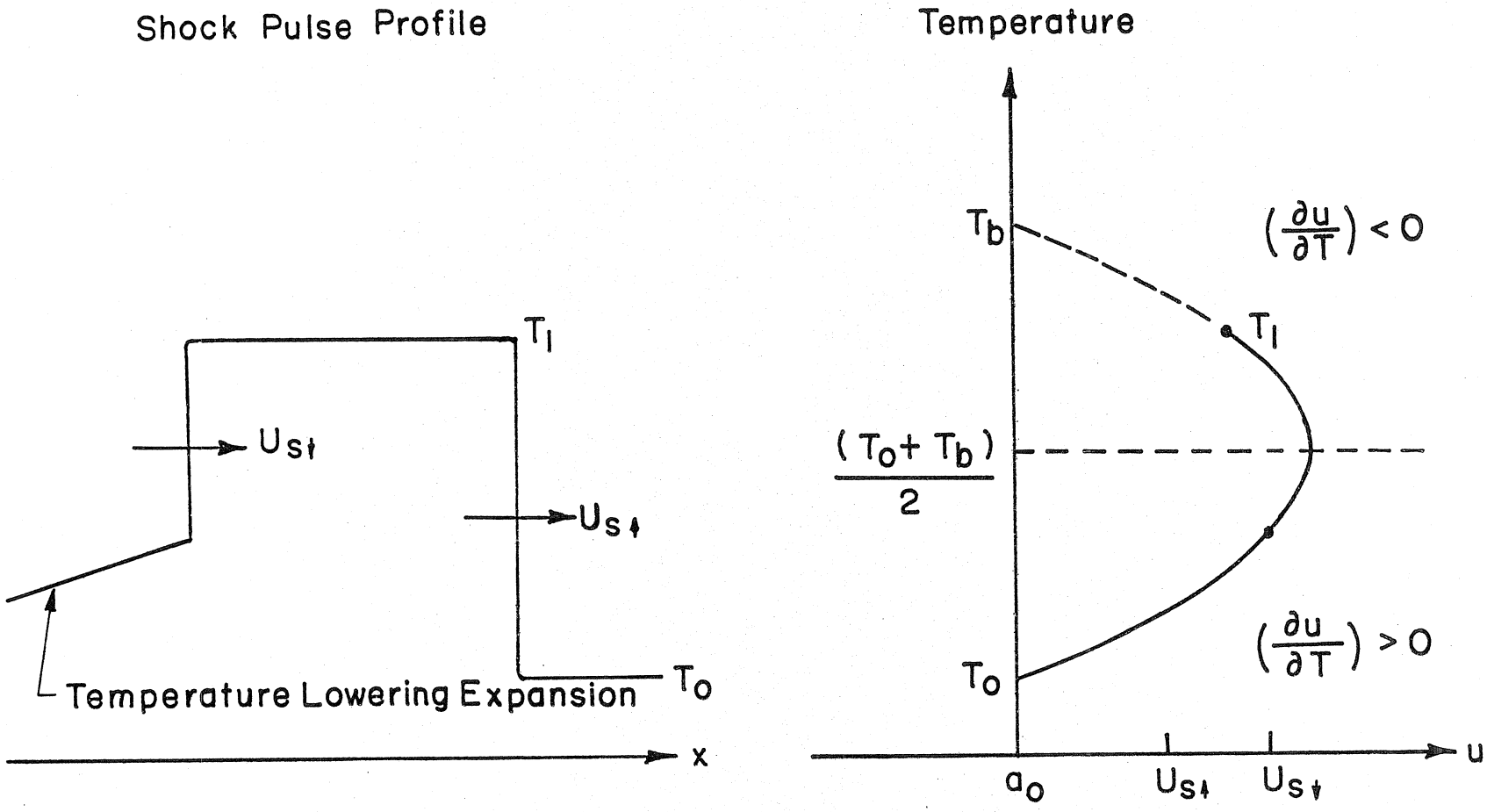

Figure 4.9 DOUBLE-SHOCK

shock followed by another expansion fan.

This double-shock configuration -- one temperature lowering and the other temperature raising -- is an unusual phenomenon only occurring in helium II when the steepening coefficient changes sign. Interestingly, double-shock configurations are not limited to second-sound shock waves, but they also occur with ordinary pressure shock waves in solids. Ultra strong shocks, having pressure jumps in the hundreds of kilobars, can compress metals sufficient to cause a polymorphic transition from one solid phase to another. When this occurs the initial shock front will split at the phase transition pressure into two shock compressions. Shock splitting, first observed in iron (Bancroft, Peterson, and Minshall, 1956), occurs in many metals and dielectric crystals. It has also been discovered that rarefactions spanning the polymorphic transition pressure will steepen into pressure lowering shock waves and form double-shock configurations, similar in appearance to those that occur with second-sound (Ivanov, Novikov, and Tarasov, 1962).

Anomalous shock behavior can also occur in a real gas near its critical point. In this region isentropes plotted in the p-V plane possess an inflection point where $(\partial^2 p/\partial V^2)_S$ changes sign. For pressure shock waves this quantity is completely analogous to the steepening coefficient of second-sound. Thus, complex configurations, containing both compression and rarefaction shock waves, are found when $(\partial^2 p/\partial V^2)_S$ changes sign (see Zel'dovich and Raizer, 1966, p. 67).

Double-shocks in liquid helium can occur near the shock thickness

divergence even if the divergence itself is not spanned. Figure 4.9 illustrates the type of double-shock which occurs when

$$0 < T_1 - \tfrac{1}{2}(T_0 + T_b) < \frac{\sqrt{2}}{4}\ (T_b - T_0)$$

In this case there is no expansion wave between the temperature raising and temperature lowering shocks. Instead the back steepened shock propagates faster than the one at the front and will eventually overtake it.

The evolution and decay of the double-shock structure is unique and quite interesting. For example, suppose a large amplitude shock pulse is generated which crosses the shock thickness divergence; this initially evolves into a double-shock having an expansion wave between the temperature raising and temperature lowering shocks. Relative to the front shock, the expansion wave will propagate towards the back shock, eventually overtake it, and in the process cause its decay. The back shock, which was initially propagating slower than the front shock causing the double-shock to spread, will actually increase in velocity as it decays. By the time the amplitude of the double-shock has decayed to the point where the in between expansion wave disappears, the back shock will be travelling faster than the front shock. The double-shock will now decay by decreasing in width, instead of amplitude, until it disappears altogether. The remnant is a simple shock-expansion pulse which then decays naturally.

The various versions of double-shocks in helium II are usually very difficult to observe experimentally because the Mach numbers of these shocks are very small, making the formation time very large.

However, double-shocks have been consistently observed when the heater power is sufficient to cause a breakdown in superfluidity. When the initial temperature, T_0, is slightly less than T_b, the shock which emerges from the breakdown region always displays a double-shock profile. The implications of this will be explored in Chapter 6.

GENERATION OF SECOND-SOUND

Second-sound waves in helium II are obviously generated by dumping in heat which turns on the counterflow mechanism and effects the reversible transport of heat away from the source. How counterflow is turned on at the interface between the liquid and heat source is not so obvious.

The boundary condition at a heater wall, that $\vec{v}$ and therefore $\vec{v}_n$ are zero (see Chapter 2), implies that heat transfer by counterflow must cease at the wall. Thus, there must be a thermal boundary layer in which heat transfer by pure counterflow far from the wall is smoothly converted into irreversible thermal conduction at the wall. Within this layer incoming superfluid is gradually converted into outgoing normal fluid. If the layer does not exist, conversion would have to occur infinitely fast at the liquid-wall interface, which would require an infinite chemical potential gradient to instantaneously stop the superfluid and start the normal fluid -- a process lacking physical reality.

In Appendix E, the boundary layer is calculated assuming equilibrium thermodynamics. This results in an exponential layer of thickness λ which is illustrated by Figure 4.10. The temperature amplitude of the thermal boundary layer is relatively large: approximately half the temperature jump in the generated shock wave. This means it plays a significant role in the generation of second-sound shock waves strong enough to break down superfluidity in a region near the heater.

Unfortunately the theoretical conclusions reached in Appendix E,

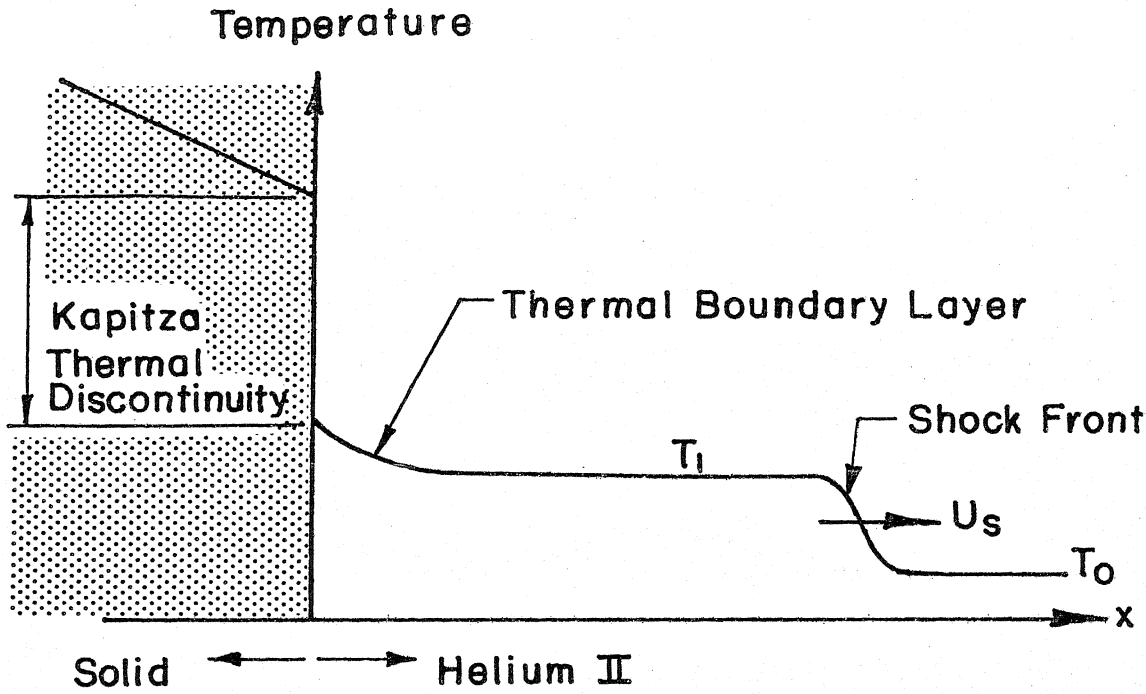

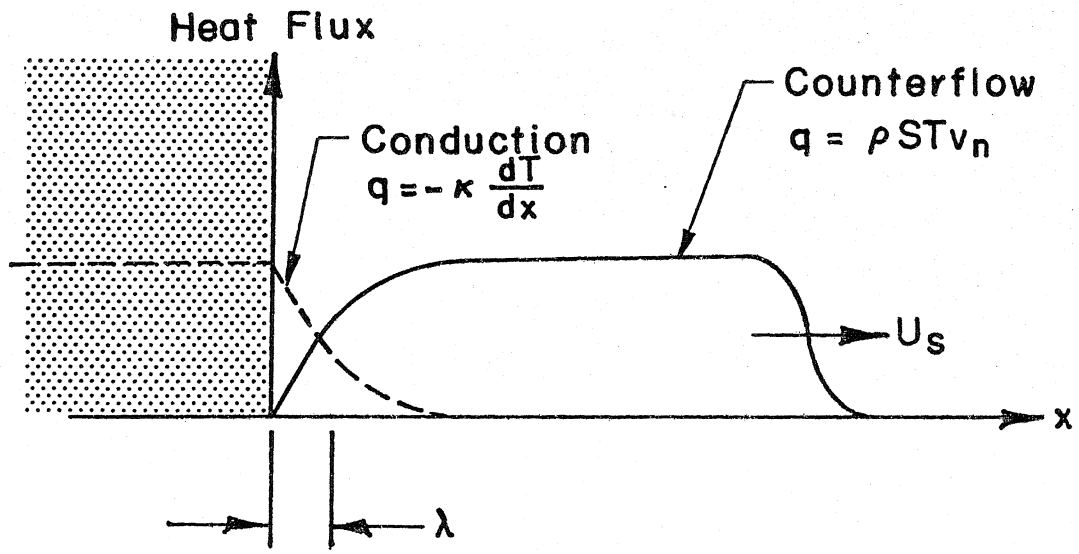

Figure 4.10 GENERATION OF A SECOND SOUND SHOCK PULSE

detailing the size and shape of the thermal boundary layer, are suspect: the assumption of complete thermodynamic equilibrium may not be valid since the evaluated layer thickness is on the order of 100 Å, while the phonon mean free path, ℓ_{pr}, is over a hundred times longer.

Since the boundary layer temperature jump is probably a significant fraction of the shock wave temperature jump, its magnitude might be experimentally determined. Unfortunately, the thermal Kapitza discontinuity at the liquid-solid interface is much larger and tends to mask the effects of the thermal boundary layer. However, a similar boundary layer must be generated at the liquid-vapor interface when heat is exchanged, and therefore, second-sound shock interactions with this interface might be employed to measure the boundary layer temperature jump.

Generation of a second-sound shock pulse is always accompanied by a much weaker first-sound wave. A temperature raising second-sound shock wave initiates a small mass flow, having a bulk velocity jump proportional to the coefficient of thermal expansion, β (see Table B.1):

$$\Delta v = - \beta T_0 \left(\frac{c^2}{c^2 - a^2} \right)_0 a_0 \Delta\theta + O(\Delta\theta^2) \qquad (4.33)$$

Since β is small and negative in helium II for temperatures exceeding 1.20 ^{o}K, the shock-induced mass flux is small and in the direction of the wave propagation.

The boundary condition at the heater wall, $v = 0$, demands that a negative pressure first-sound wave also be generated to initially

balance the mass flux to zero. The temperature amplitude of this first-sound wave is always positive and is equal to:

$$\frac{T'}{T_0} = (\beta T)_0^2 \left(\frac{c^2}{c^2 - a^2}\right)_0^2 \left(\frac{ca}{C_p T}\right)_0 \Delta\theta \qquad (4.34)$$

The thermodynamic function multiplying $\Delta\theta$ in this equation is exceedingly small -- never larger than .001 except near the λ-line -- so that these waves are not usually observable. However, when the temperature near the heater becomes so large that boiling is nucleated, the situation will be reversed. In this case the expanding bubbles will act like pistons to produce relatively large, positive pressure, first-sound waves. Since β in the normal operating range is negative, the resulting temperature amplitude will be negative.

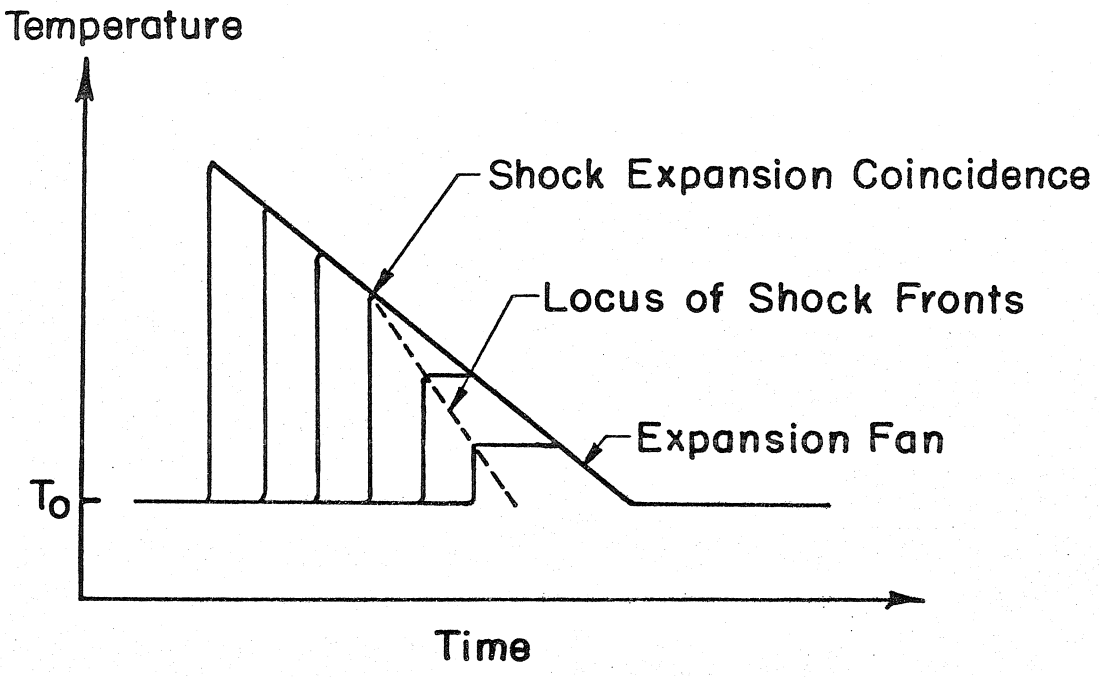

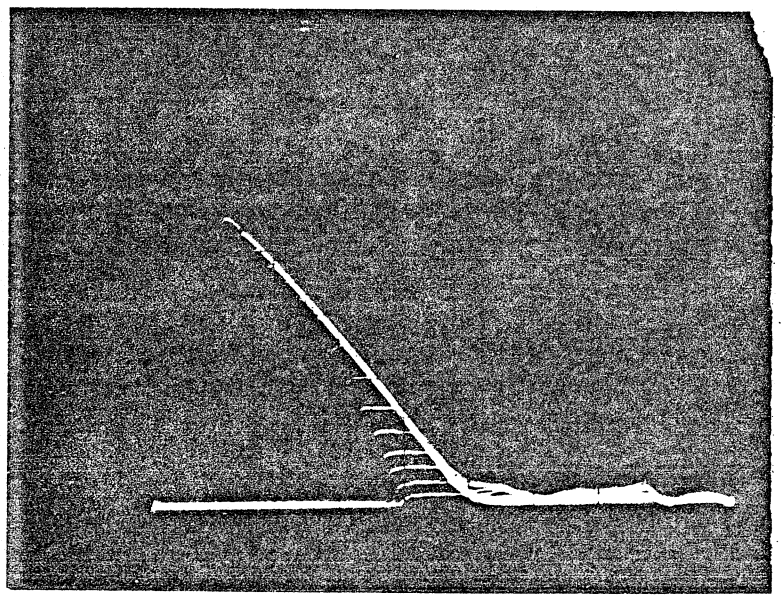

Figure 4.11 FAMILY OF SHOCK PULSES FOR WEAK WAVES OF VARIABLE POWER

Chapter 5. SHOCK AMPLITUDE MEASUREMENT

Since the main goal of this thesis, stated in the introduction, depends on the ability of second-order theory to accurately predict the shock jump conditions, it is useful to summarize its success. There are three testable predictions made by the theory, namely:

1. $U_S = \frac{1}{2}(u_0 + u_1)$
2. $M_S = 1 + \frac{1}{2}b_0\Delta\theta$
3. Shock structure

The first prediction -- the shock velocity is the average of the characteristic velocities ahead and behind the shock front -- is equivalently a statement of conservation of temperature or entropy within the shock pulse. The experimental fact that the integral of T with time is constant at any station observing the shock is thus a verification of this prediction. More refined tests of this prediction were obtained by observing the shock-expansion wave coincidence (Appendix G) and the arrival of the initial secondary waves generated at the heater seal (Appendix D). In both cases the measurable relative errors were within the acceptable tolerance: $(w/a)^2$.

The third prediction, dealing with the shock structure, is quantified by the shock thickness which was shown to compare reasonably well with experimental results obtained at a single temperature. The change in behavior of a shock pulse when the steepening coefficient changes sign, including the double-shock phenomena occurring near $T = 1.88^{o}K$, can also be viewed as further verification of this

prediction.

The second prediction, relating the Mach number to the shock strength, is the topic of this chapter. The usual procedure used to experimentally obtain this relation was to fit a straight line to the points specifying the measured shock strength versus $(at_A)^{-1}$, where t_A is the arrival time of the shock front as timed from the initial generation of the heat pulse. As $\Delta\theta \to 0$, the fitted line intercepts the axis at $t_A a = L$, where L is the distance traversed by the shock from the heater to the detecting sensor. The average Mach number of the shock front can then be calculated as $M_S = (L/at_A)$ and plotted against the shock strength. The slope of the resulting curve can then be identified as $\frac{1}{2}b(p,T)$.

Before elaborating on the results an additional point must be made concerning shock formation. The initial heat pulse generated by the heater has a finite rise time, t_r, on the order of 1 μsec. Thus, except for very weak pulses, the wave front will propagate as an unsteady wave until it has fully steepened into a steady shock profile. As can be seen on the x-t diagram of Figure 5.1, the fully developed shock front appears to originate at the heater at a time $\frac{1}{2}t_r$ later than initiation of the heat pulse. Actually, the apparent origin depends somewhat on the shape of the initial temperature rise, but as long as the shock is fully formed before it reaches the sensor, the correction to M_S required to account for its formation is on the order (t_r/t_A), which in every case was very small.

Early experiments showed that the experimental value of the

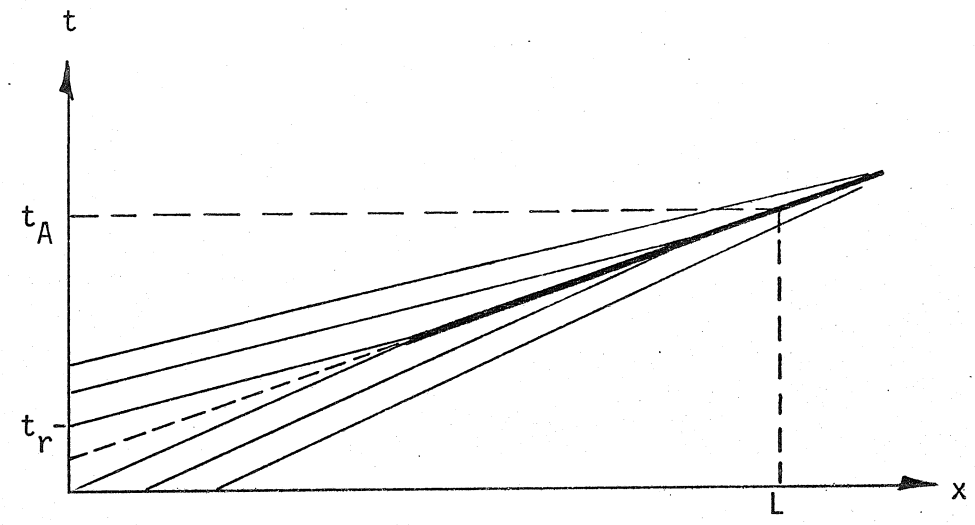

Figure 5.1 SHOCK FORMATION

steepening coefficient, b(p,T), was always significantly smaller than its predicted value. Soon it was also found that the magnitude of this discrepancy was strongly dependent on the type of sensor used to measure the temperature. Thus the problem had to be associated with the response of the temperature sensor itself.

A typical sensor consisted of a thin superconducting film physically supported on a glass substrate. The sensor was mounted on an endwall, aligned perpendicular to the longitudinal axis of the shock tube as described in Chapter 3. In this attitude, the measured temperature profile is always a superposition of the incoming wave with its simultaneous reflection from the endwall. Therefore the measured temperature jump must exceed that of the initial shock, ΔT, by an amount calculable from second-order theory.

Consider the temperature T_2 which is realized a long time after reflection. This temperature remains constant if the initial incoming wave temperature, T_1, is constant for as long as the boundary

conditions remain constant. This being the case, the initial wave front which produces the temperature jump is arbitrary and may be taken as one rising slow enough to be thermodynamically reversible. Then second-order theory may be employed to calculate R_+ on the characteristic C_{+1} in Figure 5.2 to yield:

$$w_2 + \int_{T_0}^{T_2} \frac{\rho S}{\rho_n a} dT = 2 \int_{T_0}^{T_1} \frac{\rho S}{\rho_n a} dT \qquad (5.1)$$

If the wall is adiabatic, then w_2 must be zero, and the preceding equation shows that for small amplitude temperature waves the reflected temperature jump is twice the initial jump. This doubling upon reflection is dramatically displayed in Figure 5.3, where a small

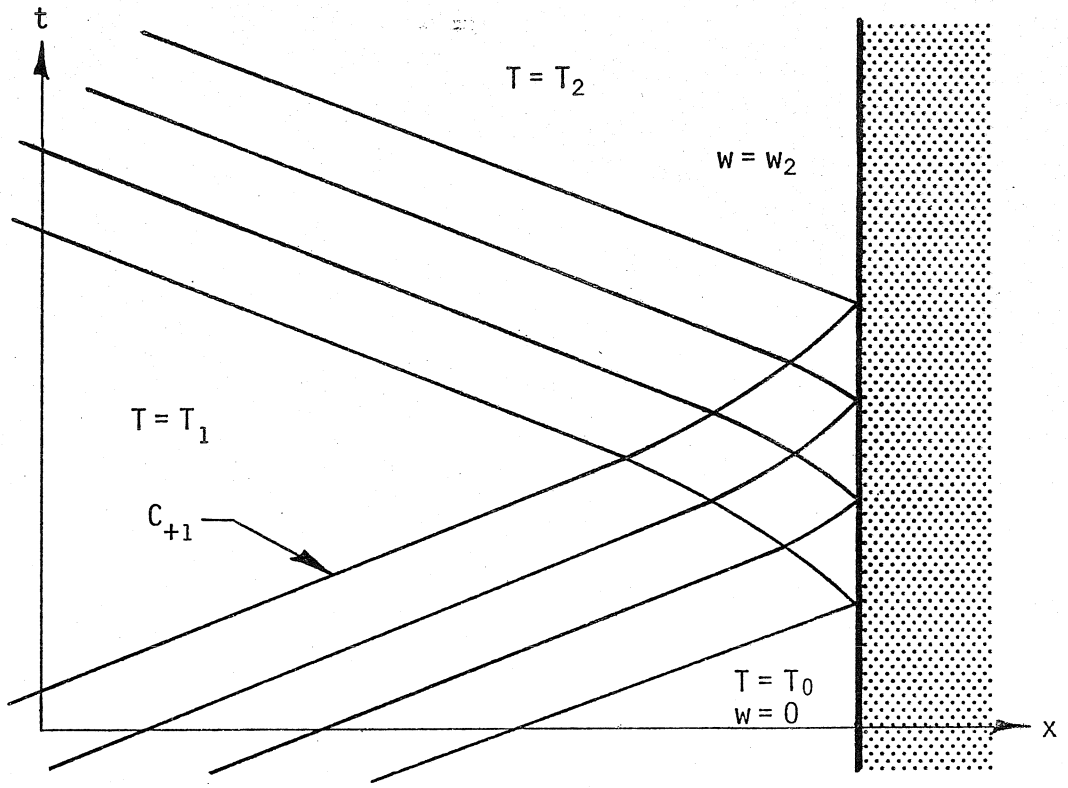

Figure 5.2 SECOND-SOUND WAVE REFLECTION

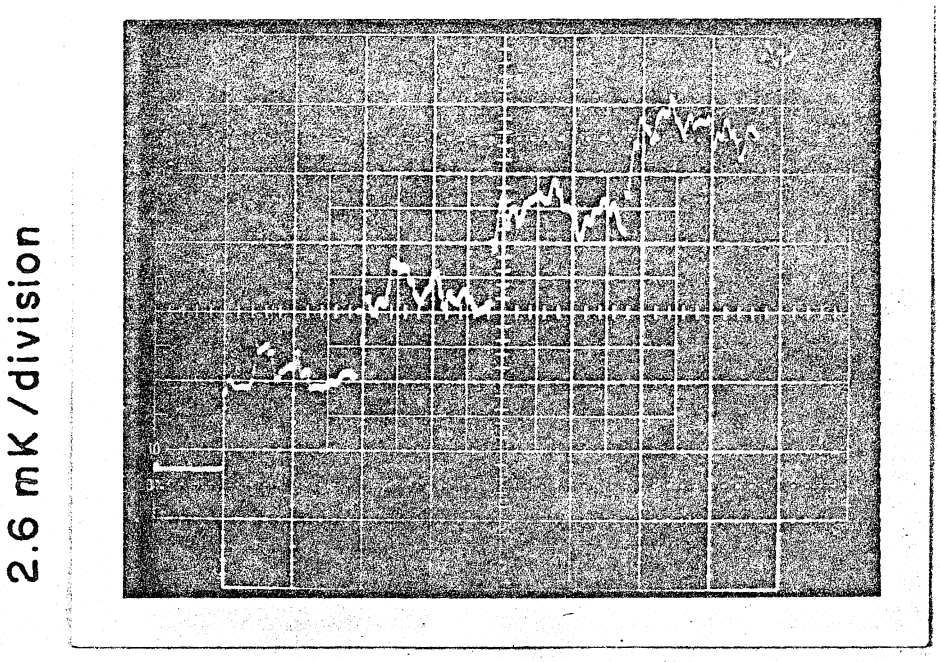

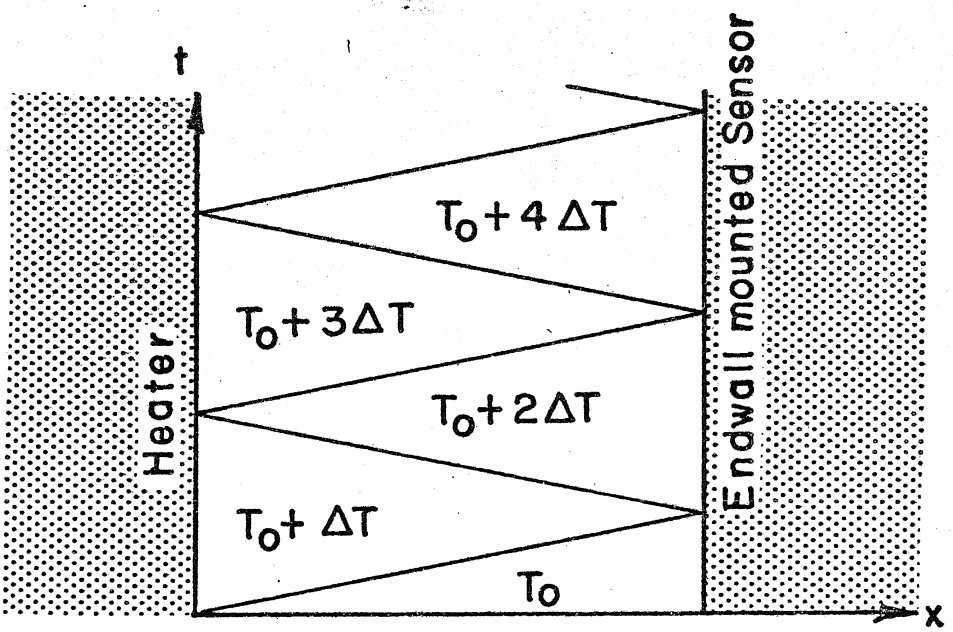

Figure 5.3 STAIRSTEP REFLECTIONS PRODUCED BY A WEAK SECOND SOUND SHOCK PULSE OF LONG DURATION (10 m sec)

amplitude, long duration wave was generated in a shock tube barely 19.3 mm long (Shock Tube IV). The time for the initial wave front to reach the endwall sensor was 0.959 msec, while the duration of the pulse exceeded 10.0 msec. During this heat pulse, the wave front reflected five times to produce a temporal, stairstep temperature profile.

In reality the wall cannot be completely adiabatic, since if there was no heat flux into it, the temperature sensor would not even register. This heat flux can be written in terms of w_2 as:

$$q_2 = \rho_s STw_2 \tag{5.2}$$

where positive q represents heat flowing into the wall. From equation (5.1) this will reduce the final temperature T_2 somewhat, but in practice this effect is unmeasurable because q is so small -- being limited by the Kapitza resistance and to a much lesser extent the thermal boundary layer resistance discussed in the preceding chapter.

In Appendix F the response of a thin-film sensor is analyzed and shown to be limited by the thermal response of the supporting substrate. It is also shown that the sensor can be accurately modelled as two temperature discontinuities occurring at the liquid-solid and metal-dielectric interfaces (which are proportional to the heat flux penetrating the interfaces), superimposed on the boundary of a semi-infinite substrate. The theoretical response at the substrate boundary to a step in the liquid temperature from $T = T_0$ to $T = T_2$ is displayed graphically as Figure 5.4a. The substrate temperature rises very quickly at first and then very much slower resulting in a characteristic

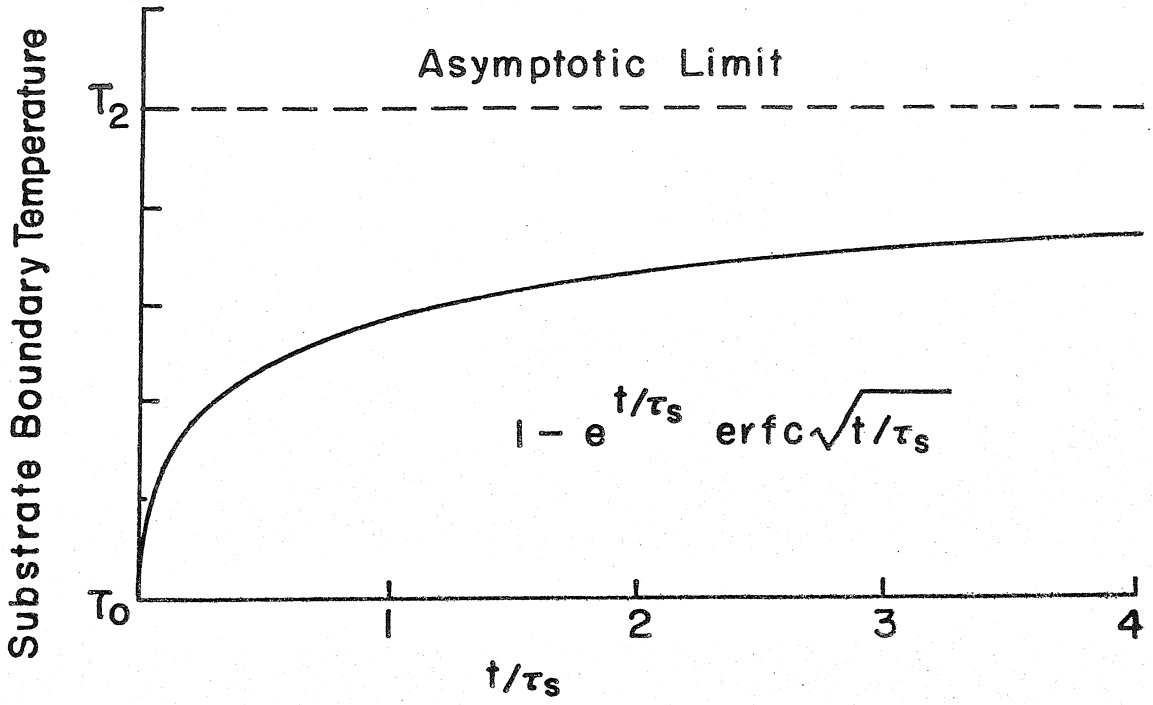

(a) Substrate Response to a Step Input

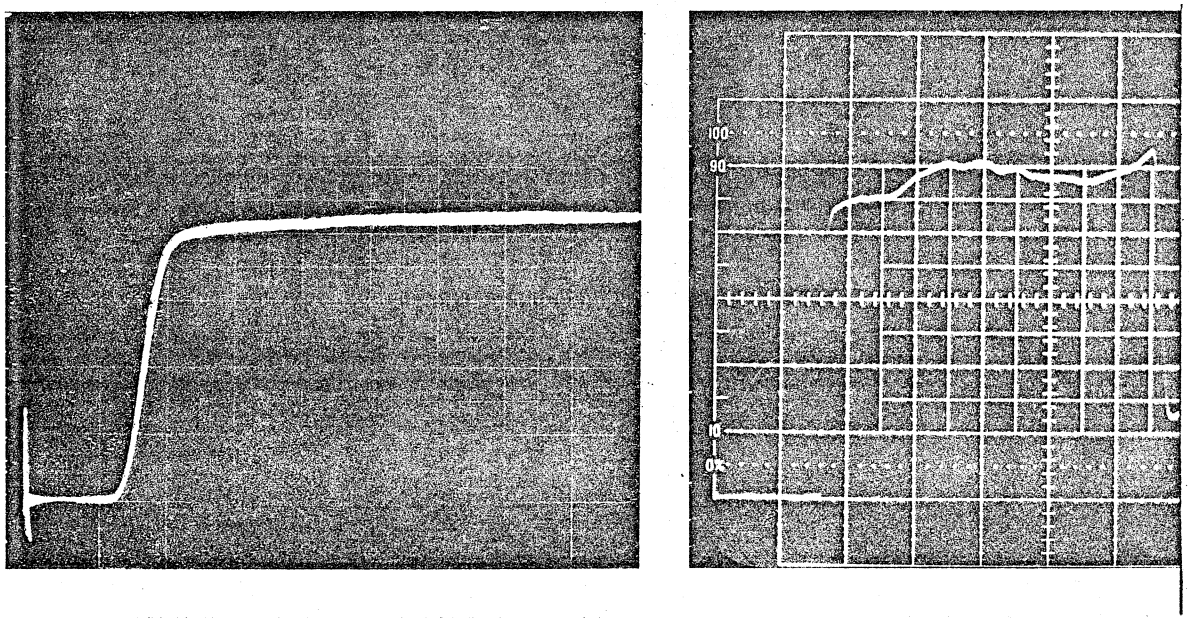

(b) 5 μ sec/division

(c) 50 μ sec/division

Figure 5.4 RESPONSE OF A THIN-FILM TEMPERATURE SENSOR

hook-shaped profile.

The temperature actually measured by the sensor is the thin-film temperature, T_3 (refer to notation of Figure F.1), since it is the thin-film resistance which is monitored. Applying the simple model shows that the thin-film temperature must initially jump from $T = T_0$ to:

$$T_3 = T_0 + \frac{R_C}{R_C + R_K} (T_2 - T_0) \qquad (5.3)$$

where R_K is essentially the Kapitza resistance, and R_C is a similar contact resistance between the film and substrate. After this initial temperature jump, the temperature rises similarly to the substrate boundary temperature, $T_4(t)$, finally asymptoting to $T = T_2$. Figures 5.4 b,c are oscillographs displaying the characteristic hook profile following the shock front typical of a thin-film sensor.

For the tin-on-gold sensors deposited on glass, the contact resistance is much greater than the Kapitza resistance. This results in a large temperature jump to 85-90% of the asymptotic limit. Previous sensors consisting of layered tantalium and titanium films deposited on silicon displayed much smaller temperature jumps on the order of 10%. This can now be explained by a combination of decreased contact resistance -- the film adheres very well to the silicon substrate -- and an increased liquid-solid resistance; when the film surface is annodized, in order to set the transition temperature, the resulting oxide layer very effectively supplements the Kapitza resistance.

There are two reasons why tin-on-gold films on glass make excellent temperature sensors. First, the high contact resistance

due to poor adherence of the film to glass allows the film to initially register 90% of the actual temperature jump in the liquid. (This property also makes the sensors very fragile -- a good sensor won't last long, but a durable sensor won't work.) Second, since the time constant of the substrate is proportional to its thermal conductivity (see appendix F) which for glass is exceedingly small, the substrate time constant is also small -- about 5 to 20 μs. Compare this to a silicon substrate whose thermal conductivity can be a thousand times that of glass (Berman, 1976); the response time could be enormously slow -- at least for measuring shock waves.

With a clear understanding of the temperature sensor response, the apparent discrepancy between the predicted and measured shock strengths can now be resolved. The typical procedure for measuring the shock strength, or equivalently the temperature jump, utilizes an electronic pulse amplitude DVM triggered to record the sensor temperature 5 μsec after the shock front is detected. After this much delay the sensor temperature is on a plateau -- the temperature is steadily rising, but very slowly. The temperature measurement taken at this time is very repeatable but slightly less than the real equilibrium value. A few time constants later the measured temperature will be much closer to the real value. This can be clearly seen in the results of an experiment where measurements were taken with both a 5 μsec and a 30 μsec delay (Table 5.1). After 30 μsec the thin-film temperature has come much closer to the theoretical doubled value caused by an endwall reflection. This and similar measurements verify the second relation predicted by second-order shock theory,

Table 5.1 NORMALIZED TEMPERATURE JUMP OF A THIN-FILM SENSOR (ENDWALL MOUNTED)

	$\frac{\Delta\theta_{sensor}}{2(M_S - 1)/b_0}$
5 μs delay*	1.89
30 μs delay*	1.99
theoretical value	2.00

*experiment C3, SEQ 1 and SEQ 1A.

stated at the beginning of the chapter.

In conclusion to this chapter, it may be stated that second-order theory accurately describes second-sound shock waves generated in the present experiments. Errors caused by neglecting higher order terms are immeasurable for the shock strengths which can be generated. Before higher order terms become important second-sound shock waves are limited in strength by a breakdown in the superfluidity of helium II to be discussed in the next chapter.

Chapter 6. THE SHOCK LIMIT AND BREAKDOWN OF SUPERFLUIDITY

The preceding two chapters have demonstrated the overwhelming agreement between nonlinear second-sound theory and experiment. This chapter will concentrate on behavior that is not predicted by second-order theory and which dramatically displays a breakdown in the superfluidity of helium II.

When a rectangular heat pulse is generated by the heater, the size and shape of the resulting second-sound shock pulse can be accurately predicted as long as the input power does not exceed a certain critical limit. When this limit is exceeded the flat top of the predicted trapezoidal waveform (see Figure 4.11) will begin to tilt; that is, the temperature following a front steepened, temperature raising shock will decrease instead of remaining constant at $T_1 = T_0 + \Delta T$. This tilt is not due to a shock-expansion coincidence, but it is a result of a breakdown in the superfluidity of helium II. As the power is increased further the amplitude of the shock front will eventually reach a maximum value -- more power will only decrease its size -- and the shape of the initially rectangular shock pulse will asymptote to a triangular or exponential-like profile, possessing a long warm tail.

This peculiar behavior is illustrated by a shock strength versus Mach number diagram (Figure 6.1) and two sets of multiple exposure oscillographs showing how the shock pulse profiles are modified with increasing heater power (Figures 6.2 and 6.3). The nomenclature applied to the $\Delta\theta$ versus M_S diagram, illustrated by Figure 6.4, will be defined as follows:

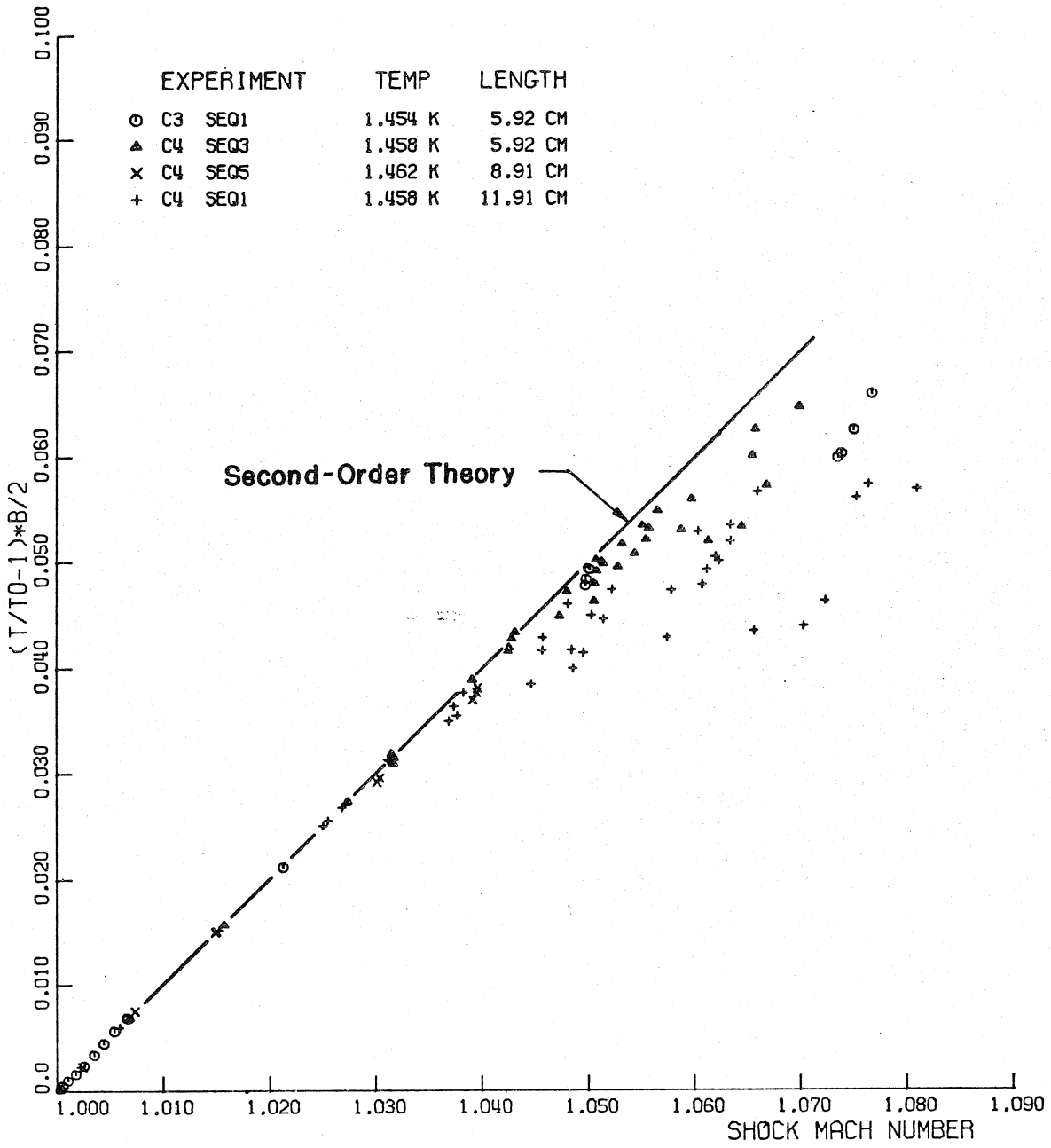

Figure 6.1 SHOCK STRENGTH VERSUS MACH NUMBER
(HEATER TO STATION)

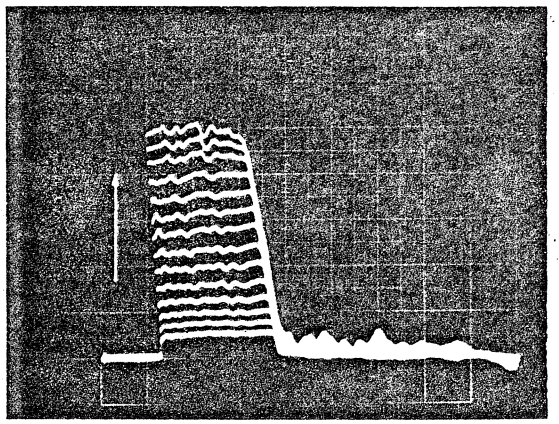

(a) Simple Formation

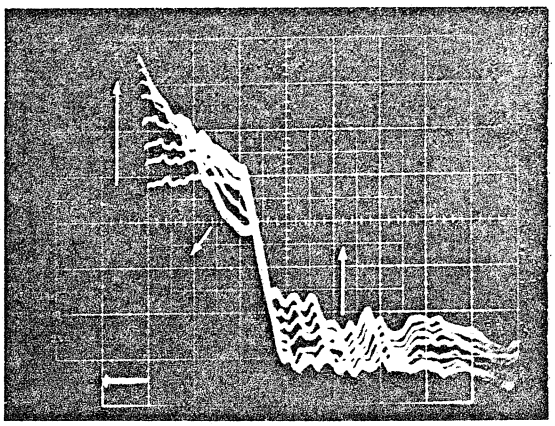

(b) Wave Modification

(c) Shock Limit

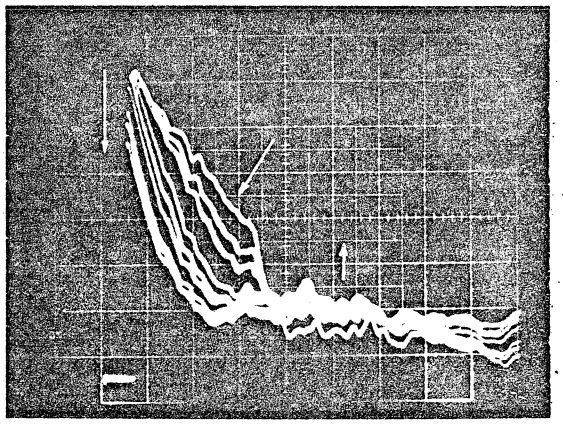

(d) Beyond the Shock Limit

Figure 6.2 EFFECTS OF HEATER POWER ON SHOCK PULSE PROFILES (200 μsec/division)

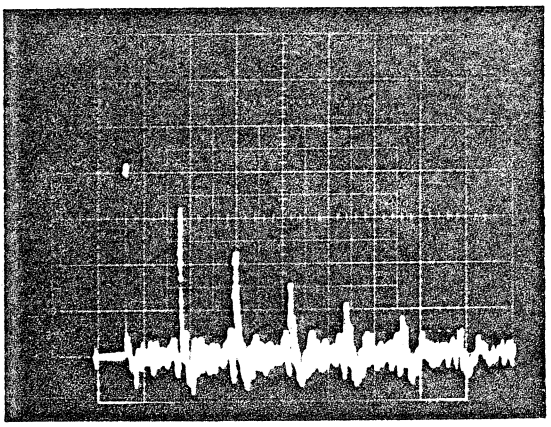

(a) Simple Formation

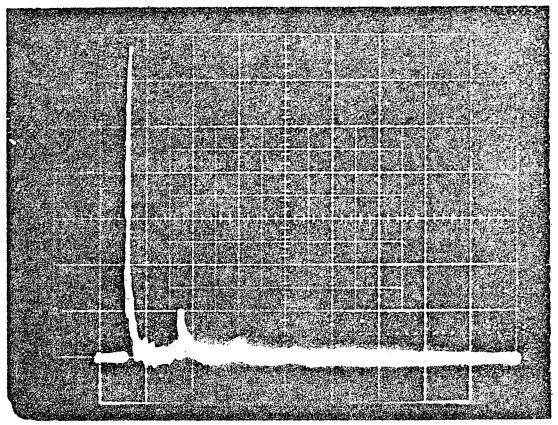

(b) Shock Limit

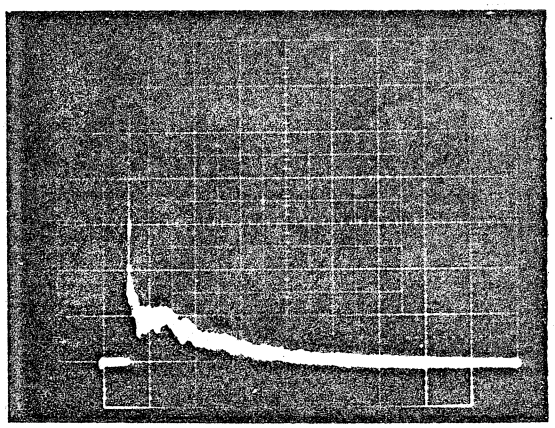

(c) Beyond the Shock Limit

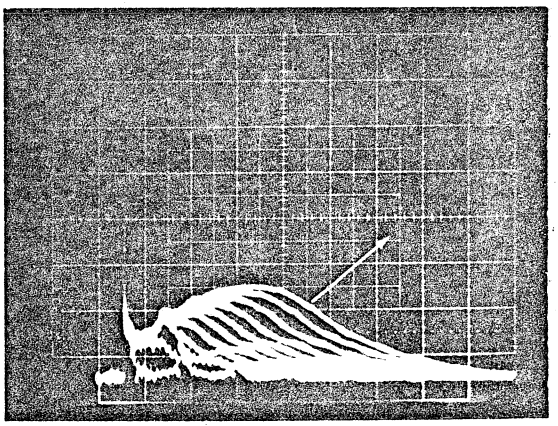

(d) Beyond the Shock Limit

Figure 6.3 EFFECTS OF HEATER POWER ON SHOCK PULSE PROFILES (10 msec / division)

1) The Simple Formation Branch applies to shock pulses whose formation and propagation conform to predictions made by second-order theory.
2) The Breakpoint occurs when the shock pulse profile begins to tilt (see Figure 6.2b). This event is also the dividing point between the simple formation and wave modification regions.
3) The Wave Modification Region contains the scatter of (M_S, $\Delta\theta$) data points which diverge from the breakpoint and display an apparent departure from second-order theory. In this region wave profiles are distorted from the simply formed trapezoidal waveform towards the limiting exponential profile. The extent of modification is directly related to the input heater power.
4) The Shock Limit is the maximum attainable shock strength.

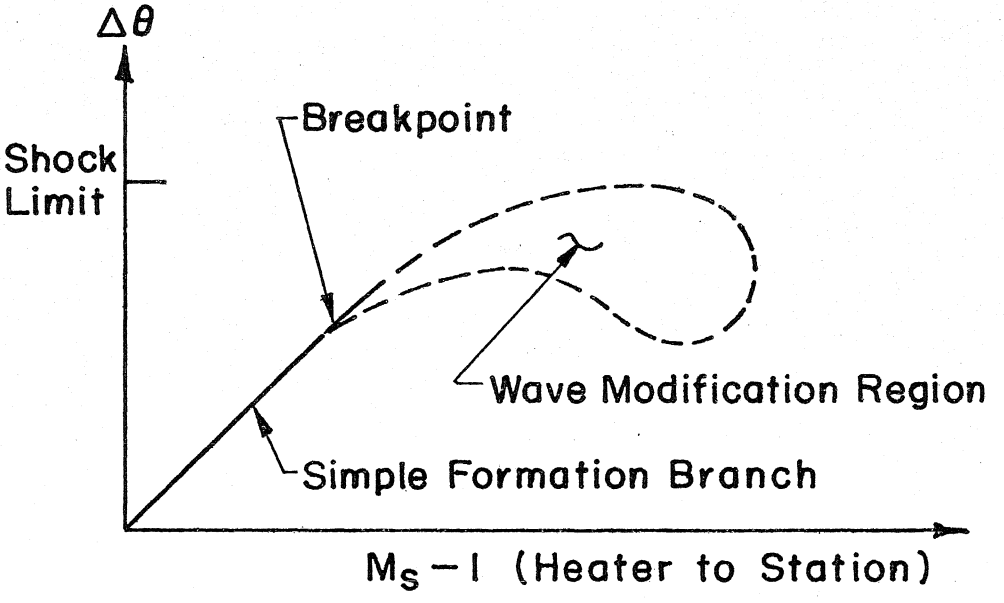

Figure 6.4 NOMENCLATURE APPLIED TO THE $\Delta\theta$ VERSUS M_S-1 DIAGRAM

SUPERCRITICAL VERSUS SUBCRITICAL SHOCK WAVES

Whether or not the observed breakdown of superfluidity is caused by an intrinsic critical velocity is an important question which demands resolution. In an endeavor to do so, the concept of subcritical and supercritical shock waves will be elucidated.

A "supercritical shock wave" will be defined as one that generates a relative velocity larger than any intrinsic critical velocity of the liquid. Conversely, a "subcritical shock wave" is one whose maximum relative velocity is less than all excitable intrinsic critical velocities.

By definition, a subcritical shock wave cannot cause any mutual interaction between the normal and superfluid components leading to extra dissipation in the flow; dissipation occurs exclusively in the shock front where the gradients in T and w are very large. If the initial shock pulse has a rectangular temperature profile, the shock strength and Mach number will be constant until the leading edge of the expansion wave overtakes the shock front. From this time on, the triangular shaped shock pulse will decrease in amplitude and velocity as the expansion wave propagates further into the shock front.

There is one important characteristic that distinguishes a subcritical shock pulse: dissipation, and thus amplitude decay, occur exclusively at the shock front. The amplitude of a point on the expansion wave remains constant until it coincides with the shock front (This is illustrated by the "marker" on a decaying subcritical shock pulse -- Figure 6.5. A marker can be any distinguishable feature in the wave profile which propagates at the characteristic

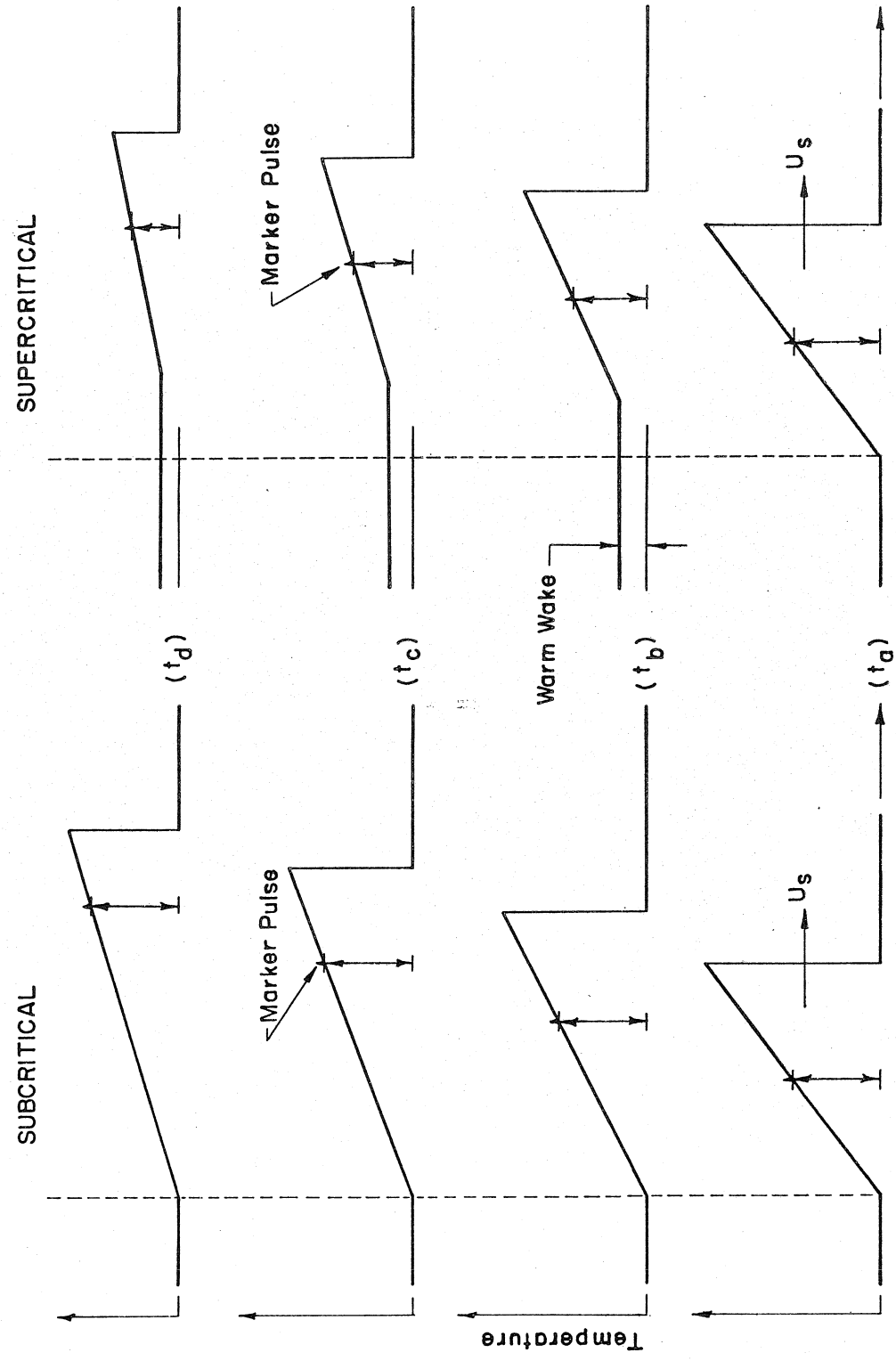

Figure 6.5 SHOCK PULSE DECAY —— SUPERCRITICAL VS SUBCRITICAL

velocity at that point -- for example, a kink or slope discontinuity.). Subcritical shock decay is common to ordinary pressure shock pulses and can be calculated for second-sound by the second-order theory derived in Chapter 4 (for example, see Appendix H).

A supercritical shock wave, on the other hand, excites dissipation producing interactions in all regions where the relative velocity is large. Consider a front steepened supercritical shock wave propagating into undisturbed fluid. The mechanism producing the extra dissipation in the flow, turned-on by the shock front passage, will cause an initially rectangular waveform to decrease in amplitude even before the leading edge of the expansion wave can overtake the shock front. This occurs because mutual interactions produce "bulk dissipation", monotonically related not to the gradient of w, but to its magnitude.

A hypothetical illustration of supercritical decay of an initially triangular shock pulse is shown in Figure 6.5. Suppose at time t_a, mutual interactions are suddenly turned on. For example, superfluid quantum vortices might be generated at the shock front leading to a Gorter-Mellink type body force in the fluid arising between the quantum vortices and the normal fluid excitations. Whatever their origin, mutual interactions will rapidly dissipate the wave energy and transform it into heat. The result is a steadily decreasing shock pulse whose dissipated energy is left behind to form a warm wake as the shock wave propagates further into undisturbed fluid.

Whether or not the wave modified shock pulse emerging from the heater is a result of critical velocities cannot yet be answered with certainty. However, there is sufficient evidence to prove that:

(1) the observed breakdown of superfluidity occurs in a region near the heater; and (2) the emerging second-sound shock pulse is subcritical.

There are three possible locations where breakdown could occur: 1) in a formation zone near the heater; 2) at the endwall where the shock strength is doubled; and 3) between the heater and endwall via supercritical propagation. The third possibility can be eliminated because wave modified shock pulses have been observed to propagate and decay subcritically. Figure 6.6 shows the propagation of a typical wave modified shock pulse in which the heater power exceeded the value necessary to reach the shock limit. The arrows point to the remnant of the expansion fan leading edge as observed from four different locations, ranging from 5.9 to 11.9 cm from the heater. Notice that as this feature propagates its temperature amplitude does not decay. This is typical of reversible wave propagation, but would not occur if the shock pulse was supercritical. The temperature amplitude of the shock front does decrease as the wave propagates, but this is due to the normal confluence of the expansion fan with the shock front.

Since the shock pulse obviously propagates subcritically one might suspect that breakdown actually occurs at the endwalls where reflection doubles the temperature amplitude of the wave. However, identical breakdown phenomena, occurring at equivalent power levels, were observed with both endwall and sidewall mounted sensors. Thus, the observed breakdown had to occur before the shock pulse reached the endwall.

This fact, however, does not exclude the possibility of a

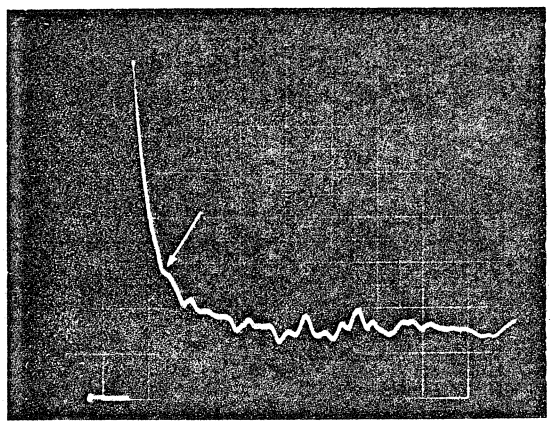

(a) L = 5.9 cm

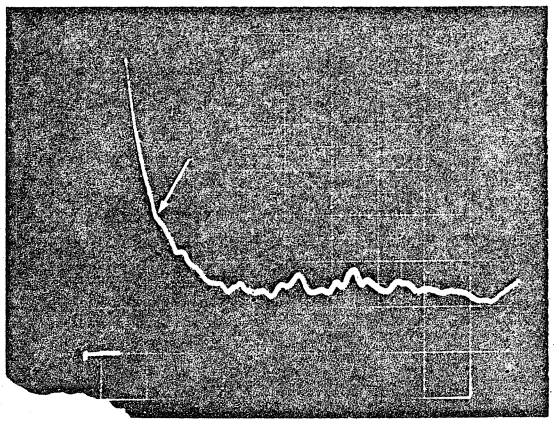

(b) L = 8.9 cm

200 μ sec/division

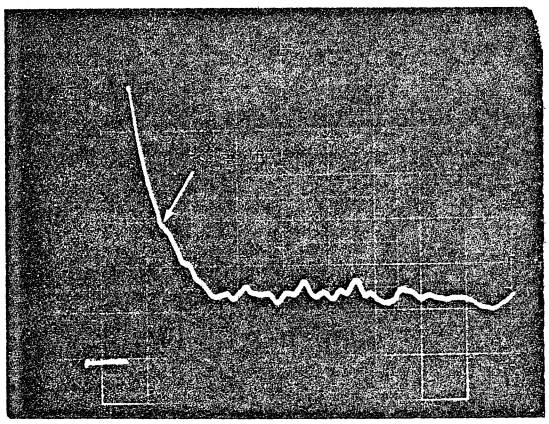

(c) L = 10.4 cm

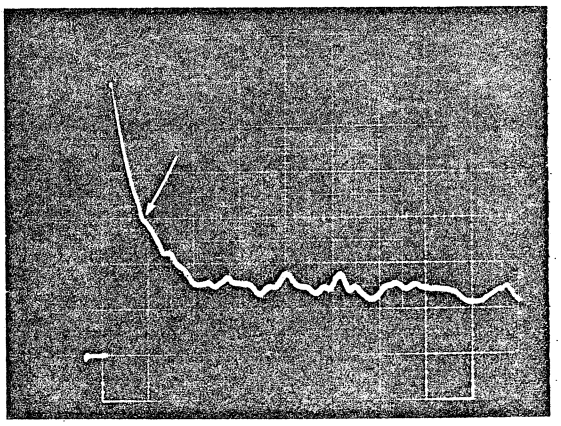

(d) L = 11.9 cm

Figure 6.6 PROPAGATION OF A FORMATION MODIFIED SHOCK PULSE WHICH EXCEEDED THE SHOCK LIMIT POWER

secondary breakdown occurring upon endwall reflection (no such breakdown was observed, but it was not searched for either). Yet, if breakdown is truly a critical velocity phenomenon, breakdown upon reflection should not occur. This is because although the temperature amplitude is doubled during reflection, the relative velocity is essentially zero, being dictated by the "boundary condition" at the wall -- $q \simeq 0$.

Breakdown does not occur upon reflection or during the propagation from heater to endwall; therefore, it must occur at, or very near, the heater. Additional evidence proving this proposition, as well as the subcritical nature of the emerging shock pulse, can be gleaned from the $\Delta\theta$ versus M_S diagrams. The Mach number in these diagrams is actually the average Mach number between two fixed points. The shock propagation time used to calculate the Mach numbers in Figure 6.1 was the arrival time at the sensor location measured from the initiation of the heat pulse. Therefore, this Mach number is an average from the heater to the sensor station, which necessarily includes delays or advances primarily associated with the initial formation of the wave.

In fact, for heater powers exceeding the breakpoint, the departure of the observed (M_S, $\Delta\theta$) points from second-order theory always displays a definite advance meaning that a wave modified shock pulse propagates faster than demanded by simple theoretical considerations. If, on the other hand, the Mach number is calculated from one sensor station to another, both substantially displaced from the heater, the resulting $\Delta\theta$ versus M_S diagram does not depart from second-order theory even for heater powers exceeding the shock limit.

This fact has two implications: First, propagation of the shock pulse between sensor stations is describable by second-order theory, as it must be if the shock pulse is subcritical. Second, the wave advance, which is one clear indication of breakdown, occurs between the heater and the first sensor. The mechanisms responsible for the wave advance are revealed in a subsequent section.

WAVE MODIFICATION AND BOILING

There are three distinct phenomena that commence at the breakpoint heater power: 1) wave modification; 2) arrival time jitter; and 3) boiling. The occurrence of boiling was obvious at heater powers greatly exceeding the breakpoint since the sound generated by the nucleating bubbles was heard as a sharp "ping". Boiling could also be visually observed in the optical shock tube as a thin sheath covering the heater, which appeared every time a shock was fired. Using a stethoscope applied to the outside dewar, these pings were audible until the heater power was reduced to the breakpoint; as this limit was crossed into the simple formation region the pings suddenly stopped.

The effects of boiling were also observed with the superconducting temperature sensors. Recall that the heater boundary condition requires that a simply formed, positive temperature, second-sound shock pulse be accompanied by a negative pressure, first-sound wave (see Generation of Second-Sound, Chapter 4). The temperature excursion of this first-sound wave is positive and exceedingly small -- so small in fact, that it was not observable within the noise limits of the sensor. However, after the breakpoint power was exceeded a first-sound wave was observed, but it initially produced a negative temperature excursion (see Figure 6.7). Thus the pressure perturbation in this wave was positive, which can only be explained by boiling. As the nucleating bubbles expand they act like pistons pushing the fluid away from the heater, and in the process, they generate relatively large, positive pressure, first-sound waves.

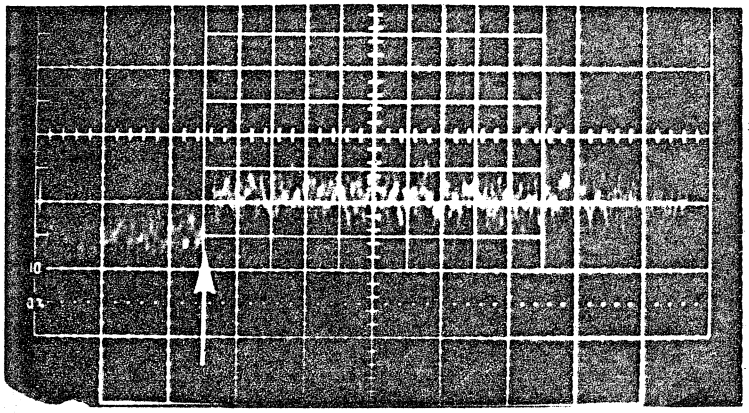

(a) No observable pressure wave for simply formed shocks (arrow points to electrical pulse termination)

100 μ sec/division

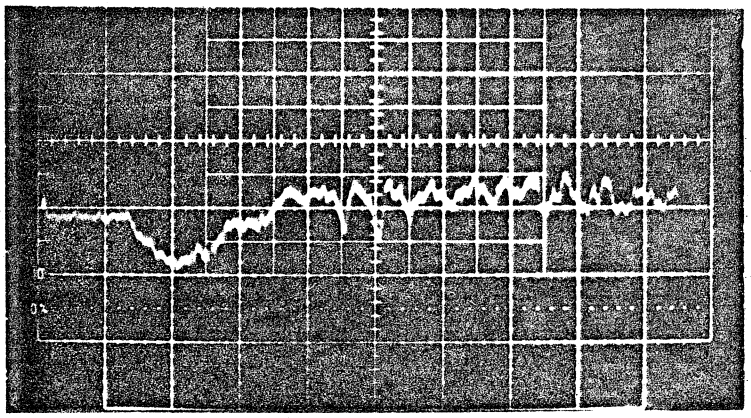

(b) Positive pressure wave observed for shocks exceeding the breakpoint

T = 1.51°K

Figure 6.7 BOILING INDUCED PRESSURE WAVES

Arrival time jitter is a measure of the randomness in the formation process that began at the breakpoint and increased steadily with heater power. In the simple formation region the repeatability of the arrival time between shock pulses of equal amplitude was about 10 parts per million, but as soon as the break point was exceeded the repeatability dropped to one part in ten thousand, or one part in one thousand. This randomness in the formation process must be attributed to nucleate boiling.

With the information presented so far, a couple of scenarios describing the observed breakdown of superfluidity can be hypothesized.

The presence of boiling, concurrent with the other phenomena signalling the breakdown, strongly suggests that boiling initiates the entire process. All the experimental data comprising the present thesis were obtained when the equilibrium pressure was slightly above the saturated vapor pressure of the liquid. The pressure increment was maintained by a head of liquid helium ranging from 5 to 50 centimeters high. At 1.85 ^{o}K the corresponding temperature increment necessary to cross the equilibrium saturated vapor pressure curve ranges from 10.7 mK to 107 mK, while the experimentally determined shock limit at this temperature was $\Delta T = 36 \pm 2$ mK. It is possible that this temperature jump, supplemented by the temperature increase in the thermal boundary layer, could nucleate bubbles that would quickly form an insulating layer over the heater surface. The heat flux, which generates the shock pulse, has to penetrate this layer, and thus it would decrease with time as the layer grows. In this manner the observed shock pulse profile would be modified into the

observed triangular waveforms.

A second scenario would have the breakdown initiated by an intrinsic critical velocity transition. The resulting supercritical shock pulse would decay quickly near the heater until the relative velocity within the pulse was subcritical. The energy dissipated from the supercritical shock wave would form a hot layer near the heater which in turn would nucleate boiling.

The evidence obtained so far is not sufficient to determine the mechanism responsible for the observed breakdown of superfluidity. However, it is interesting that the experimental shock limit did not change when the equilibrium temperature differential from the SVP curve varied by a factor of two or three, due to evaporation of the head of liquid helium during the course of the experiment. This poses a problem for the boiling triggered hypothesis; the initiation of boiling should occur at a fixed temperature jump, not with respect to the equilibrium temperature, T_0, but relative to the SVP curve. Also, the observation that some shock limited pulses may have superheated the liquid is not a problem; superheating has been observed even in steady counterflows dominated by Gorter-Mellink dissipation (Childers and Tough, 1972). These facts make the critical velocity triggered scenario a better bet. However, a final conclusion must await the results of forthcoming experiments conducted at pressures exceeding the critical point of liquid helium.

THE SHOCK LIMITED RELATIVE VELOCITY

Whether the breakdown of superfluidity is critical velocity triggered or otherwise, the maximum relative velocity, produced by the subcritical shock pulse which emerges from the breakdown region, represents a lower limit to the long sought fundamental critical velocity. This makes the maximum relative velocity a very important quantity to determine.

Since the emerging shocks are always subcritical, second-order theory can be confidently applied. The trick is to determine either the Mach number or shock strength of the shock wave just as it emerges from the formation zone. This is complicated by the fact that shock limited pulses are highly modified into triangular shock pulses which decay as they propagate. That is, as the expansion fan merges with the shock front, it continually reduces the shock amplitude and velocity.

If the modified shock pulse can be well approximated by an initially triangular profile, then its trajectory and decay in amplitude will be proportional to the square root of the propagation time (see appendix H). By measuring the shock limit at different positions from the heater, the rate of decay can be deduced and the original formation temperature amplitude of the subcritical shock pulse can be determined. The relation connecting the formation shock strength, $\Delta\theta_F$, to the measured shock strength, $\Delta\theta$, is:

$$\frac{1}{(\Delta\theta)^2} = \frac{1}{(\Delta\theta_F)^2} + \frac{t}{\tau} \qquad (6.1)$$

where t is the propagation time of the shock pulse. Note that the data in Figure 6.1 definitely display a larger shock strength limit for measurements made closer to the heater. If the shock limited data are plotted against arrival time, then from equation (6.1) the decay time, τ, and the formation strength can be extrapolated. The results of this determination yield a relative velocity limit of 3.67 m/sec for T = 1.458 ^{o}K. Compare this to the lower limit, 3.10 m/sec, which is the result obtained for the maximum observed shock strength.

Values of the shock limited relative velocity can also be determined from measurements of the Mach number. The maximum observed Mach number, which recall is an average value, yields a relative velocity slightly larger than the value associated with the extrapolated shock strength; it is 3.82 m/sec. The initial formation Mach number must be larger than the measured average value, $\langle M_S \rangle$, again due to the decay of the triangular shock pulse. Using the theory developed in Appendix H, the decay in the shock strength can be calculated from the measured shock strength and Mach number as:

$$\frac{\Delta\theta \; b/2}{\langle M_S - 1 \rangle} = \frac{1}{2} + \frac{1}{2} \frac{\Delta\theta}{\Delta\theta_F} \tag{6.2}$$

With this method the calculated limiting relative velocity is found to range from 4.4 to 8.3 m/sec with decays from $(\Delta\theta_F/\Delta\theta)$ = 1.5 to 4.2. The larger the decay, the larger the wave advance, and the larger the apparent initial relative velocity.

The fact that the calculated relative velocity limit depends on the decay means that other mechanisms must also be responsible for

the wave advance rather than just the natural decay of a triangular shock pulse. One that is obvious is a result of boiling. Boiling-induced, positive pressure, first-sound waves convect the shock pulse forward, resulting in a larger apparent Mach number without affecting the shock amplitude. Substitution of these data into equation (6.2) results in an artificially large decay and an inflated value of the shock limited relative velocity.

Another factor that contributes to the difficulty of determining the true shock limit is the sensitivity of the breakdown to disturbances already present in the fluid before a shock is fired. This effect is clearly illustrated by Figure 6.8 which shows the effect of repetition rate on shock pulse profiles. The two oscillograph traces are shock pulse profiles generated by equivalent input power pulses. The only difference in the two cases is the time between shock firings. If one waits about 200 seconds between firings, the resulting shock pulse is simply formed, but if the heat pulse is applied every second, the resulting shock pulse degenerates to a typical wave modified profile.

One reason why there is so much scatter in the wave modification region of Figure 6.1 is due to the fact that the duration between shots was not precisely the same each time -- varying from 100 to 300 seconds. The repeatability of the shock pulse profiles was much greater in the data presented as Figures 6.2 and 6.3 where shocks were periodically generated one per second.

When breakdown occurs, slowly decaying disturbances are generated which nucleate the breakdown mechanism. If breakdown is due to an

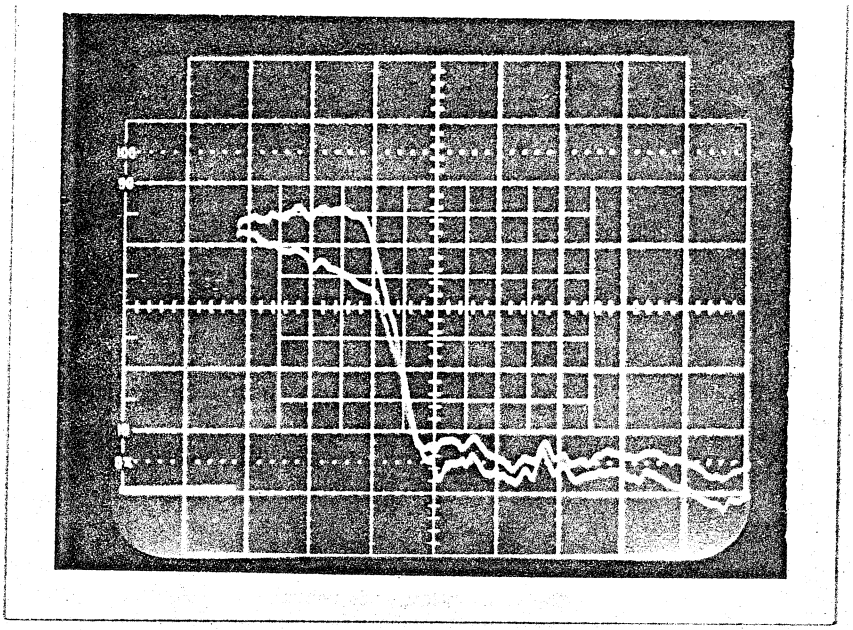

200 μ sec / division

Pulse Repetition Rate

.005 Hz → Simple Formation
1.0 Hz → Wave Modification

Figure 6.8 EFFECT OF REPETITION RATE ON SHOCK PULSE PROFILES

intrinsic critical velocity via homogeneous nucleation of superfluid vortices, then the observed facts are not difficult to explain. For example, the sensitivity to repetition rate is explained by the slow decay rate of these vortices. A supercritical shock initiating breakdown would multiply the superfluid vortices which in turn would dissipate energy from the wave by a Gorter-Mellink type interaction. Since these vortices move with the superfluid they would be pushed back near the heater resulting in an insulating layer whose temperature would very quickly become hot enough to nucleate boiling.

The shock limited relative velocities presented in this chapter and the concluding graph, Figure 7.1, do not include data obtained at rapid repetition rates. The shock limit of the latter (one shock per second) is only 25 or 30% of the limit obtained by low repetition shock generation.

SHOCK LIMITED DOUBLE-SHOCKS AND BACK STEEPENED SHOCKS

The problems encountered when determining the shock limit of front steepened shocks do not appear for double-shocks. At $T = 1.85^{o}K$, the breakdown of superfluidity modifies the input heat pulse into a double-shock whose profile does not change appreciably as it propagates. The reason for this is that the steepening coefficient is very small; therefore, the nonsteady wave evolution brought on by nonlinearity is very slow.

Figure 6.9c shows the profiles of double-shocks as the heater power is increased and the shock limit is attained. Notice that after a limiting temperature is reached a further increase in heater power may lengthen the double-shock pulse, but it will not increase its amplitude. Figure 6.9d shows the limiting profile which resulted when the heat pulse power was fixed, but its duration was varied over a range from 10 μsec to 1 msec. The amplitude of the initial pulse again remained shock limited; the duration of the double-shock varied slightly, but only over a range from 4 to 7 μsec.

From the temperature amplitude limit of the double-shocks shown in Figure 6.9 abc, a limiting relative velocity of 3.20 m/sec can be deduced for the initial temperature, $T_0 = 1.852^{o}K$.

Figure 6.10 displays the profiles of some back steepened shock pulses produced when $T_0 = 1.951^{o}K$. As the heater power is increased the shock limit is attained, but the shock limited profiles are very much different than those observed for front steepened shocks. The leading expansion wave, whose profile is convex shaped, does not

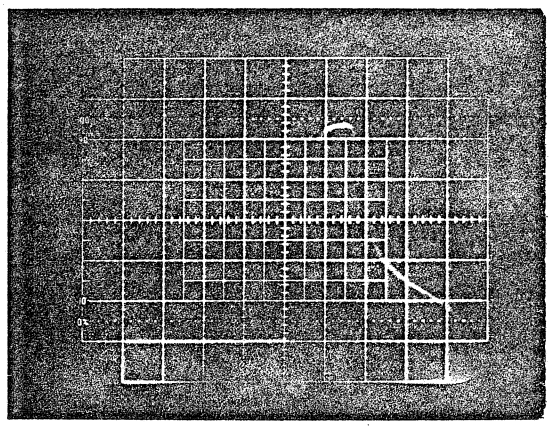

(a) 5 μ sec/division
6.8 mK/division
T_0 = 1.852° K

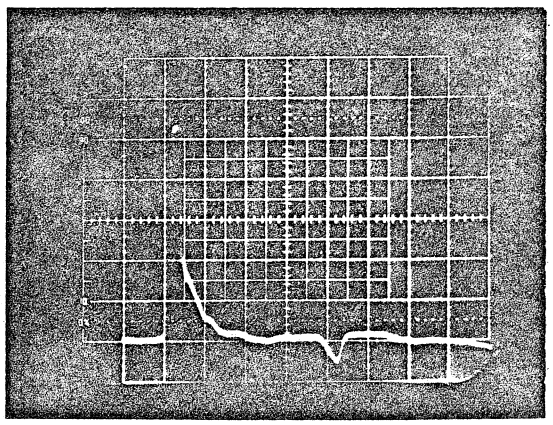

(b) 20 μ sec/division
6.8 mK/division
T_0 = 1.852° K

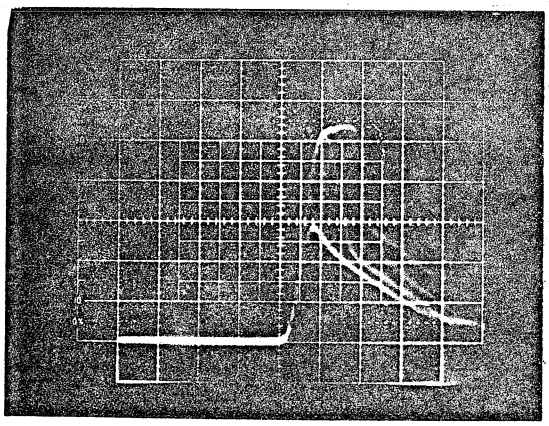

(c) 5 μ sec/division
6.8 mK/division
T_0 = 1.852° K

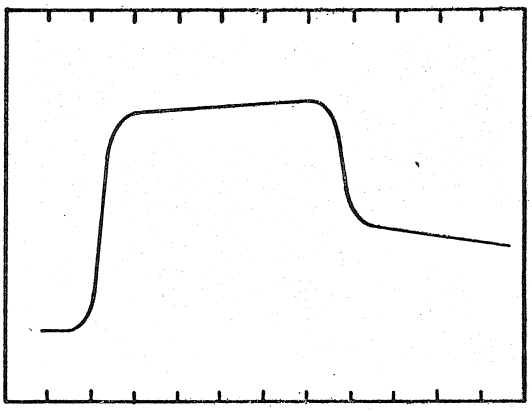

(d) 1 μ sec/division

T_0 = 1.849° K

Figure 6.9 DOUBLE-SHOCKS FORMED BY WAVE MODIFICATION

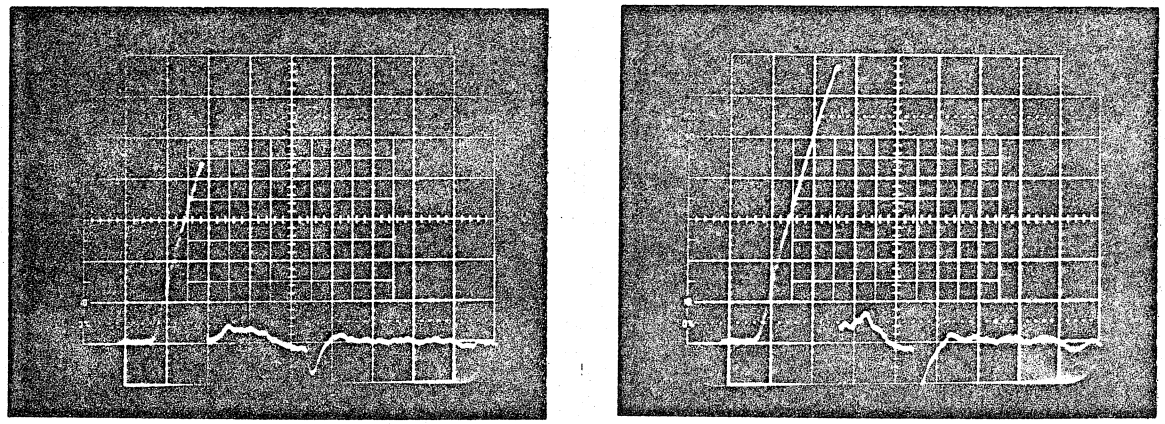

(a) Simply Formed
1.3 mK/division

(b) Simply Formed
1.3 mK/division

20 μ sec/division

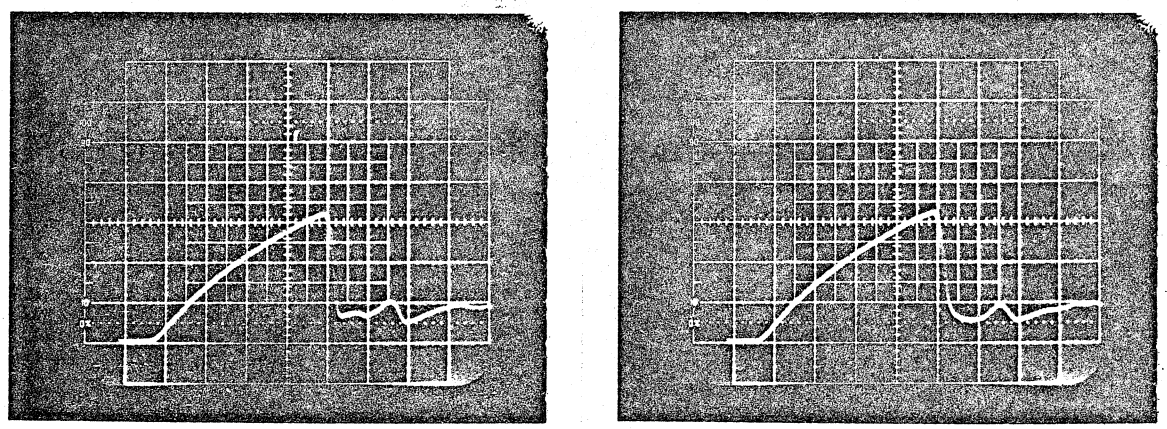

(c) Shock Limited
5.2 mK/division

(d) Shock Limited
5.2 mK/division

Figure 6.10 BACK STEEPENED SHOCKS ATTAINING THE SHOCK LIMIT (T_o = 1.951° K)

possess any steep gradients before the temperature lowering shock is encountered. Because of this shape, the natural decay of the emerging shock pulse is slow and an accurate value of the maximum temperature amplitude can be obtained. From this the maximum relative velocity was calculated to be 1.60 m/sec.

The first signals of breakdown, clearly visible for the front steepened shocks, are masked by the leading expansion wave in the present case. However, the convex shape of shock limited profiles indicates that breakdown began slowly at a temperature amplitude below the shock limit (recall that the profile of a simply formed expansion fan would be triangular).

Finally, note that the thickness of the temperature lowering shock appears to grow when the shock limit is attained. Since these results are only preliminary, one can only speculate as to their meaning. However, could it be that superfluid vortices, generated in the temperature raising expansion wave at some critical velocity, are causing the shock front to ripple? Whether or not these shock pulses were supercritical could not be ascertained since they were not generated in the variable length shock tube. Further research should prove interesting.

Chapter 7. CONCLUSIONS

The ability of second-sound shock waves to produce and measure large relative velocities away from walls has been successfully demonstrated. The fact that second-order theory has been verified up to the maximum temperature amplitudes generated allows one to accurately and unobtrusively obtain the shock-induced relative velocity by measuring either the shock Mach number or shock strength. The problems originally encountered when measuring the temperature amplitude with superconducting thin-films have been resolved, and techniques allowing one to calibrate these sensors and to measure the shock velocity to five significant figures have been developed and demonstrated.

The breakdown of superfluidity was found to occur upon formation in a region close to the heater. Many of the processes involved, including boiling and wave modification, have been identified, and the causes of amplitude decay and wave advance with increasing heater power have been found. Unfortunately, the mechanism triggering the breakdown could not be positively identified; it may be an intrinsic critical velocity, or it may be related to nucleate boiling on the heater face, or even some other unidentified mechanism.

However, not being able to positively identify the observed breakdown of superfluidity as a critical velocity triggered phenomena does not detract from the significance of the results obtained: the maximum shock-induced relative velocity is as large as those formerly obtained only in highly restricted geometries. Figure 7.1 shows the maximum obtained shock-induced relative velocity with

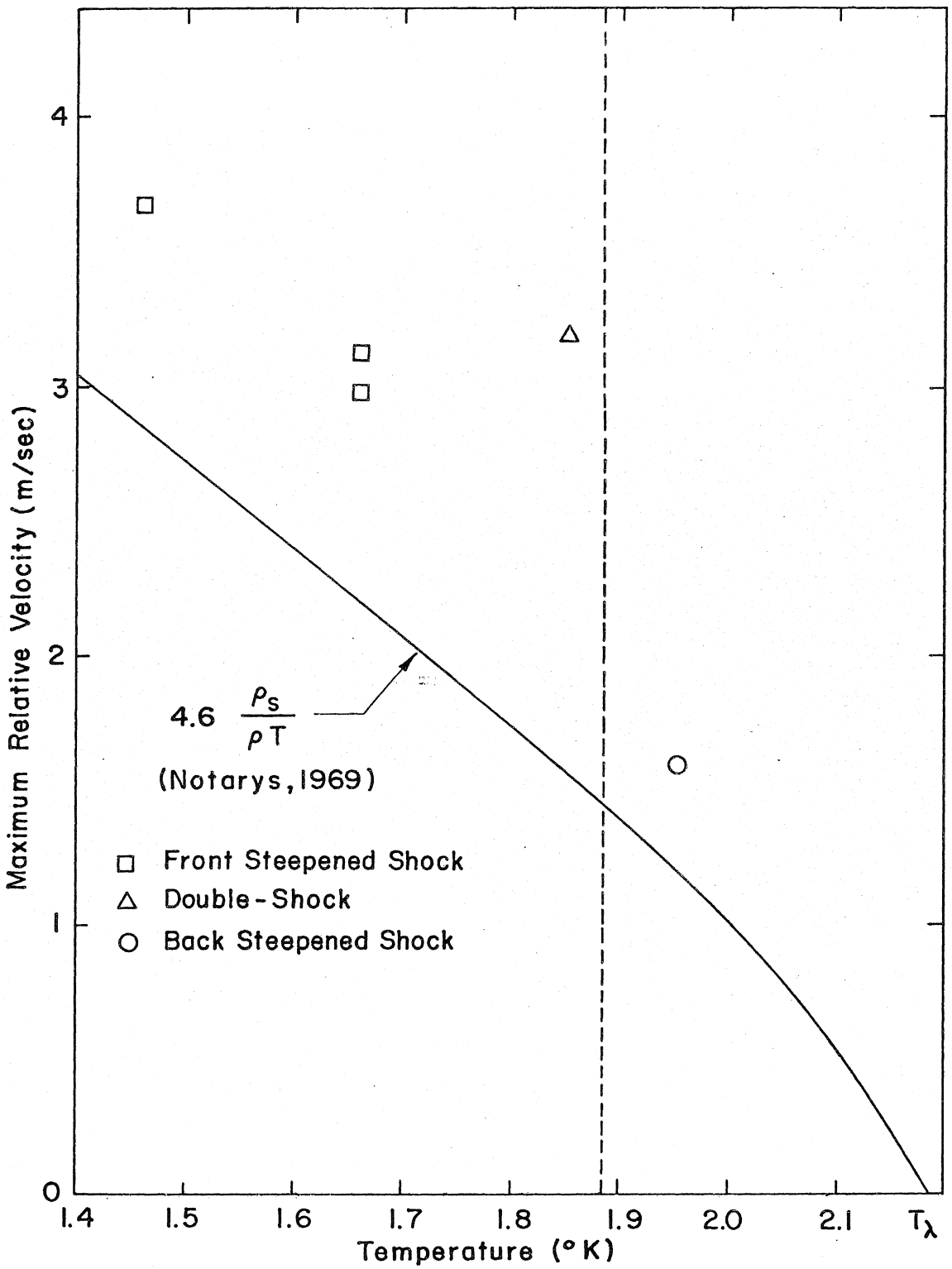

Figure 7.1 MAXIMUM SHOCK-INDUCED RELATIVE VELOCITY

respect to the initial fluid temperature. Also plotted is the intrinsic relative velocity measured by Notarys (1969) in 200 to 800 Å wide pores. The present results, which represent a lower bound to the fundamental or true intrinsic critical velocity, show a temperature dependent decline as T_λ is approached, and they are somewhat larger than the critical velocities reported in microscopic pores.

Pressurized experiments now underway should be able to determine if the breakdown is triggered by boiling. If it is, then pressurizing the test section above the critical pressure of liquid helium (2.29 bar) will eliminate its interference so that the fundamental critical velocity can be identified. However even when this is done the breakdown will still occur near the heater where the shock is formed. Ultimately this problem can be eliminated by strengthening the shock wave in converging channels -- a process which will move the spatial location of breakdown away from the heater.

In conclusion, it is evident that second-sound shock waves, used as a tool to probe the mutual interactions between the two-fluid components of helium II, can provide the clearest picture of the fundamental critical velocity phenomenon that has ever been obtained.

Appendix A. THE EQUILIBRIUM THERMODYNAMICS OF LIQUID HELIUM II

The state of a system consisting of an ordinary homogeneous fluid in thermodynamic equilibrium can be described by three variables: the total mass of the system, M; the total volume, V; and the total entropy S. The change in total internal energy, E = E(S,V,M), can then be written as:

$$dE = \left(\frac{\partial E}{\partial S}\right)_{V,M} dS + \left(\frac{\partial E}{\partial V}\right)_{S,M} dV + \left(\frac{\partial E}{\partial M}\right)_{S,V} dM \qquad (A.1)$$

The partial derivatives in this statement can be identified with the temperature, T, negative of the pressure, p, and the chemical potential, μ. With these substitutions the fundamental thermodynamic identity results:

$$dE = TdS - pdV + \mu dM \qquad (A.2)$$

The three variables, S, V, and M, which have been chosen to describe the system are not independent, because they are all proportional to the mass of the system (that is, they are extensive variables). Thus a homogeneous fluid system can be described by two independent variables--for example the specific entropy, s = S/M, and the density, ρ = M/V. Also since the internal energy is an extensive quantity, the thermodynamic identity can be easily integrated as follows:

$$\lambda E(S,V,M) = E(\lambda S, \lambda V, \lambda M)$$

$$d(\lambda E) = T\, d(\lambda S) - p d(\lambda V) + \mu d(\lambda M)$$

$$\lambda dE + E d\lambda = (TdS - pdV + \mu dM)\lambda + (TS - pV + \mu M)d\lambda$$

Since λ is arbitrary this last equation implies:

$$E = TS - pV + \mu M \tag{A.3}$$

It is often convenient to express the thermodynamic state of a system in variables other than the entropy, volume, and mass. This is simply done by forming a new thermodynamic potential from the internal energy via a Legendre transformation. For helium II it will be convenient to take the temperature and pressure as independent variables. To do this, the Gibb's free energy, defined as

$$G \equiv E - TS + pV = \mu M \tag{A.4}$$

becomes the thermodynamic potential describing the system. The thermodynamic identity written in terms of this potential becomes:

$$dG = dE - TdS - SdT + pdV + Vdp$$

$$dG = Vdp - SdT + \mu dM \tag{A.5}$$

Written in terms of specific variables and cancelling the μdM terms results in the Gibbs-Duhem relation:

$$d\mu = \frac{1}{\rho} dp - sdT \tag{A.6}$$

The thermodynamic principles which have been applied to an ordinary fluid can equally well be applied to helium II. The major difference between the two systems is that for an ordinary homogeneous fluid there is always a coordinate frame in which the macroscopic velocity of the fluid is zero, whereas for helium II no such frame

exists. This fluid, in general, executes two distinct simultaneous motions, corresponding to the superfluid and normal fluid velocities; this means that there will always be a velocity dependence intrinsic in the thermodynamic functions. The velocity which naturally appears is the relative velocity, w, because it is the difference between two velocity fields ($\vec{w} \equiv \vec{v}_n - \vec{v}_s$) and therefore it is an invariant quantity with respect to a Galilean transformation. Liquid helium is isotropic; therefore, the thermodynamic state of a fluid particle cannot depend on the direction of $\vec{w}$, but only on its magnitude. This means that the velocity parameter which enters into the thermodynamics is actually the scalar product of the relative velocity with itself, w^2.

The coordinate frame in which the motions of helium II are the simplest is the frame in which the superfluid component is at rest, called the "superfluid frame". In this frame only the excitations comprising the normal fluid component are in motion. The macroscopic average of these motions is the normal fluid velocity, which in this frame is $\vec{w}$. The frame of reference in which one customarily views helium II is the "laboratory frame" where the superfluid velocity is $\vec{v}_s$ and the normal fluid velocity is $\vec{w} + \vec{v}_s = \vec{v}_n$.

In the superfluid frame the total energy, E_0, is a function of entropy, volume, mass, and the internal momentum due to the macroscopic normal fluid motion: $E_0 = E_0 (S, V, M, J_0)$. A change in the internal energy can be expanded in terms of these variables just as was done for an ordinary fluid:

$$dE_0 = TdS - pdV + \mu dM + \vec{w} \cdot d\vec{J}_0 \tag{A.7}$$

where

$$T = \left(\frac{\partial E}{\partial S}\right)_{V,M,\vec{J}_0}$$

$$p = -\left(\frac{\partial E}{\partial V}\right)_{S,M,\vec{J}_0}$$

$$\mu = \left(\frac{\partial E}{\partial M}\right)_{S,V,\vec{J}_0}$$

$$\vec{w} = \left(\frac{\partial E}{\partial \vec{J}_0}\right)_{S,V,M}$$

Since the internal momentum, $\vec{J}_0$, is an extensive variable like, S, V, M, and E_0, equation (A.7) can easily be integrated to the following form:

$$E_0 = TS - pV + \mu M + \vec{w} \cdot \vec{J}_0 \tag{A.8}$$

It is usually more convenient to work with the energy density, $\varepsilon_0 = E_0/V$. Equation (A.8) divided by the volume and written in terms of specific quantities becomes:

$$\varepsilon_0 = \rho s T - p + \mu\rho + \vec{w} \cdot \vec{J}_0 \tag{A.9}$$

Equation (A.7) can also be rewritten in this form by writing the extensive variables as densities times the volume and then expanding the differentials:

$$d\varepsilon_0 = T\, d(\rho s) + \mu d\rho + \vec{w} \cdot d\vec{J}_0 \tag{A.10}$$

The internal momentum density, as seen in the superfluid frame, can be identified as the product of the normal fluid velocity with a

normal fluid density:

$$\vec{j}_0 = \rho_n \vec{w} \tag{A.11}$$

which is simply the defining relationship for the normal fluid mass density, ρ_n.

In order to transform the thermodynamics into the laboratory frame a Galilean transformation is required, and the transformation for energy density is (Landau and Lifshitz, 1959, chapter 16):

$$\varepsilon = \varepsilon_0 + \tfrac{1}{2}\rho v_s^2 + \vec{v}_s \cdot \vec{j}_0 \tag{A.12}$$

Substituting in for ε_0 and $\vec{j}_0$, expanding, and then collecting terms, yields the following result for total energy density in the laboratory frame:

$$\varepsilon = \rho s T - p + \mu\rho + \tfrac{1}{2}\rho_n w^2 + \tfrac{1}{2}\rho_s v_s^2 + \tfrac{1}{2}\rho_n v_n^2 \tag{A.13}$$

If a specific internal energy, e, is defined by the following equation:

$$\rho e \equiv \rho s T - p + \mu\rho + \tfrac{1}{2}\rho_n w^2 \tag{A.14}$$

then the total energy density may be written in a more familiar form:

$$\varepsilon = \rho e + \tfrac{1}{2}\rho_s v_s^2 + \tfrac{1}{2}\rho_n v_n^2 \tag{A.15}$$

As stated earlier, it is convenient to write the fundamental thermodynamic identity in terms of the chemical potential. This can be done with the equations written for the superfluid frame by taking the differential of equation (A.9) and then using (A.10) to eliminate terms. The result is a relationship which happens to be valid in any

coordinate frame, since all the variables are frame invariant quantities:

$$d\mu = \frac{1}{\rho} dp - s dT - \tfrac{1}{2} \frac{\rho_n}{\rho} dw^2 \tag{A.16}$$

This last equation expresses the fact that the complete thermodynamics of helium II are known if the chemical potential is known as a function of pressure, temperature and relative velocity squared. Other thermodynamic variables are identified in the usual way as derivatives of the chemical potential:

$$s = -\left(\frac{\partial \mu}{\partial T}\right)_{p,w^2} \tag{A.17a}$$

$$\frac{1}{\rho} = \left(\frac{\partial \mu}{\partial p}\right)_{T,w^2} \tag{A.17b}$$

$$\xi \equiv \frac{\rho_n}{\rho} = -2\left(\frac{\partial \mu}{\partial w^2}\right)_{p,T} \tag{A.17c}$$

The major problem that remains is to determine the chemical potential as a function of w^2. Experimentally μ has only been determined as a function of pressure and temperature with w equal to zero, because it has not been possible to measure the dependence on w^2 consistently. This is because moving the fluid to get the required w inevitably introduces hydrodynamic effects, such as turbulence, which mask the thermodynamic effects. Using second-sound shock waves to generate uniform relative velocities may be the one way to experimentally determine the thermodynamic dependence on w^2, but this endeavor must be left for the future.

The relative velocity dependence in the limit of vanishing w, can be deduced theoretically by expanding the chemical potential in terms of w^2:

$$\mu(p,T,w^2) = \mu(p,T)_{w=0} + \left(\frac{\partial\mu}{\partial w^2}\right)_{p,T,w=0} w^2 \quad . \quad . \quad . \qquad (A.18)$$

Using previous results to identify the coefficient of the w^2 term leads to the following equation:

$$\tilde{\mu}(p,T,w^2) = \mu(p,T) - \tfrac{1}{2}\xi(p,T)w^2 + O(w^4) \qquad (A.19)$$

In this expansion, and those to follow, there needs to be a distinction between the quantities which show the full dependence on p, T, and w^2, and those that are evaluated at w = 0. The former type will be accompanied by a tilde, whereas the latter, which are the quantities that are measured experimentally, will be left unadorned. The expansions for the entropy and density proceed in the same manner with the partial derivatives being evaluated by "Maxwell relations":

$$\left(\frac{\partial s}{\partial w^2}\right)_p = -\left(\frac{\partial^2\mu}{\partial T\partial w^2}\right)_p = -\frac{\partial}{\partial T}\left(-\tfrac{1}{2}\xi\right) \equiv \tfrac{1}{2}\xi_T \qquad (A.20)$$

$$\left(\frac{\partial 1/\rho}{\partial w^2}\right)_T = \left(\frac{\partial^2\mu}{\partial p\partial w^2}\right)_T = \frac{\partial}{\partial p}\left(-\tfrac{1}{2}\xi\right) \equiv -\tfrac{1}{2}\xi_p \qquad (A.21)$$

The equations for entropy and density expanded to first order in w^2 are therefore:

$$\tilde{s}(p,T,w^2) = s(p,T) + \tfrac{1}{2}\xi_T(p,T)w^2 + O(w^4) \qquad (A.22)$$

$$\frac{1}{\tilde{\rho}(p,T,w^2)} = \frac{1}{\rho(p,T)} - \tfrac{1}{2}\xi_p(p,T)w^2 + O(w^4) \qquad (A.23)$$

Finally it is usually assumed, with some experimental verification, that the normal fluid fraction is independent of the relative velocity to lowest order:

$$\left(\frac{\tilde{\rho}_n}{\rho}\right)(p,T,w^2) = \left(\frac{\rho_n}{\rho}\right)(p,T) + O(w^4) \qquad (A.24)$$

Appendix B. LINEAR WAVES IN HELIUM II

The properties of reversible first- and second-sound, in the limit of infinitesimal amplitude, can be calculated from the linearized, dissipationless, two-fluid equations. Linearization is accomplished by a perturbation expansion from the steady, rest state of the fluid, with terms higher than second order in the perturbation quantities ignored. These quantities will be denoted by primes while steady state values are left unadorned. The resulting four equations are shown below (note that the energy equation is replaced by conservation of entropy since all processes are assumed reversible):

$$\frac{\partial \rho'}{\partial t} + \rho \nabla \cdot \vec{v}' = 0 \tag{B.1}$$

$$\frac{\partial \vec{v}'}{\partial t} + \frac{1}{\rho} \nabla p' = 0 \tag{B.2}$$

$$\frac{\partial \vec{w}'}{\partial t} + \frac{\rho S}{\rho_n} \nabla T' = 0 \tag{B.3}$$

$$\rho \frac{\partial S'}{\partial t} + \rho_s S \nabla \cdot \vec{w}' = 0 \tag{B.4}$$

Now consider the important case of one-dimensional or plane wave motion. The set of linear equations can be solved to get four characteristic velocities, which are the propagation velocities of linear waves. Two velocities are for first-sound waves traveling parallel or anti-parallel to the x-axis, which is defined normal to the wave front. The remaining two velocities relate to the propagation of second-sound.

It is well known that a complex plane wave field can be described

by a superposition of simple waves. Each simple wave is characterized by motion occurring only along one set of characteristics which can be completely described by a single dependent variable. To see how this occurs, examine the motion of an arbitrary dependent variable, f. The perturbation to f propagates at the wave velocity, u, so that its functional form in space and time can be written as:

$$f'(x,t) = f'(x - ut) = f'(\xi)$$

The partial derivatives of this perturbation quantity are:

$$\frac{\partial}{\partial t} f' = - uf_{\xi}' \tag{B.5}$$

$$\frac{\partial}{\partial x} f' = f_{\xi}' \tag{B.6}$$

Applying these results to the basic differential equations results in relations between dependent variables. For example, an application to the momentum equation (B.2) results in:

$$- uv_{\xi}' + \frac{1}{\rho} p_{\xi}' = 0$$

Integrate this with respect to ξ and note that the integration constant is zero since p' and v' are, by definition, perturbations from an equilibrium rest state. The final result is:

$$v' = \frac{p'}{\rho u}$$

This technique can be applied to each of the basic four equations stated previously, and to two additional relations in which the dependence of velocities v' and w' is eliminated (see Equations B.7 and

B.8). It should be noted from these results, presented in Table B.1, that positive pressure and temperature excursions produce perturbation velocities, v' and w', which always head in the direction of the wave propagation for both first and second sound. If the excursions are negative the fluid and propagation velocities are oppositely directed.

$$\frac{\partial^2 \rho'}{\partial t^2} - \nabla^2 p' = 0 \tag{B.7}$$

$$\frac{\partial^2 S'}{\partial t^2} - \frac{\rho_s}{\rho_n} S^2 \nabla^2 T' = 0 \tag{B.8}$$

With the aid of the thermodynamic relations below, equation B.7 and B.8 can be reexpressed as a set of two coupled wave equations (B.12 and B.13).

$$d\rho = \frac{\gamma}{c_0^2} dp - \rho\beta dT \tag{B.9}$$

$$dS = \frac{C_p}{T} dT - \frac{\beta}{\rho} dp \tag{B.10}$$

$$\gamma = 1 + \frac{T\beta^2}{C_p} c_0^2 \tag{B.11}$$

where $\gamma \equiv C_p/C_v$

$$\beta \equiv \frac{1}{V}\left(\frac{\partial V}{\partial T}\right)_p , \qquad V = \text{volume}$$

$$c_0 \equiv \sqrt{\left(\frac{\partial p}{\partial \rho}\right)_S}$$

$$\gamma \frac{\partial^2 p'}{\partial t'} - \rho\beta c_0^2 \frac{\partial T'}{\partial t^2} - c_0^2 \nabla^2 p' = 0 \qquad \text{(B.12)}$$

$$\frac{\rho C_p}{\beta T} \frac{\partial^2 T'}{\partial t^2} - \frac{\partial^2 p'}{\partial t^2} - \frac{\rho C_p}{\beta T} a_0^2 \nabla^2 T' = 0 \qquad \text{(B.13)}$$

where $a_0 \equiv \sqrt{\frac{\rho_s}{\rho_n} \frac{S^2 T}{C_p}}$

Note that coupling is achieved solely via the coefficient of thermal expansion, which approaches zero at very low temperatures. Therefore, in many instances, the coupling between pressure and temperature may be neglected. In this case first-sound is purely a pressure and density wave traveling at the speed c_0. Similarily second-sound is an unadulterated temperature and entropy wave propagating with speed a_0.

For now however, the coefficient of thermal expansion will be asssumed not zero, but small. Thus, first-sound waves will also produce temperature and entropy variations, while second-sound waves will correspondingly display pressure and density perturbations. The wave speeds, which are altered slightly by this coupling, may be calculated by the method of characteristics applied to the last equation set. To do this the first equation is multiplied by an arbitrary constant parameter and added to the second. For convenience, the constant parameter will be chosen λ/ε, where ε is small ($\varepsilon \equiv \gamma - 1 = O(\beta^2)$) and λ is to be determined.

$$\frac{1}{\varepsilon}(\lambda\gamma - \varepsilon)\left[\frac{\partial}{\partial t^2} - \frac{c_0^2\lambda}{\lambda\gamma - \varepsilon}\nabla^2\right]p' \qquad (B.14)$$

$$+ \frac{\rho C_p}{\beta T}(1 - \lambda)\left[\frac{\partial}{\partial t^2} - \frac{a_0^2}{1 - \lambda}\nabla^2\right]T' = 0$$

This equation can be put in characteristic form if the propagation velocities for both p' and T' are real and equal, namely:

$$u^2 = \frac{c_0^2\lambda}{\lambda\gamma - \varepsilon} = \frac{a_0^2}{1 - \lambda} \qquad (B.15)$$

This can be solved for the parameter λ to get two solutions:

$$\lambda_+ = 1 - \frac{a_0^2}{c_0^2} + \varepsilon\frac{a_0^2}{c_0^2}\frac{a_0^2}{c_0^2 - a_0^2} + O(\varepsilon^2)$$

$$\lambda_- = -\frac{\varepsilon a_0^2}{c_0^2 - a_0^2} + O(\varepsilon^2)$$

When these results are substituted back into (B.15) the wave speeds to first order in ε are obtained (recall that $\varepsilon \equiv \gamma - 1$):

$$u_-^2 = a_0^2\left\{1 - \varepsilon\frac{a_0^2}{c_0^2 - a_0^2} + O(\varepsilon^2)\right\} \qquad (B.16)$$

$$u_+^2 = c_0^2\left\{1 + \varepsilon\frac{a_0^2}{c_0^2 - a_0^2} + O(\varepsilon^2)\right\} \qquad (B.17)$$

Finally to complete the analysis, it is necessary to calculate the relationship between the pressure and temperature perturbations for both first- and second sound waves. This is done by eliminating ρ' and S' in the thermodynamic expansions (B.9 and B.10), with the previous results already tabulated, to obtain:

$$\left[\gamma - \frac{c_0^2}{u^2} \right] p' = \rho\beta c_0^2 T' \qquad \text{(B.18)}$$

$$\left[1 - \frac{a_0^2}{u^2} \right] T' = \frac{\beta T}{\rho C_p} p' \qquad \text{(B.19)}$$

Inserting the wave velocities to order ε, the p':T' relations can be calculated to the same order. These results are compiled with those obtained previously, in Table B.1, which provides a convenient summary of this section.

It is interesting to note that a positive pressure first-sound wave generates a negative temperature excursion for temperatures above 1.2^{o}K which occurs because the coefficient of thermal expansion of liquid helium is negative. This also accounts for the fact that a positive temperature second-sound wave generates a positive pressure perturbation.

Table B.1 SIMPLE LINEAR PLANE WAVES IN HELIUM II AT REST

PERTURBATION QUANTITIES:

$$\vec{v}' = \frac{p'}{\rho \vec{u}} \qquad \vec{w}' = \frac{\rho S}{\rho_n} \frac{T'}{\vec{u}}$$

$$\rho' = \frac{p'}{u^2} \qquad S' = \frac{C_p}{T} \frac{a_0^2}{u^2} T'$$

$$T' = \beta \frac{T}{C_p} \left(\frac{c_0^2}{c_0^2 - a_0^2} \right) \frac{p'}{\rho} + O(\beta^2) \qquad \text{(first sound)}$$

$$p' = -\beta\rho \left(\frac{c_0^2 a_0^2}{c_0^2 - a_0^2} \right) T' + O(\beta^2) \qquad \text{(second sound)}$$

WAVE VELOCITIES:

First-sound: $\vec{u} = \vec{c}$

Second-sound: $\vec{u} = \vec{a}$

where:
$$c^2 = c_0^2 \left\{ 1 + (\gamma - 1) \left(\frac{a_0^2}{c_0^2 - a_0^2} \right) + O(\gamma - 1)^2 \right\}$$

$$a^2 = a_0^2 \left\{ 1 - (\gamma - 1) \left(\frac{a_0^2}{c_0^2 - a_0^2} \right) + O(\gamma - 1)^2 \right\}$$

$$c_0 \equiv \sqrt{\left(\frac{\partial p}{\partial \rho} \right)_S} \qquad a_0 \equiv \sqrt{\frac{\rho_s}{\rho_n} \frac{S^2 T}{C_p}}$$

$$\gamma \equiv C_p / C_v = 1 + \frac{T\beta^2}{C_p} c_0^2$$

Appendix C. THEORETICAL STRUCTURE OF WEAK SECOND-SOUND SHOCK WAVES

Calculation of shock waves in a complex medium such as helium II can be done using techniques from singular perturbation theory. The solution sought is one consisting of two equilibrium states which are connected by a thin shock layer or shock front. The jump conditions between the two equilibrium states form the outer solution, which is gotten by neglecting all the dissipative terms. These terms are zero in the outer solution since there are no gradients in any of the dependent variables in the equilibrium states. Gradients do exist and are important in the shock layer. In fact, it is the balance between the dissipative terms and the nonlinear steepening terms which governs the shock structure.

The model of helium II, which serves as a starting point for the following calculations, is the two-fluid theory as set down by Landau (1941). The derivation begins by integrating the steady, one-dimensional equations for a superfluid and then evaluating the constants of integration using values for one of the equilibrium states. This results in the shock equations presented in Tables C.2 and C.3. Next the shock equations, in the linearized dissipationless approximation, are solved to obtain solutions for steady, first- and second-sound waves. These results are used to simplify the solution of the second-order equations which eventually yield the shock velocity and the jump conditions to second order.

In the shock layer the gradients become so large that even though the kinetic coefficients are small, their products are dominant

terms in the equations. These dissipative terms are of order $(T')^2 \sim w^2$; that is they are second order in the characterizing variables for second-sound. Therefore, to balance these terms, the shock equations must be solved with all the other second order terms being retained. The order of the dissipative terms depends on the fact that for weak shock waves, the shock thickness is inversely proportional to the shock strength, $\Delta\theta$, which will be taken as the temperature jump normalized by an equilibrium state temperature. The shock layer must therefore be scaled by $1/\Delta\theta$, which means the derivative with respect to the spatial dimension, x, must be order $\Delta\theta$. Since the temperature and velocity perturbations are also of this order their derivatives must be order $(\Delta\theta)^2 \propto w^2$. Although these relations are true for weak shock waves in any substance, there validity for second-sound shock waves will be reaffirmed by direct calculation.

DERIVING THE SHOCK EQUATIONS

Calculation of shock wave jump conditions traditionally make use of conservation equations for mass, momentum, and energy; these quantities are conserved from one equilibrium state to the other across the shock, even though the details within the shock itself may be unknown. The same approach is applicable to temperature shocks in helium II, except in this case an additional equation describing the superfluid velocity field must be included.

The major problem arising when calculating the shock conditions in helium II is caused by the thermodynamics of the liquid, which are not completely known due to their intrinsic dependence on the relative velocity between the two fluids. The only recourse to date has been to expand the thermodynamics in terms of the relative velocity, which must be assumed small in some sense. This was done by Landau and is reproduced in Appendix A. It should be noted that the thermodynamics are expansions in the square of the relative velocity and that only the coefficients for the terms second order in w are known. This makes it possible to solve the shock equations to third order in w, but no higher. Since w is a first order quantity in a second-sound shock wave, this necessarily means that the results to be obtained are valid only for weak temperature shocks.

The following derivations are done in the reference frame which travels along with the shock wave -- the shock-stationary frame. In this reference frame the shock profile is assumed steady. In the laboratory frame, where the undisturbed fluid is at rest, the shock

will be traveling in the positive x-direction. In the shock-stationary frame the mass flux, $\vec{j}$, therefore will be in the negative x-direction.

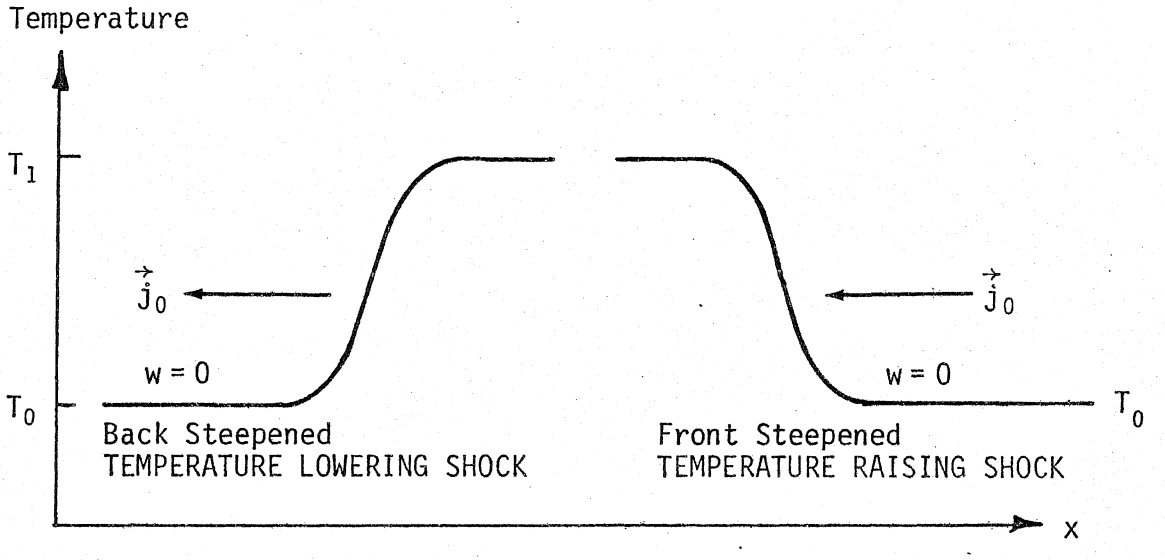

Figure C.1. SECOND-SOUND SHOCK LAYER PROFILES

The shock profiles for two types of temperature shocks possible in helium II are shown in Figure C.1. The front steepened one is a temperature raising shock in which the entropy density following the shock is greater than before it. The back steepened one is a temperature lowering shock; in this case the entropy density is decreased following passage of the shock front.

In the chosen reference frame the applicable equations describing a plane shock wave are the steady, one-dimensional form of the conservation equations previously mentioned. This set of equations is reproduced as Table C.1. The dissipative effects are included so that a shock profile and thickness can be calculated. The form of the dissipative terms follows from a consistent derivation made by

Table C.1. THE STEADY, ONE-DIMENSIONAL FORM OF THE TWO-FLUID EQUATIONS INCLUDING DISSIPATION

MASS:
$$\frac{d}{dx} j = 0$$

MOMENTUM:
$$\frac{d}{dx}\left[\tilde{\rho} v^2 + \frac{\tilde{\rho}_n \tilde{\rho}_s}{\tilde{\rho}} w^2 + p + \tau^*\right] = 0$$

SUPERFLUID:
$$\frac{d}{dx}\left[\tilde{\mu} + \frac{1}{2} v_s^2 + h^*\right] = 0$$

ENERGY:
$$\frac{d}{dx}\left[j\left(\tilde{\mu} + \frac{1}{2} v_s^2\right) + \tilde{\rho}\tilde{S}T v_n + \tilde{\rho}_n v_n^2 w + Q^*\right] = 0$$

where:
$$j \equiv \tilde{\rho} v \equiv \tilde{\rho}_n v_n + \tilde{\rho}_s v_s$$

$$w \equiv v_n - v_s$$

$$\tau^* = -\left(\frac{4}{3}\eta + \zeta_2\right)\frac{dv_n}{dx} + \zeta_1 \frac{d}{dx}\left(\tilde{\rho}_s w\right)$$

$$h^* = \zeta_3 \frac{d}{dx}\left(\tilde{\rho}_s w\right) - \zeta_1 \frac{dv_n}{dx}$$

$$Q^* = -\kappa \frac{dT}{dx} - \left(\frac{4}{3}\eta + \zeta_2\right) v_n \frac{dv_n}{dx} + \zeta_1 \tilde{\rho}_s w \frac{dv_n}{dx}$$

$$+ \zeta_1 v_n \frac{d}{dx}\left(\tilde{\rho}_s w\right) - \zeta_3 \tilde{\rho}_s w \frac{d}{dx}\left(\tilde{\rho}_s w\right)$$

Khalatnikov (1965, chapter 9) which requires the assumption that the superfluid is free of vorticity; this is no restriction in the analysis which follows.

The one-dimensional equations are easily integrated and the constants of integration are evaluated for the equilibrium state where the relative velocity is zero. This state will be indicated by a subscript zero. The other equilibrium state will be denoted by a subscript one. Unsubscripted variables will be considered as a function of x. For example, the integrated equation for mass conservation is:

$$j \equiv \tilde{\rho} v = - \rho_0 U_S \tag{C.1}$$

This can be solved for the bulk velocity, v, to get:

$$v = \frac{-\rho_0}{\tilde{\rho}} U_S = - \frac{\rho_0}{\rho} U_S + \tfrac{1}{2} \rho_0 U_S w^2 \xi_p + O(w^4) \tag{C.2}$$

where the last step was to expand the density in terms of w^2. The thermodynamic variables without the tilde are functions only of pressure and temperature. The other three equations can be integrated and expanded in terms of w^2; then the bulk velocity, v, can be eliminated by use of the previous formula. The resulting "shock equations" can be found in Table C.2. Two equations which are linear combinations of the three original shock equations and which are useful when calculating second-sound shock waves are presented in Table C.3.

The same procedure of expanding in the relative velocity and then eliminating any bulk velocity dependence must also be applied to the dissipative terms, τ^*, h^*, and Q^*. From the definition of v_n

we have:

$$v_n \equiv v + \frac{\tilde{\rho}_s}{\tilde{\rho}} w = v + \frac{\rho_s}{\rho} w + O(w^4)$$

By using equation (C.2), the normal fluid velocity can be expanded in terms of w and the shock velocity with the result:

$$v_n = -\frac{\rho_0}{\rho} U_S + \frac{\rho_s}{\rho} w + \tfrac{1}{2}\rho_0 U_S w^2 \xi_p + O(w^4) \qquad (C.3)$$

When calculating the derivatives, use will be made of the fact that the shock thickness is inversely proportional to the shock strength. For second-sound shocks this means that the spatial dimension, x, is scaled by w^{-1}:

$$\frac{d}{dx} \sim w$$

With this simplification, the normal velocity gradient written out to third order in w is:

$$\frac{d}{dx} v_n = \left(\rho_s w - \rho_0 U_S\right) \frac{d}{dx} \frac{1}{\rho} + \frac{1}{\rho} \frac{d}{dx} \rho_s w + \tfrac{1}{2}\rho_0 U_S \frac{d}{dx} \xi_p w^2 + O(w^4) \qquad (C.4)$$

The product of the normal velocity with equation (C.4) is:

$$v_n \frac{dv_n}{dx} = \frac{\rho_0}{\rho} U_S \left(\rho_0 U_S - 2\rho_s w\right) \frac{d}{dx} \frac{1}{\rho} + \frac{1}{\rho^2} \left(\rho_s w - \rho_0 U_S\right) \frac{d}{dx} \rho_s w$$
$$- \left(\tfrac{1}{2}\rho_0 U_S^2\right) \frac{\rho_0}{\rho} \frac{d}{dx} \xi_p w^2 + O(w^4) \qquad (C.5)$$

These results allow for further expansion and simplification of the kinetic fluxes which are valid for second-sound shocks. These expansions are reproduced in Table C.4.

Table C.2. SHOCK EQUATIONS*

MOMENTUM

$$\frac{p-p_0}{\rho U_S^2} = \left(1 - \frac{\rho_0}{\rho}\right)\frac{\rho_0}{\rho} - \left[\frac{\rho_n\rho_s}{\rho^2} - \frac{\rho_0}{\rho}\left(\tfrac{1}{2}\rho_0 U_S^2 \xi_p\right)\right]\left(\frac{w}{U_S}\right)^2 - \frac{\tau^*}{\rho U_S^2} + O(w^4)$$

SUPERFLUID

$$\frac{\mu-\mu_0}{U_S^2} = \tfrac{1}{2}\left[1 - \left(\frac{\rho_0}{\rho}\right)^2\right] - \frac{\rho_n}{\rho}\frac{\rho_0}{\rho}\left(\frac{w}{U_S}\right) + \tfrac{1}{2}\left[\frac{\rho_n\rho_s}{\rho^2} + \frac{\rho_0}{\rho}\left(\rho_0 U_S^2 \xi_p\right)\right]\left(\frac{w}{U_S}\right)^2$$
$$+ \frac{1}{2}\frac{\rho_n}{\rho}\left(\rho_0 U_S^2 \xi_p\right)\left(\frac{w}{U_S}\right)^3 - \frac{h^*}{U_S^2} + O(w^4)$$

TOTAL ENERGY

$$\frac{ST - S_0T_0}{U_S^2} = \left[\left(\frac{\rho_0}{\rho}\right)^2 + \frac{\rho_s}{\rho_n}\frac{ST}{U_S^2}\right]\frac{\rho_n}{\rho_0}\frac{w}{U_S} - \left[2\frac{\rho_s}{\rho} + \tfrac{1}{2}\left(\frac{\rho}{\rho_n}T\xi_T\right)\right]\frac{\rho_n}{\rho}\left(\frac{w}{U_S}\right)^2$$
$$+ \left[\left(\frac{\rho_s}{\rho}\right)^2 + \tfrac{1}{2}\frac{\rho_s}{\rho_n}\left(T\xi_T + \rho ST\xi_p\right) - \frac{\rho_0}{\rho}\left(\rho_0 U_S^2 \xi_p\right)\right]\frac{\rho_n}{\rho_0}\left(\frac{w}{U_S}\right)^3$$
$$+ \frac{Q^*}{\rho_0 U_S^3} + \frac{h^*}{U_S^2} + O(w^4)$$

*Since these equations make use of the expanded thermodynamic functions, they are strictly valid only when the relative velocity is small.

Table C.3. SHOCK EQUATIONS USEFUL FOR SECOND SOUND SHOCK WAVES

"W" EQUATION

$$\left(\frac{\mu-\mu_0}{U_S^2}\right) - \left(\frac{p-p_0}{\rho U_S^2}\right) = \tfrac{1}{2}\left[1-\frac{\rho_0}{\rho}\right]^2 - \frac{\rho_n}{\rho}\frac{\rho_0}{\rho}\left(\frac{w}{U_S}\right) + \frac{3}{2}\frac{\rho_n\rho_s}{\rho^2}\left(\frac{w}{U_S}\right)^2 + \frac{1}{2}\frac{\rho_n}{\rho}\left(\rho_0 U_S^2 \xi_p\right)\left(\frac{w}{U_S}\right)^3 + \frac{\tau^*}{\rho U_S^2} - \frac{h^*}{U_S^2} + O(w^4)$$

MODIFIED ENERGY EQUATION

$$\frac{(\mu-\mu_0)}{U_S^2} + \frac{ST-S_0T_0}{U_S^2} - \frac{p-p_0}{\rho U_S^2} = \tfrac{1}{2}\left[1-\frac{\rho_0}{\rho}\right]^2 + \frac{\rho_s}{\rho_0}\frac{ST}{U_S^2}\left(\frac{w}{U_S}\right) - \tfrac{1}{2}\left[\frac{\rho_s}{\rho} + \left(\frac{\rho}{\rho_n}T\xi_T\right)\right]\frac{\rho_n}{\rho}\left(\frac{w}{U_S}\right)^2 + \frac{\rho_n}{\rho_0}\left[\left(\frac{\rho_s}{\rho}\right)^2 + \frac{1}{2}\frac{\rho_s}{\rho_n}\left(T\xi_T + \rho ST\xi_p\right) - \frac{1}{2}\frac{\rho_0}{\rho}\left(\rho_0 U_S^2 \xi_p\right)\right]\left(\frac{w}{U_S}\right)^3 + \frac{Q^*}{\rho_0 U_S^3} + \frac{\tau^*}{\rho U_S^2} + O(w^4)$$

Table C.4. DISSIPATIVE TERMS FOR SECOND-SOUND SHOCKS*

$$\tau^* = -\left(\frac{4}{3}\eta + \zeta_2\right)\left(\rho_s w - \rho_0 U_S\right)\frac{d}{dx}\frac{1}{\rho}$$

$$- \left(\frac{4}{3}\eta + \zeta_2 - \rho\zeta_1\right)\frac{1}{\rho}\frac{d}{dx}\rho_s w$$

$$- \tfrac{1}{2}\left(\frac{4}{3}\eta + \zeta_2\right)\rho_0 U_S \frac{d}{dx}\xi_p w^2 + O(w^4)$$

$$h^* = -\zeta_1\left(\rho_s w - \rho_0 U_S\right)\frac{d}{dx}\frac{1}{\rho}$$

$$- \left(\zeta_1 - \rho\zeta_3\right)\frac{1}{\rho}\frac{d}{dx}\rho_s w$$

$$- \tfrac{1}{2}\zeta_1 \rho_0 U_S \frac{d}{dx}\xi_p w^2 + O(w^4)$$

$$Q^* = -\kappa\frac{dT}{dx} - \left(\frac{4}{3}\eta + \zeta_2\right)\frac{\rho_0}{\rho}\left(\rho_0 U_S^2\right)\frac{d}{dx}\frac{1}{\rho}$$

$$+ 2\left(\frac{4}{3}\eta + \zeta_2 - \tfrac{1}{2}\rho\zeta_1\right)\frac{\rho_0}{\rho}\left(\rho_s w U_S\right)\frac{d}{dx}\frac{1}{\rho}$$

$$+ \left(\frac{4}{3}\eta + \zeta_2 - \rho\zeta_1\right)\frac{\rho_0 U_S}{\rho^2}\frac{d}{dx}\rho_s w$$

$$- \left(\frac{4}{3}\eta + \zeta_2 - 2\rho\zeta_1 + \rho^2\zeta_3\right)\frac{\rho_s w}{\rho^2}\frac{d}{dx}\rho_s w$$

$$+ \left(\frac{4}{3}\eta + \zeta_2\right)\frac{\rho_0}{\rho}\left(\tfrac{1}{2}\rho_0 U_S^2\right)\frac{d}{dx}\xi_p w^2 + O(w^4)$$

*These equations, besides being expansions in the relative velocity, make use of the fact that d/dx is of order w. Thus these equations are strictly valid only for weak second-sound shock waves.

LINEARIZED SOLUTIONS

Now since the shock waves under consideration are assumed small, the thermodynamic functions may be expanded further in terms of pressure and temperature perturbations, p' and T', defined by:

$$p \equiv p_0 + p'$$
$$T \equiv T_0 + T'$$

For liquid helium the coefficient of thermal expansion is very small, and it will be neglected in the calculations to follow. The assumption that the coefficient of thermal expansion is zero is equivalent to assuming that the entropy is a function only of temperature and that density is a function only of pressure. Also, the specific heat at constant pressure and volume are equivalent and will be denoted by C_p. Table C.5 lists a set of thermodynamic perturbations expansions when this assumption is invoked.

In order to see the role the various thermodynamic variables play in the two forms of shock wave motion occurring in helium II, a solution to the linearized equations will be sought first. To do this the shock equations of Table C.3 will be expanded in terms of the pressure and temperature perturbations with only linear terms being retained. Now to solve for the jump conditions, the perturbations p', and T', and w, will become the differences between the two equilibrium states:

$$p' \to p_1 - p_0 \equiv \Delta p$$
$$T' \to T_1 - T_0 \equiv \Delta T$$
$$w \to w_1 \equiv \Delta w$$

Table C.5. THERMODYNAMIC PERTURBATION EXPANSIONS*

Independent variables:

$$p = p_0 + p' \qquad T = T_0 + T'$$

where $\frac{p'}{p_0} << 1$ and $\frac{T'}{T_0} << 1$

Expansions of dependent variables:

$$\mu(p,T) = \mu_0 - S_0 T' + \frac{1}{\rho_0} p' - \left(\frac{C_p}{T}\right)_0 \frac{(T')^2}{2} - \left(\frac{1}{\rho^2 c^2}\right)_0 \frac{(p')^2}{2} + \ldots$$

$$S(T) = S_0 + \left(\frac{C_p}{T}\right)_0 T' + \left[\frac{1}{T}\frac{dC_p}{dT} + \frac{C_p}{T^2}\right]_0 \frac{(T')^2}{2} + \ldots$$

$$\rho(p) = \rho_0 + \frac{p'}{c_0^2} + \left(\frac{d^2\rho}{dp^2}\right)_0 \frac{(p')^2}{2} + \ldots$$

$$ST - S_0 T_0 = \left(S + C_p\right)_0 T' + \left[\left(\frac{dC_p}{dT}\right) + \frac{C_p}{T}\right]_0 \frac{(T')^2}{2} + \ldots$$

$$\left(1 - \frac{\rho_0}{\rho}\right) = \frac{p'}{\rho_0 c_0^2} + \ldots$$

$$\frac{\rho_n}{\rho} = \left(\frac{\rho_n}{\rho}\right)_0 + \xi_T T' + \xi_p p' + \ldots$$

$$\frac{\rho_s}{\rho} = \left(\frac{\rho_s}{\rho}\right)_0 - \xi_T T' - \xi_p p' + \ldots$$

where $C_p \equiv T\left(\frac{dS}{dT}\right)_p$ = specific heat

$c \equiv \sqrt{\left(\frac{\partial p}{\partial \rho}\right)_S}$ = speed of first-sound

$\xi_T \equiv \frac{\partial}{\partial T}\frac{\rho_n}{\rho}$ $\qquad \xi_p \equiv \frac{\partial}{\partial p}\frac{\rho_n}{\rho}$

---

*The coefficient of thermal expansion is assumed to be negligible, which implies that entropy is a function only of temperature, density is a function only of pressure, and $C_v = C_p$.

When this is done, all the dissipative terms will disappear because they depend only on derivatives, which are zero in the equilibrium states. Carrying out this procedure on the momentum, superfluid and total energy shock equations, yields the following set:

$$\left[1 - \frac{U_S^2}{c_0^2}\right] \Delta p = 0 \qquad (C.6)$$

$$\frac{1}{\rho_0}\left[1 - \frac{U_S^2}{c_0^2}\right] \Delta p - S_0 \Delta T + \frac{\rho_{n0}}{\rho_0} U_S \, \Delta w = 0 \qquad (C.7)$$

$$\left(S_0 + C_{p0}\right)\Delta T - \left[\frac{\rho_{s0}}{\rho_{n0}} S_0 T_0 + U_S^2\right] \frac{\rho_{n0}}{\rho_0} \frac{\Delta w}{U_S} = 0 \qquad (C.8)$$

For a nontrivial solution to exist the determinate of the coefficients of Δp, ΔT, and Δw must vanish. This requirement yields the following characteristic equation:

$$\left(1 - \frac{U_S^2}{c_0^2}\right)\left(\frac{\rho_{s0}}{\rho_{n0}} \frac{S_0^2 T_0}{C_{p0}} - U_S^2\right) = 0 \qquad (C.9)$$

therefore:

$$U_S = \pm c_0$$

$$\text{or} \quad U_S = \pm a_0$$

where the second-sound speed has been defined as:

$$a = \sqrt{\frac{\rho_s}{\rho_n} \frac{S^2 T}{C_p}} \qquad (C.10)$$

The result of this linearized analysis is simply to find steady first and second sound waves. Thus the propagation velocity, U_S, is independent of amplitude, since nonlinear terms have not been included. However, the jumps in the thermodynamic variables--ΔT, Δp, Δw, etc.--

are those occurring in shock waves to lowest order.

Substituting the second-sound speed in equation (C.8) yields the following relation:

$$\Delta T = \left(\frac{\rho_n}{\rho S}\right) U_S \, \Delta w \ , \text{ for } U_S = a_0 \tag{C.11}$$

which can also be written as:

$$\frac{\Delta w}{U_S} = \left(\frac{\rho}{\rho_s} \ \frac{C_p}{S}\right)_0 \Delta\theta, \text{ for } U_S = a_0 \tag{C.12}$$

where $\Delta\theta \equiv \frac{\Delta T}{T_0}$

Substituting this result into equation (C.7) reveals that the pressure jump, Δp, is zero to this level of approximation. Thus the pressure jump in a second-sound wave must be of order w^2 or higher.* The only first order quantities in second-sound waves will therefore be fluctuations of entropy, temperature, relative velocity, and normal fluid fraction (ρ_n/ρ).

---

*This statement must be modified when the coefficient of thermal expansion cannot be neglected. In that case the pressure jump will be of order w times the coefficient of thermal expansion which is still small, although not negligible. See Appendix B.

SOLVING FOR THE JUMP CONDITIONS AND SHOCK VELOCITY

When solving the shock equations to order w^2 for second-sound it is useful to use the equations of Table C.3, since terms involving pressure and density are order w^3. These equations expanded in terms of T' and w are:

$$\left(\frac{\rho_n}{\rho}\right)_0 U_S w - S_0 T' = \frac{3}{2}\left(\frac{\rho_n \rho_s}{\rho^2}\right)_0 w^2 - \xi_T T' U_S w + \left(\frac{C_p}{T}\right)_0 \frac{(T')}{2} + \frac{\tau^*}{\rho} - h^* + O(w^3) \tag{C.13}$$

$$C_{p0} T' - \left(\frac{\rho_s}{\rho} ST\right)_0 \frac{w}{U_S} = -\tfrac{1}{2}\left(\frac{\partial C_p}{\partial T}\right)_0 (T')^2 + \left[\frac{\rho_s}{\rho}\left(S + C_p\right) - ST\xi_T\right]_0 T' \frac{w}{U_S} - \tfrac{1}{2}\left[\frac{\rho_s}{\rho} + \frac{\rho}{\rho_n} T\xi_T\right]_0 \left(\frac{\rho_n}{\rho}\right)_0 w^2 + \frac{Q^*}{\rho_0 U_S} + \frac{\tau^*}{\rho} + O(w^3) \tag{C.14}$$

The dissipative terms similarily expanded but restricted to second-sound shocks are:

$$\frac{\tau^*}{\rho} - h^* = -\left[\frac{4}{3}\frac{\eta}{\rho} + \frac{\zeta_2}{\rho} - 2\zeta_1 + \rho\zeta_3\right]_0 \left(\frac{\rho_s}{\rho}\right)_0 \frac{dw}{dx} + O(w^3) \tag{C.15}$$

$$\frac{Q^*}{\rho_0 U_S} + \frac{\tau^*}{\rho} = -\frac{\kappa}{\rho_0 U_S} \frac{dT}{dx} + O(w^3) \tag{C.16}$$

From the first order solutions for second-sound (see Eq. C.12):

$$w = \frac{\rho_0 S_0}{\rho_{n0} U_S} T' + O(T')^2$$

This expression may be substituted into the second order terms of equations (C.13) thru (C.16) to eliminate w, since the error involved will be of third order. This substitution may not be made into the

first order terms however, so there will still be a linear dependence of w in the two shock equations. The result of this simplification is the following set of four equations:

$$\left(\frac{\rho_n}{\rho}\right)_0 U_S w - S_0 T' = \left(\frac{S}{T}\right)_0 \left[2\frac{C_p}{S} - \left(\frac{\rho}{\rho_n} T\xi_T\right)\right]_0 (T')^2 + \frac{\tau^*}{\rho} - h^* \qquad (C.17)$$

$$C_{p0} T' - \left(\frac{\rho_s}{\rho} ST\right)_0 \frac{w}{U_S} = \frac{C_{p0}}{T_0}\frac{a_0^2}{U_S^2}\left[\frac{1}{2} + \frac{C_p}{S} - \frac{1}{2}\left(\frac{T}{C_p}\frac{\partial C_p}{\partial T}\right)\right. \qquad (C.18)$$

$$\left. - \left(\frac{3}{2}\frac{\rho_n}{\rho_s} + \frac{1}{2}\right)\left(\frac{\rho}{\rho_n} T\xi_T\right)\right]_0 (T')^2 + \frac{Q^*}{\rho_0 U_S} + \frac{\tau^*}{\rho}$$

$$\frac{\tau^*}{\rho} - h^* = -\left[\frac{4}{3}\frac{\eta}{\rho} + \frac{\zeta_2}{\rho} - 2\zeta_1 + \rho\zeta_3\right]_0 \left(\frac{\rho_s S}{\rho_n U_S}\right)_0 \frac{dT}{dx} \qquad (C.19)$$

$$\frac{Q^*}{\rho_0 U_S} + \frac{\tau^*}{\rho} = -\frac{\kappa}{\rho_0 U_S}\frac{dT}{dx} \qquad (C.20)$$

Finally w can be eliminated by multiplying equation (C.17) by (T/S) and equation (C.18) by $(T/C_p)_0\ (U_S/a_0)^2$, and adding. The result is:

$$\left[\frac{U_S^2}{a_0^2} - 1\right] T_0 T' = \left[\frac{1}{2} + 3\frac{C_p}{S} - \frac{1}{2}\left(\frac{T}{C_p}\frac{\partial C_p}{\partial T}\right) - \frac{3}{2}\left(\frac{\rho_n}{\rho_s} + 1\right)\left(\frac{\rho}{\rho_n} T\xi_T\right)\right]_0 (T')^2$$

$$+ \left(\frac{T}{C_p}\right)_0 \left[\frac{Q^*}{\rho_0 U_S} + \frac{\tau^*}{\rho} + \left(\frac{\tau^*}{\rho} - h^*\right)\frac{C_p}{S}\right]_0 \qquad (C.21)$$

Note when writing down the dissipative terms use was made of the fact that these terms are of order w^2 and that U_S^2 equals a_0^2 plus a correction of order w.

From this point the jump equations can be simply solved by letting $T' \to \Delta T$ and by noting that the dissipative terms disappear

because two equilibrium states are being used.

$$\left(\frac{U_S^2}{a_0^2} - 1\right) = \left[\frac{1}{2} + 3\frac{C_p}{S} - \frac{1}{2}\left(\frac{T}{C_p}\frac{\partial C_p}{\partial T}\right) - \frac{3}{2}\left(\frac{\rho_n}{\rho_s} + 1\right)\left(\frac{\rho}{\rho_n} T\xi_T\right)\right]_0 \frac{\Delta T}{T_0}$$

$$= \left[T\frac{\partial}{\partial T}\log\left(a^3\frac{C_p}{T}\right)\right]_0 \Delta\theta \qquad (C.22)$$

This yields Khalatnikov's well known second-sound shock velocity formula (see Khalatnikov, 1965, chapter 13):

$$U_S = \pm a\left(1 + \frac{1}{2} b_0 \Delta\theta\right) \qquad (C.23)$$

where b(p,T) is the steepening coefficient of second-sound defined by:

$$b(p,T) \equiv T\frac{\partial}{\partial T}\log\left(a^3\frac{C_p}{T}\right) \qquad (C.24)$$

This solution to shock velocity can be substituted into equation (C.17) to yield a second-order result for the relative velocity jump. Equation (C.17) rewritten as a jump equation and solving for Δw is:

$$\frac{\Delta w}{a_0} = \left(\frac{\rho S}{\rho_n T}\right)_0 \frac{T_0 \Delta T}{U_S a_0}\left[1 + \left(2\frac{C_p}{S} - \frac{\rho}{\rho_n} T\xi_T\right)_0 \Delta\theta\right] \qquad (C.25)$$

but from equation (C.22):

$$\frac{1}{U_S} = \frac{1}{a_0}\left(1 - \frac{b_0}{2}\Delta\theta\right)$$

which substituted into equation (C.25) yields:

$$\frac{\Delta w}{a_0} = \left(\frac{\rho}{\rho_s}\frac{C_p}{S}\right)_0 \Delta\theta\left\{1 + \frac{1}{4}\left[2\frac{C_p}{S} + \frac{T}{C_p}\frac{\partial C_p}{\partial T} + \left(3\frac{\rho_n}{\rho_s} - 1\right)\left(\frac{\rho}{\rho_n} T\xi_T\right) - 1\right]_0 \Delta\theta\right\}$$

$$= \left(\frac{\rho}{\rho_s}\frac{C_p}{S}\right)_0 \Delta\theta\left\{1 + \frac{1}{2} T_0 \frac{\partial}{\partial T}\left[\log a\frac{C_p}{T}\left(\frac{\rho}{\rho_s}\right)^2\right]\Delta\theta\right\} \qquad (C.26)$$

SHOCK STRUCTURE SOLUTION

The shock structure can now be solved directly from equation (C.21) which is rewritten below:

$$\left[\frac{U_S^2}{a_0^2} - 1\right] T_0 T' = b_0 (T')^2 + \frac{T_0}{\rho_0 a_0}\left[\frac{\kappa}{C_p} + \frac{\rho_S}{\rho_n}\left(\frac{4}{3}\eta + \zeta_2 - 2\rho\zeta_1 + \rho^2\zeta_3\right)\right]_0 \frac{dT}{dx} \qquad (C.27)$$

This equation can be rearranged with the aid of the shock velocity result to the following nondimensional form:

$$\frac{d\overline{T}}{dy} = \Delta\theta\overline{T} - \overline{T}^2 \qquad (C.28)$$

where $\overline{T} \equiv \dfrac{T-T_0}{T_0}$

$$y \equiv \left(\frac{ab}{D}\right)_0 x$$

$$D(p,T) \equiv \frac{1}{\rho}\left[\frac{\kappa}{C_p} + \frac{\rho_S}{\rho_n}\left(\frac{4}{3}\eta + \zeta_2 - 2\rho\zeta_1 + \rho^2\zeta_3\right)\right] \qquad (C.29)$$

The remaining question that needs to be answered before solving equation (C.28) concerns whether quadratic or just linear terms are required to balance the differential term. The shock layer is a very narrow part of the entire shock solution when expressed in the non-dimensional variable y; therefore it is useful to rewrite the equation in stretched coordinates as follows:

Set $\quad \overline{y} \equiv \dfrac{y}{\phi(\theta)}$

Define $f(\bar{y})$ such that:

$$T(\bar{y}) = T(\bar{y}\ \ \phi(\Delta\theta)) \equiv \Delta\theta f(\bar{y})$$

Note that $\phi(\Delta\theta)$, which is a measure of the shock thickness, is some unknown function of the shock strength. Also note that the new dependent variable is magnified by some function of the shock strength which in this case must be $\Delta\theta$ itself. With these substitutions equation (C.28) becomes:

$$\frac{\Delta\theta}{\phi(\Delta\theta)} \frac{df}{d\bar{y}} = \Delta\theta^2 f - \Delta\theta^2 f^2 \qquad \text{(C.30)}$$

Clearly in order to balance the differential term, both the linear and quadratic terms are required since they are of the same order in the small parameter $\Delta\theta$. Also, the shock thickness must be inversely proportional to the shock strength:

$$\phi = \frac{1}{\Delta\theta} \qquad \text{(C.31)}$$

Finally equation (C.30) can be solved for $f(\bar{y})$ to yield:

$$f(\bar{y}) = \frac{1}{2} + \frac{1}{2} \tanh \frac{\bar{y}}{2} \qquad \text{(C.32)}$$

When the original variables are resubstituted the shock structure is found to be:

$$T(x) = \frac{1}{2}(T_1 + T_0) + \frac{1}{2}(T_1 - T_0) \tanh \frac{2x}{\delta} \qquad \text{(C.33)}$$

$$\delta = \frac{4D}{ab\Delta\theta} = \frac{2D}{a} \frac{1}{M_S - 1} \qquad \text{(C.34)}$$

The profile of a second-sound shock wave given by equation (C.33)

has the same shape as an ordinary pressure shock profile for weak shock waves. Also the form of the shock thickness, δ, is totally analogous to the ordinary weak shock case (Landau and Lifshitz, 1959). In both cases the shock thickness is inversely proportional to the shock strength; in the second-sound shock case this parameter is the temperature jump divided by the temperature of the initial rest state. Also in both cases the shock thickness includes a thermodynamic coefficient whose sign determines whether the shock is a compression or expansion. For ordinary pressure shocks this coefficient is the "fundamental derivative of gas dynamics", $(\partial^2 p/\partial V^2)_S$, (where V is specific volume). For the second sound case this coefficient is the steepening coefficient b(p,T) defined by equation (C.24).

The analogy is made complete by the constant terms of proportionality which are equal to the absorption of sound per frequency squared. Khalatnikov (1965, Chapter12) has shown that the absorption of second-sound is given by:

$$\alpha = \tfrac{1}{2}\omega^2 \frac{1}{\rho a^3}\left[\frac{\kappa}{C_p} + \frac{\rho_s}{\rho_n}\left(\frac{4}{3}\eta + \zeta_2 - 2\rho\zeta_1 + \rho^2\zeta_3\right)\right] \qquad (C.35)$$

thus

$$D = \frac{2\alpha}{\omega^2} a^3 \qquad (C.36)$$

At first thought such a complete analogy between ordinary pressure shock waves and temperature shock waves in a superfluid may seem surprising since the basic equations of motion as well as the thermodynamics of helium II are very different from those of an ordinary fluid. This analogy however is not a coincidence, but is due to the fact that in both cases the steady profile of a shock wave is due to a

balance of the nonlinear steepening effects by dissipative mechanisms. Furthermore it can be shown quite generally for weak shocks, that when a steady wave front is formed by balancing nonlinear steepening with some dissipative process -- whether it be heat conduction, viscosity, or diffusion -- the result will be a shock wave front whose thickness is inversely proportional to the shock strength.

IRREVERSIBLE ENTROPY JUMP

Like an ordinary pressure shock wave, weak second-sound shock waves generate entropy in proportion to the third power of the shock strength. However, the total entropy jump caused by the passage of a second-sound shock front can be either positive or negative, since the entropy jump to lowest order is proportional to the shock-induced temperature jump. This happens, of course, because entropy can be reversibly transported by second-sound. Thus, it is necessary to distinguish between the entropy reversibly transported and the entropy irreversibly generated.

The irreversible entropy may be calculated by integrating the rate of entropy production over time as the shock front passes a fixed point. This production rate is proportional to the square of the temperature and velocity gradients (Khalatnikov, 1965), and therefore, the irreversible entropy jump is always a positive-definite function of the shock strength. For one-dimensional second-sound (where the fluid density is assumed constant to first order in the temperature perturbation) the entropy production rate can be written as follows:

$$\left(\frac{\partial \rho S}{\partial t}\right)_{\text{irreversible}} = \frac{1}{T}\left\{\frac{\kappa}{T}\left(\frac{\partial T}{\partial x}\right)^2 + \left(\frac{4}{3}\eta + \zeta_2 - 2\rho\zeta_1 + \rho^2\zeta_3\right)\left(\frac{\partial v_n}{\partial x}\right)^2\right\} \tag{C.37}$$

An integration over distance in the shock steady frame is equivalent to an integration over all time at a fixed point: $dx = dt/U_S$. From the last section, the temperature and velocity gradients produced in the shock front are known to be:

$$\frac{\partial T}{\partial x} = \frac{\Delta T}{\delta} \operatorname{sech}^2 \frac{2x}{\delta} \tag{C.38}$$

$$\frac{\partial v_n}{\partial x} = \frac{\Delta v_n}{\delta} \operatorname{sech}^2 \frac{2x}{\delta} \tag{C.39}$$

Integration and substitution of previous results shows that the total entropy generated is indeed proportional to $(\Delta\theta)^3$:

$$(\Delta S)_{\text{irreversible}} = \frac{1}{6} \left| b(\Delta\theta)^3 \right| C_p + O(\Delta\theta)^4 \tag{C.40}$$

It is also remarkable that the total entropy jump is independent of the dissipative coefficients. This again is analogous to the result obtained for weak pressure shocks in ordinary substances.

Appendix D. SECONDARY WAVES ORIGINATING FROM AN UNSEALED HEATER

Any open space between the heater and the sidewalls of the shock tube will create a secondary wave field which will perturb the otherwise one-dimensional shock pulse generated by the heater. In general the open space can act as a source or sink of heat flux depending on the configuration of the heating element and the sidewall.

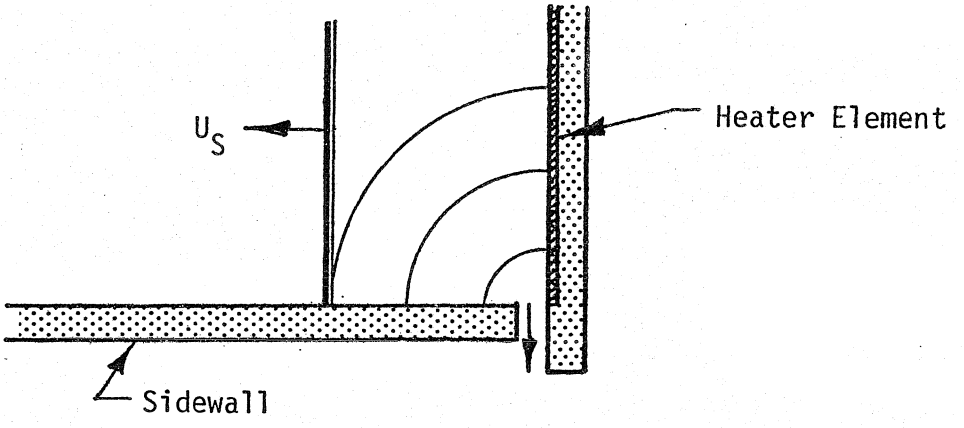

Figure D.1 SECONDARY WAVE FIELD PRODUCED BY AN OPEN HEATER

The first figure shows a typical configuration where the heating element does not overlap the end of the sidewall. In this case, when a shock pulse is being generated, some heat flux leaks out through the opening which acts as a heat sink. Therefore, the secondary wave which results will display an initially negative temperature excursion.

An open heater can also act as a source of heat flux if the heating element overlaps the end of the sidewall. This happens because the temperature is amplified within the opening by multiple reflections of the heat pulse occurring between the heater and the end of the sidewall. In this case the initial temperature excursion

will be positive.

Secondary waves of both types, which resulted from an open heater, have been observed during experiments which employed a square cross section shock tube (Shock Tube I). Since the walls of this shock tube are flat and parallel to one another, the position of the secondary waves can be calculated without difficulty as they travel down the shock tube, reflecting from sidewall to sidewall. The angle of propagation of the portion of the secondary wave front which eventually encounters the temperature sensor depends on the location of the sensor and the number of reflections made during the passage of the wave. For the configuration under consideration, which is shown in Figure D.2, the propagation angle is given by:

$$\tan \phi_n = \frac{d(n+1)}{L} \qquad (D.1)$$

where n is the number of reflections.

In the linear approximation the wave velocity is independent of amplitude and the arrival time of the secondary wave front can be calculated as:

$$t = \frac{L}{a \cos \phi} \qquad (D.2)$$

where a is the velocity of second-sound. Table D.1 gives the theoretically calculated values of propagation angle and arrival times for experiments conducted at 1.65^{o}K. Figure D.3a is an oscilloscope trace of temperature versus time for both sensors #1 and #2. The experimental results and the theoretical predictions agree exactly to within the experimental precision which was about 0.1 msec. A

Figure D.2. GEOMETRY OF SHOCK TUBE I

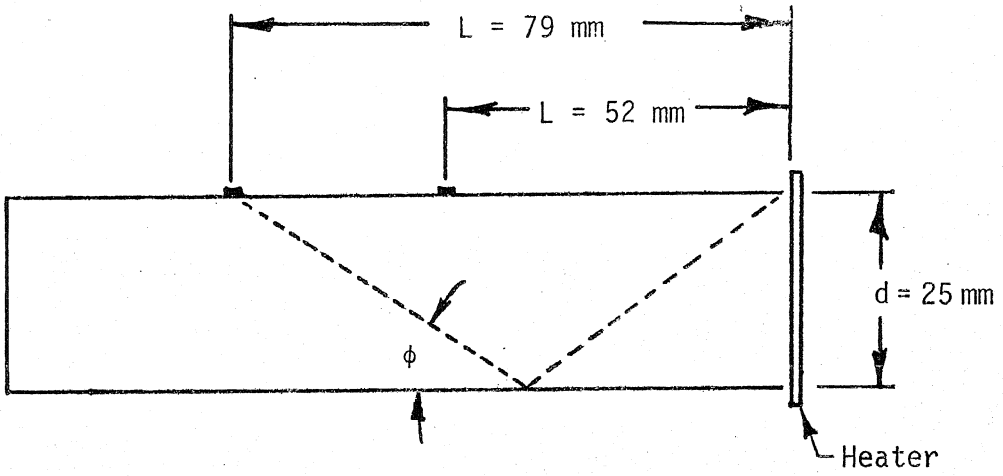

Propagation angle: $\tan \phi_n = \frac{d(n+1)}{L}$

where n is the number of reflections.

Table D.1. PREDICTED ARRIVAL TIMES OF THE SECONDARY WAVES

	Sensor #1 (L/a = 2.55 ms)		Sensor # 2 (L/a = 3.87 ms)	
n	ϕ	t(msec)	ϕ	t(msec)
0	25.7	2.8	17.6	4.1
1	43.8	3.6	32.3	4.6
2	55.3	4.5	43.5	5.3
3	62.5	5.5		
4	67.4	6.6		

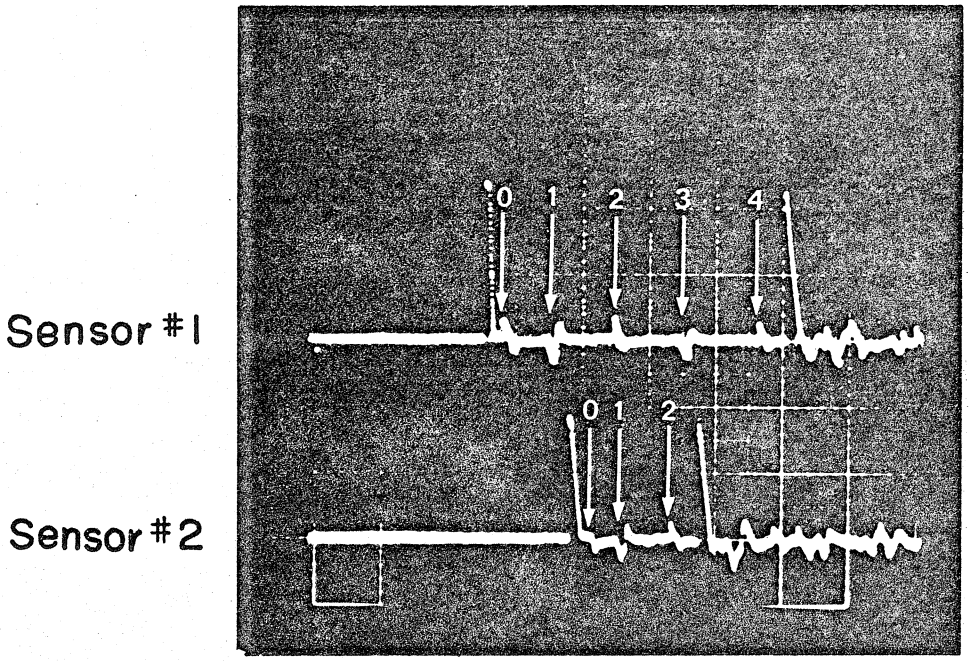

(a) 1 m sec/division

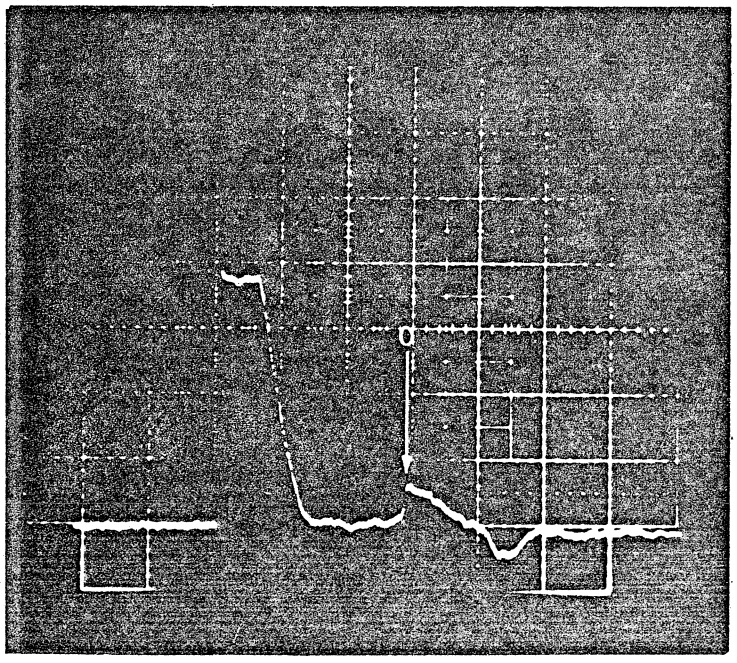

(b) 100 μ sec/division

Figure D.3 SECONDARY WAVES IN SHOCK TUBE I

number of interesting results can be obtained from this oscilloscope trace. First note that both source and sink generated waves appear alternately. This can easily be explained if the heater was displaced with respect to the end of the shock tube. On the side opposite the sensors the heating element overlapped the sidewall sufficiently to produce a heat flux source, while the other side acted as a heat flux sink.

The shape of a typical secondary wave is characteristic of an N-wave, but it should be emphasized that it is not an N-wave in the sense of the asymtotic limiting form, shock-expansion-shock, brought about by nonlinearity. Instead the wave shape is a consequence of the complex generating mechanism at the open heater. The length of the first triangular portion is equal to the length of the generating heat pulse as might be expected. The second half of the wave form does not have the same duration or amplitude as the first half, but it is always opposite in sign. Apparently the heat sink became a source and the source became a sink for a short while after the heat pulse was terminated.

The theoretical ideas for predicting the arrival times of secondary waves, which have been discussed so far, are valid only for linear waves since the convection by the shock pulse was ignored. To calculate the arrival time of the initial secondary wave front it is usually imperative to take into account the change in characteristic velocity caused by the shock pulse. This is because the direct propagating secondary wave always resides within the shock pulse as they both travel down the shock tube (except for large angles of propagation

where the sensor is located close to the heater). Now assuming that the secondary wave has a small amplitude so that it can be treated as linear, and assuming it always resides within the unexpanded region of the shock pulse, the arrival time is simply:

$$t = \frac{L}{u(\phi)\cos\phi} \tag{D.3}$$

where u is the characteristic velocity behind the shock front. This velocity of propagation is a function of the propagation angle, ϕ, since the fluid within the shock pulse forms an anisotropic medium. The jump in characteristic velocity at the shock front, denoted by Δu, is in the direction of the shock propagation for $T < 1.88^{o}K$ and for weak shock waves its magnitude is given by:

$$\frac{\Delta u}{a_0} = 2(M_S - 1) \tag{D.4}$$

where a_0 is the second-sound velocity in the undisturbed fluid (w=0) and M_S is the Mach number of the shock wave. Referring to Figure D.4, a wave which originates at point A at time t=0 appears to have radiated from point B at a later time, t_B. From this diagram the actual wave velocity can be deduced as:

$$\frac{u(\phi)}{a_1} = \left(\frac{\Delta u}{a_1}\right)\cos\phi + \sqrt{1 - \left(\frac{\Delta u}{a_1}\right)^2 \sin^2\phi} \tag{D.5}$$

where a_1 is the velocity of second-sound in the equilibrium region following the shock front.

During the initial experiments, employing the Shock Tube I, no real effort was made to seal the heater. In later experiments, using the variable length shock tube, a serious attempt was made to seal

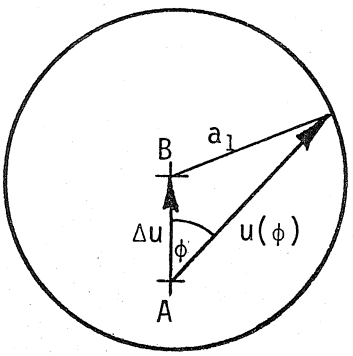

Figure D.4 WAVE PROPAGATION IN AN ANISOTROPIC MEDIUM

the heater with a machined teflon gasket. The heater is held tight against a sharp edged teflon seal, spring loaded with a force of about 10 pounds. Figure D.5 shows the basic configuration of this seal.

Unfortunately this seal was not totally successful as can be seen in the oscilloscope traces of Figure D.6. These traces were made by an endwall sensor located on the centerline of the cylindrical shock tube, and they represent time histories for the same strength shock wave (M_S = 1.0054) at different distances from the heater.

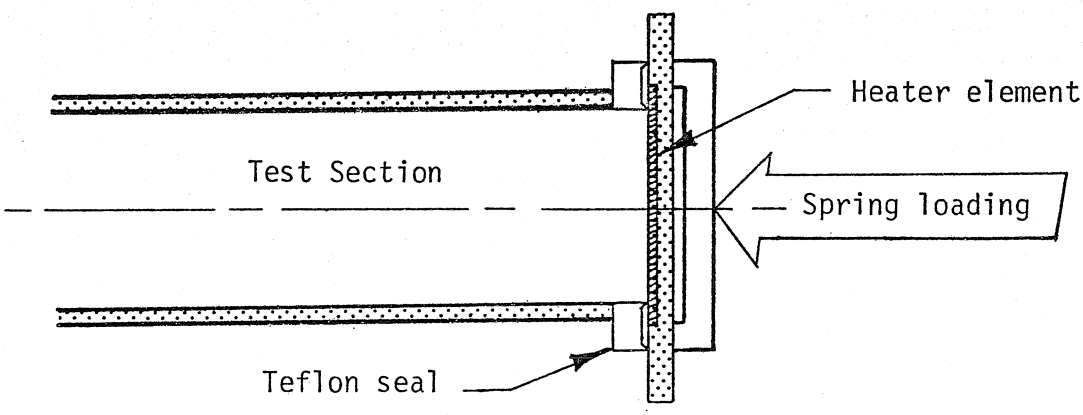

Figure D.5 TEFLON SEALED HEATER

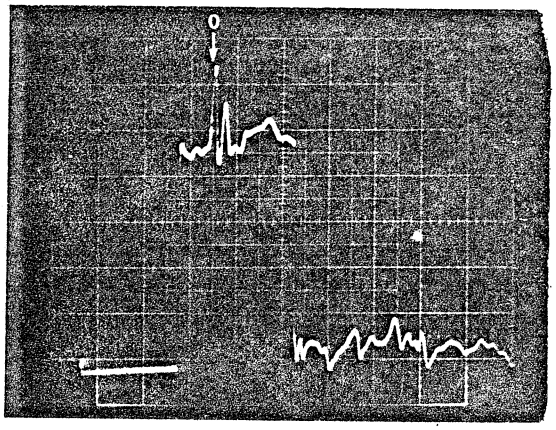

(a) L = 1.99 cm

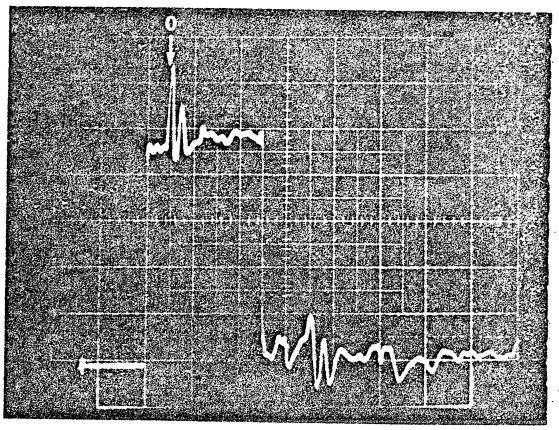

(b) L = 3.12 cm

200 μ sec / division

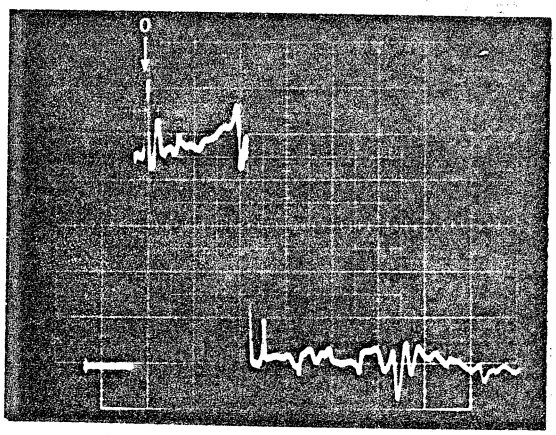

(c) L = 5.59 cm

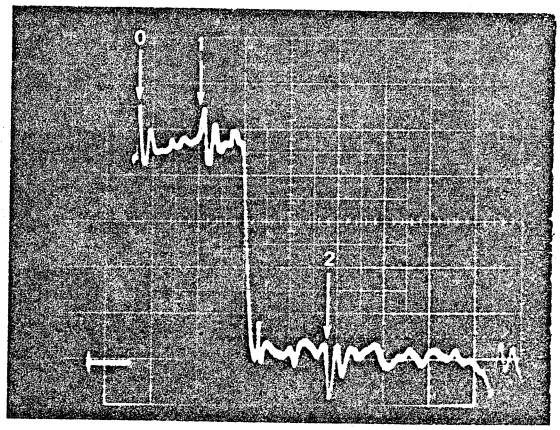

(d) L = 8.10 cm

Figure D.6 SECONDARY WAVES FOCUSING ON THE AXIS OF A CYLINDRICAL SHOCK TUBE

The arrival of the secondary wave front propagating directly and its first two reflections can be picked out as large amplitude, high frequency, oscillations. Their arrival times were measured quite accurately (at least for the n = 0 or nonreflecting wave) by locating the point when the slope of the trace changed abruptly with respect to the shock front. Results of these measurements and the comparison with theory is shown as Figure D.7. The theoretical calculations took into account the convection of the secondary waves, equations (D.3) and (D.5), where the angle of propagation was determined from:

$$\tan\phi = \frac{d}{L}(n + 1/2) \qquad (D.6)$$

As is evident, the theory can predict the arrival times very accurately as long as the characteristic velocity jump across the shock front is taken into account (the difference in arrival time due to convection is as much as 60 μsec for the n = 0 wave). Arrival times for all the secondary waves through the fourth reflection were predicted quite accurately using this simple theory. The largest discrepancy appears with the n = 1 reflection and is probably due to incorrect interpretation of the oscillations when trying to choose the initial arrival. This problem does not arise for the first wave, since the wavelets preceding it are very small and can be easily differentiated from the arrival of the secondary wave front.

It is interesting to note the difference in shape between these secondary waves and the ones described earlier occurring in Shock Tube I. Apparently the teflon seal did work partially, because disturbances were produced only at the beginning and end of the heat pulse. Recall

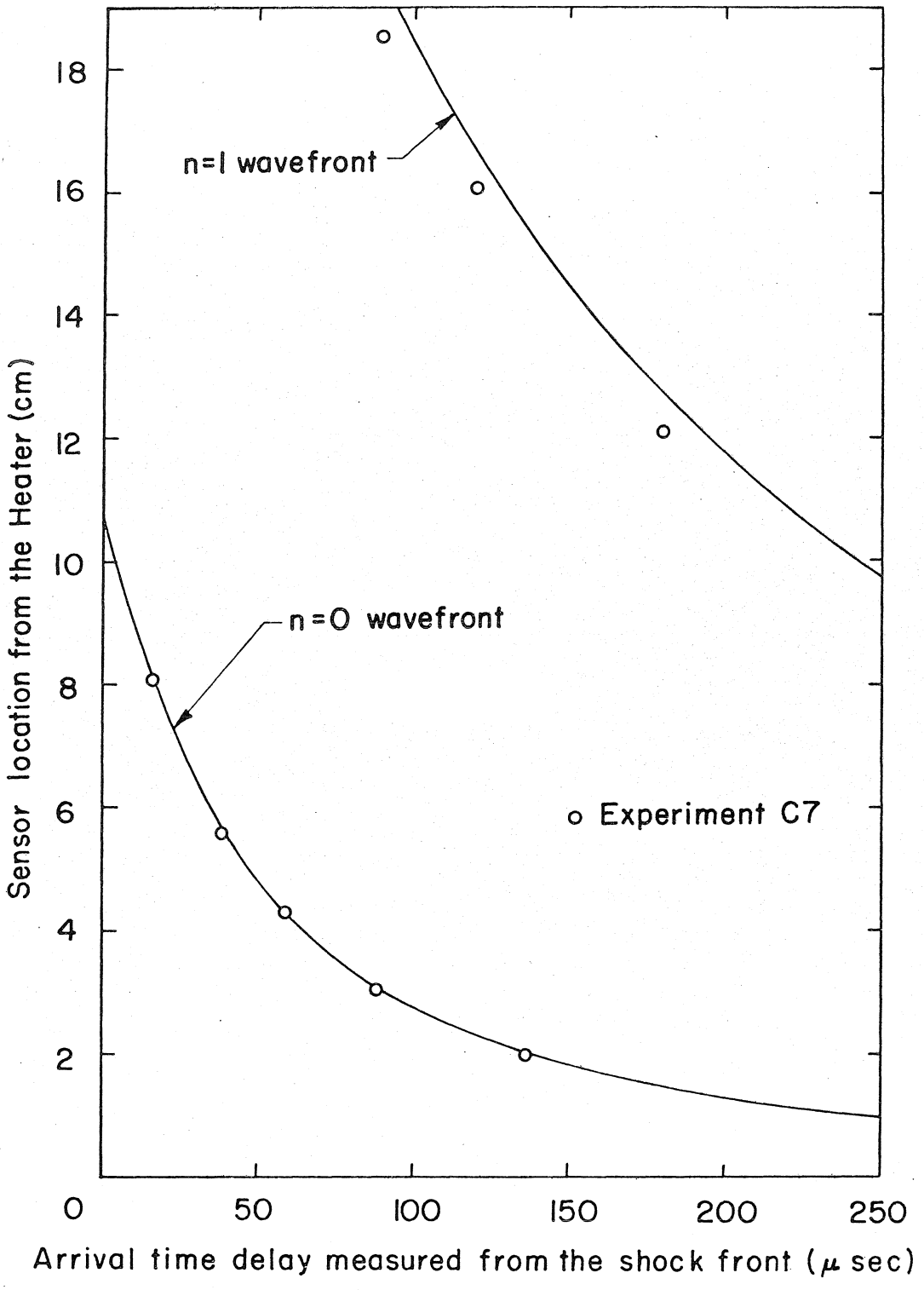

Figure D.7 ARRIVAL TIMES OF SECONDARY WAVEFRONTS

that the disturbance made in the Shock Tube I appeared continuously during the heat pulse generation and even for a short time after its termination.

One final observation concerning the amplitude of the secondary waves is interesting. When using an endwall sensor mounted off the shock tube axis, only very small secondary wavelets were detected. The observed large amplitude oscillations were produced by amplification of these radial mode secondary waves focusing on the axis of the cylindrical shock tube.

Appendix E. THE THERMAL BOUNDARY LAYER

The heat from a hot object immersed in helium II is quickly carried away by internal counterflow. On the liquid side, very close to the solid-liquid interface, incoming superfluid must be quickly converted into outgoing normal fluid in order to sustain the process. If conversion takes place exactly at the interface then it must occur infinitely fast, and it would require an infinite gradient in the chemical potential to instantaneously stop the superfluid and start the normal fluid. Such an unnatural process must in reality be smoothed out into a thermal boundary layer, where conversion takes place over a small, but nevertheless finite, distance.

In order to discover this boundary layer, the two-fluid equations will be solved for a steady flux of heat passing perpendicularly through a solid-liquid helium II interface. The flow will be assumed laminar, one-dimensional, and steady. From the conservation of mass, the mass flux, ρv, must be constant everywhere and equal to zero, since at the wall $v = 0$. The applicable form of the equations for momentum, energy, and superfluid flow, including dissipation, are given below:

$$\frac{d}{dx}\left[\frac{\tilde{\rho}_n\tilde{\rho}_s}{\hat{\rho}} w^2 + p + \tau^*\right] = 0 \qquad (E.1)$$

$$\frac{d}{dx}\left[\tilde{\rho}\tilde{S}Tv_n + \tilde{\rho}_n v_n^2 w + Q^*\right] = 0 \qquad (E.2)$$

$$\frac{d}{dx}\left[\tilde{\mu} + \tfrac{1}{2} v_s^2 + h^*\right] = 0 \qquad (E.3)$$

These equations are integrated and the constants of integration evaluated in the liquid far from the interface. At this location, denoted by $(\ )_\infty$, pure counterflow will have been established, all gradients will have vanished, and hence, the dissipative terms will be zero. Written out to second-order in the normal fluid velocity, the results are:

$$\frac{\rho_n}{\rho_s}\rho v_n^2 + p + \tau^* = \left(\frac{\rho_n}{\rho_s}\rho v_n^2 + p\right)_\infty \tag{E.4}$$

$$\rho S T v_n + Q^* = (\rho S T v_n)_\infty \tag{E.5}$$

$$\mu - \frac{1}{2}\frac{\rho_n}{\rho_s} v_n^2 + h^* = \left(\mu - \frac{1}{2}\frac{\rho_n}{\rho_s} v_n^2\right)_\infty \tag{E.6}$$

These second-order equations will be useful later, but first in order to obtain a solution, only a linearized set is required. Thus, all the thermodynamics can be expanded in terms of pressure and temperature perturbations:

$$p' = p - p_\infty \quad , \quad p' \ll p$$

$$T' = T - T_\infty \quad , \quad T' \ll T$$

A normal velocity variation from equilibrium, v_n', will also be used, but it is noteworthy that the equilibrium value, $v_{n\infty}$, will be assumed the same order as T' or p'. In the resulting set of equations, the momentum equation can be used to eliminate p', which reduces the problem to two variables, T' and v_n', and two equations:

$$(\rho S)_\infty T' = \left[\frac{4}{3}\eta + \zeta_2 - 2\rho\zeta_1 + \rho^2\zeta_3\right]_\infty \frac{dv_n'}{dx} \tag{E.7}$$

$$(\rho ST)_\infty v_n' = \kappa_\infty \frac{dT'}{dx} \tag{E.8}$$

The solution of these two coupled ordinary differential equations is an exponential layer of thickness λ:

$$v_n' = v_{nB}' \, e^{-x/\lambda} \tag{E.9}$$

$$\lambda = \frac{1}{\rho a}\sqrt{\frac{\kappa}{C_p}\frac{\rho_s}{\rho_n}\left(\frac{4}{3}\eta + \zeta_2 - 2\rho\zeta_1 + \rho^2\zeta_3\right)} \tag{E.10}$$

where v_{nB}' is the normal velocity variation from $v_{n\infty}$ in the fluid at the boundary.

This exponential layer solution has been obtained by many authors (see Atkins, 1959, pg. 202, and Putterman, 1974), but there has always been a question about how to fix the constant v_{nB}'. As pointed out in the text, the boundary condition $\rho_s \to 0$ implies that the component of $\vec{v}_n$ perpendicular to a solid wall must be zero as well as its tangential component. Therefore $v_{nB}' = -v_{n\infty}$.

Since $v_n \to 0$ at the boundary at least as fast as $\rho_s \to 0$, then the nonlinear terms -- all are of order v_n^2/ρ_s -- also go to zero. Thus, they were properly neglected. Now, after the boundary conditions have been set, it is convenient to write the final solution in terms of the relative velocity:

$$w(x) = w_\infty(1 - e^{-x/\lambda}) \tag{E.11}$$

$$T(x) = T_\infty + \left(\frac{\rho_n a}{\rho S}\right) w_\infty g e^{-x/\lambda} \tag{E.12}$$

where $$g \equiv \sqrt{\frac{\frac{\rho_s}{\rho_n}\left(\frac{4}{3}\eta + \zeta_2 - 2\rho\zeta_1 + \rho^2\zeta_3\right)}{\kappa/C_p}} \qquad \text{(E.13)}$$

The coefficient g has a value of about 0.5 and is not strongly temperature dependent (see Wilks, 1967, Chapter 8, Figure 16). The layer thickness, λ, can be evaluated in terms of g and the damping coefficient of second-sound, D (see Appendix C):

$$\lambda = \frac{g}{1+g^2}\,\frac{D}{a} = g\,\frac{\kappa}{\rho C_p a} \qquad \text{(E.14)}$$

Plugging in the numbers shows that the thermal boundary layer has a thickness rarely exceeding 100 Å (at $T = 1.60^{\circ}K$, $\lambda \simeq 60$ Å). This thickness is much larger than the length scaling the abrupt change in the superfluid density at the wall. Thus, although the existence of the ρ_s boundary layer sets the boundary condition which in turn causes the thermal boundary layer, the scale of the former does not set the scale of the latter. The normal fluid velocity cannot change abruptly; it is limited by the collisional rates between excitations constituting the normal fluid.

It is remarkable that the thermal boundary layer thickness, λ, is much shorter than the mean free path of phonons scattered by rotons, ℓ_{pr}. This scattering mechanism is the one principally responsible for maintaining thermal equilibrium between the relative number of phonons and rotons (Khalatnikov and Chernikova, 1966a). Thus, it appears that within the thermal boundary layer, the phonon and roton gases, separately in equilibrium, may not be in equilibrium with one another. A more accurate calculation of the thermal boundary layer

must therefore treat the phonon and roton gases separately.

Appendix F. RESPONSE OF A THIN-FILM TEMPERATURE SENSOR

When the boundary temperature of a thin-film sensor jumps instantaneously from T_0 to T_2, the temperature registered by the sensing element will asymptote to T_2 after a finite length of time. If a measurement of the temperature is attempted before final equilibrium is attained the resulting value will always be less than the actual temperature jump. In order to obtain a correct temperature measurement, the theoretical response of a thin-film sensor must be known.

A typical temperature sensor consists of a metallic superconducting thin-film -- about 1000 Å thick -- vacuum deposited on a dielectric substrate, usually glass or fused quartz. Figure F.1 shows a snapshot of the nonsteady temperature profile in such a temperature sensor,

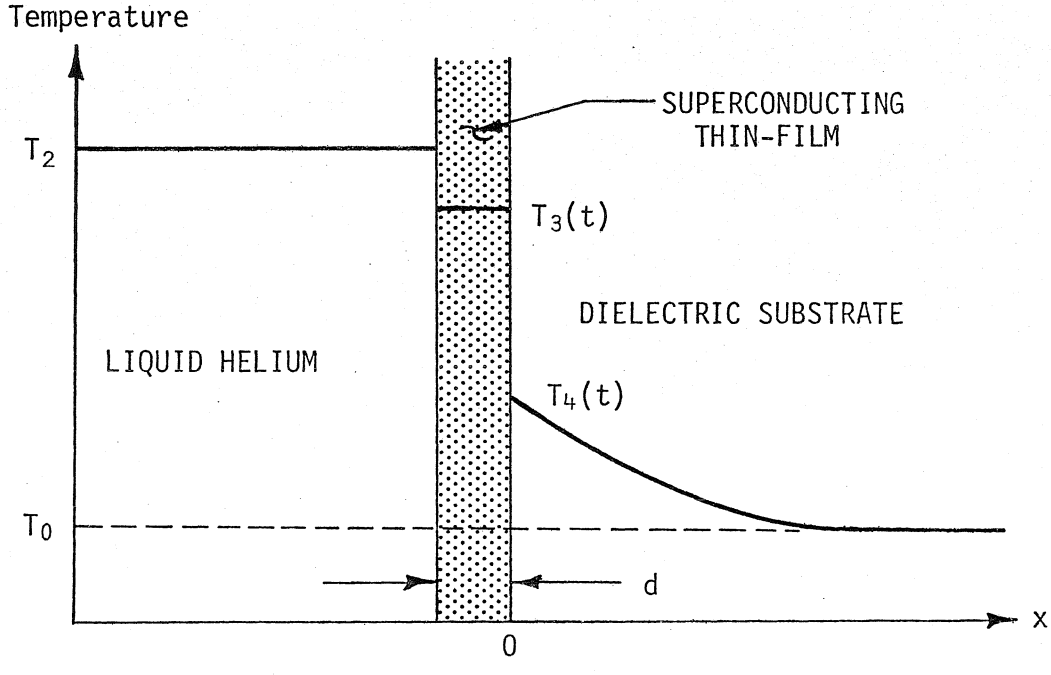

Figure F.1 MODEL OF A THIN-FILM SENSOR

which was initiated by a temperature jump in the liquid helium from T_0 to T_2.

In general, the interface between any two dissimilar materials will be the site of a temperature discontinuity whose magnitude, to lowest order, is proportional to the penetrating heat flux. If the impedance match of the thermal excitations in both materials were perfect, heat could flow reversibly across the interface without producing a temperature jump, but such a coincidence never occurs in practice.

The temperature jump occurring at the liquid-solid interface is proportional to the Kapitza resistance, R_K. Khalatnikov (1952a) has shown that if the heat flux pentrating the interface is due solely to phonon exchange, then the Kapitza resistance will be inversely proportional to T^3 -- that is, the effect becomes dominate only at low temperatures. The experimentally determined temperature dependence of R_K for copper is reported by Challis (1961) to be:

$$R_K(^oK - cm^2/w) \simeq 15\ T^{-2.5}$$

This is only a small fraction of the theoretical value; apparently other mechanisms aid the transfer of energy across the liquid-solid interface (Possible transfer mechanisms, involving rotons in helium II and electrons in the metal film, should be severely limited by the improbability of achieving a detailed balance of momentum and energy for other types of interface interactions between rotons, electrons and phonons).

At the metal-dielectric interface a similar temperature jump

will appear, again due to phonon impedance mismatch. However, for this type of interface the measured contact resistance, R_C, is a few times larger than the value predicted by the phonon transfer theory (Little, 1959). Thus, although the phonon or acoustic impedance mismatch is largest at the liquid-solid interface, the anomalously small Kapitza resistance results in $R_C > R_K$. For example, both lead and indium films vacuum deposited on sapphire substrates have experimental contact resistances ranging 30-33 $^oK\text{-}cm^2/W$ at $T = 1.45^oK$ (Wolfmeyer, Fox, and Dillinger, 1970), while R_K is typically 4 $^oK\text{-}cm^2/W$

Obviously the processes generating the observed temperature discontinuities are not well understood. Fortunately this deficiency will not present an obstacle in the following analysis where R_K and R_C will be taken as phenomenological constants of proportionality to be determined experimentally.

$$T_2 - T_3 = R_K\, q_{23} \tag{F.1}$$

$$T_3 - T_4 = R_C\, q_{34} \tag{F.2}$$

(Note that the temperature jump at the liquid-solid interface, $T_2 - T_3$, includes the actual Kapitza discontinuity together with the thermal boundary layer temperature jump occurring in the liquid (Appendix E); both effects are lumped together into the interface resistance, R_K.)

The temperature distribution within the thin-film element itself is assumed to be spatially uniform. This assumption is valid because the film is so thin that any arbitrary temperature distribution must

quickly relax to a constant gradient; then the temperature rise across the film due to its finite thermal conductivity can be absorbed into the two boundary discontinuities. The relaxation time for this process is on the order of

$$\tau_{internal} \simeq \frac{d^2}{\chi_f} \sim 0.006 \text{ nsec} \qquad \text{(F.3)}$$

where $\chi_f = \dfrac{\kappa_f}{\rho_f C_f}$

ρ_f = film density

C_f = film specific heat

κ_f = film thermal conductivity

This time, which has been evaluated for a 1250 Å thick tin-on-gold film, is at least one million times faster than the observed relaxation time!

The average film temperature, $T_3(t)$, can therefore be calculated as the integral over time of the net heat flux entering the film:

$$T_3(t) = T_0 + \int_{-\infty}^{t} \frac{q_{23} - q_{34}}{\rho_f C_f d} \, dt' \qquad \text{(F.4)}$$

Now for the moment, if the influence of the substrate is ignored -- $q_{34}(t) = 0$ -- then a step input in the helium temperature will result in an exponential rise of the film temperature asymptoting to T_2; the rise time of this process is:

$$\tau_f = R_K \rho_f C_f d \sim 14 \text{ nsec} \qquad \text{(F.5)}$$

which is still very short. Thus it must be concluded that the rise time actually observed for a complete thin-film temperature sensor is almost exclusively due to the thermal inertia of the substrate.

In every situation the temperature actually measured by the sensor is the thin-film temperature, $T_3(t)$, via the element's total resistance. When the film is calibrated the temperature is varied so slowly that the film is always in equilibrium with the liquid helium bath, but when the film is used to measure the amplitude of a second-sound shock front full equilibrium is never attained because of the long time required to heat up the substrate.

It is useful to calculate the response of the substrate to a step input in temperature including the influence of the temperature discontinuities at the two interfaces. In this analysis the thermal inertia of the film can be ignored because of the great disparity in time constants of the film by itself and the substrate; consequently $q_{23} = q_{34} = q$. The substrate will be assumed semi-finite in extent and describable by the linear heat equation (the temperature excursions must therefore be small compared to temperature dependence of C_s and κ_s):

$$\frac{\partial T}{\partial t} = \chi_s \frac{\partial^2 T}{\partial x^2} \qquad \text{on } 0 < x < \infty \qquad \text{(F.6)}$$

where $\chi_s = \dfrac{\kappa_s}{\rho_s C_s}$

The boundary condition at $x = 0$ is derivable from the initial temperature jump in the liquid, $T_2 - T_0$, and equations (F.1) and (F.2):

$$T(x,t) = T_0 \quad \text{for } t < 0 \tag{F.7}$$

$$T(0,t) = T_2 - (R_K + R_C)q$$

$$= T_2 + L_s \left.\frac{\partial T}{\partial x}\right|_{x=0} \quad \text{for } t > 0$$

where $L_s = (R_K + R_C)\kappa_s$

The length, L_s, should be identified as the thickness of a slab of substrate material required to reproduce the temperature differential actually present as discontinuities at the interfaces. As long as L_s is much shorter than the actual substrate thickness, then the latter may be properly assumed semi-infinite in extent.

The problem defined by equation (F.6) and boundary conditions (F.7) can be conveniently solved with Laplace transforms. The solution at the boundary x = 0 is:

$$T_4(t) = T_0 + (T_2 - T_0)\left[1 + e^{t/\tau_s}\,\text{erfc}\,\sqrt{t/\tau_s}\right] \tag{F.8}$$

where $\text{erfc}\, x \equiv \frac{2}{\sqrt{\pi}} \int_x^\infty e^{-\xi^2}\, d\xi$

$$\tau_s = L_s^2/\chi_s$$

The substrate boundary temperature rises initially very quickly from the equilibrium temperature T_0, but for times longer than $t = \tau_s$, the final rise to its asymptotic value, T_2, is very slow ($T_3(t)$ attains 98% of its equilibrium temperature after $t = 948\ \tau_s$; compare this to an exponential decay which would reach the same level after only 4

time constants). This behavior is graphically illustrated in Figure 5.4a and can also be deduced from the following asymptotic expansions for small and large time:

$$1 + e^{\xi} \operatorname{erfc} \sqrt{\xi} \sim \begin{cases} 2\sqrt{\xi/\pi} & \text{for } \xi << 1 \\ 1 - 1/\sqrt{\pi\xi} & \text{for } \xi >> 1 \end{cases} \qquad \text{(F.9)}$$

Under the assumptions required for calculating the substrate boundary temperature, T_4-- the time constant τ_s is much larger than all other time constants -- the average film temperature, T_3, must be a linear interpolation between T_2 and T_4:

$$T_3(t) = T_4(t) + \frac{R_C}{R_C + R_K} \left(T_2 - T_4(t) \right) \qquad \text{(F.10)}$$

This means that the sensor, which actually measures the film temperature, will initially register a fraction of the temperature jump actually occurring in the liquid equal to:

$$\frac{R_C}{R_C + R_K}$$

Since R_C is usually larger than R_K, the initial jump is a sizable fraction of $T_2 - T_0$.

Appendix G. SHOCK-EXPANSION WAVE COINCIDENCE

A rectangular heat pulse of duration Δt results in a second-sound shock pulse having a leading shock front and a trailing expansion fan when the steepening coefficient, $b(p,T)$, is positive. For temperatures where $b(p,T)$ is negative, this configuration is reversed in that the expansion fan leads the shock front. In the first case the leading edge of the expansion fan travels faster than the shock front which allows the expansion wave to overtake the shock after the shock pulse has traversed at distance, L. The coincidence of these waves, which can be calculated from the x-t diagram of Figure G.1, provides an additional opportunity to compare second-order theory with experiment.

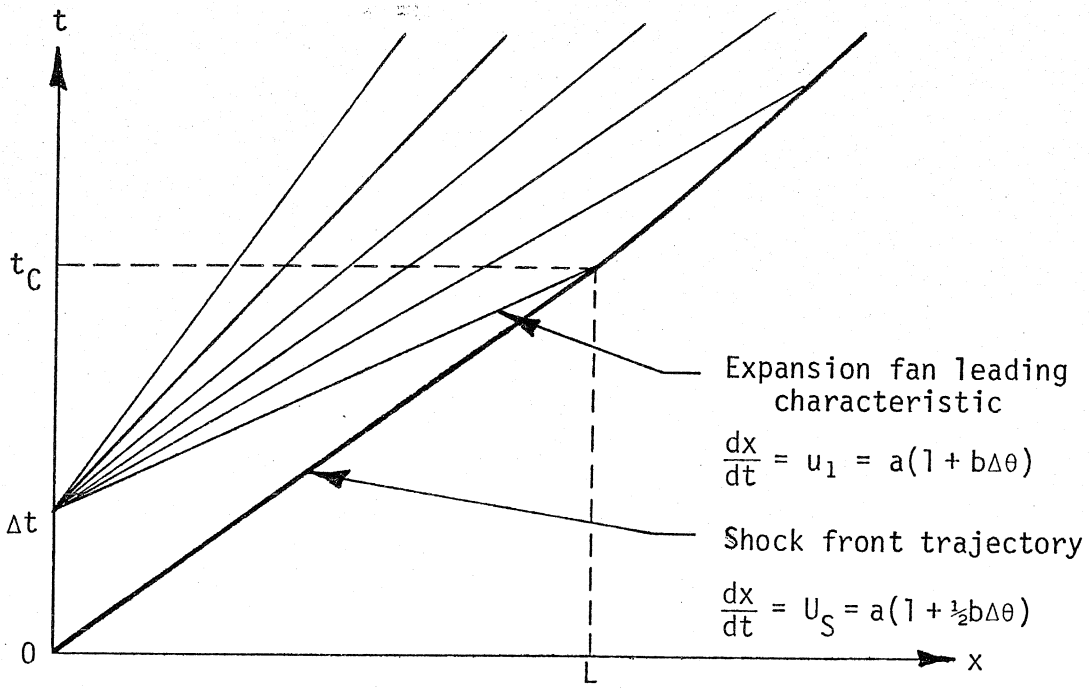

Figure G.1. COINCIDENCE OF A FRONT STEEPENED SHOCK WITH THE EXPANSION FAN

The distance propagated by the shock by the time the expansion fan catches up to it can be written as:

$$L = t_C U_S = (t_C - \Delta t)u_1 \qquad (G.1)$$

where t_C is the coincidence time to be determined.

The velocities U_S and u_1 written in terms of the shock Mach number are:

$$U_S = a M_S \qquad (G.2)$$

$$u_1 = a(2M_S - 1) \qquad (G.3)$$

where a = speed of second-sound

The relation for the characteristic velocity u_1 follows from the second-order shock theory which is valid only for shock waves.

From equation (G.1) the time of coincidence can be solved for:

$$t_C = \Delta t \ \frac{(2M_S - 1)}{(M_S - 1)} \qquad \text{for } M_S > 1 \qquad (G.4)$$

It is clear from the x-t diagram that the expansion wave will eventually overtake the shock front no matter how weak the shock (as long as $M_S \neq 1$). Now consider shock pulses of varying amplitude, but constant duration. What is the Mach number of the shock pulse whose expansion wave will just catch up to the shock front at a specified distance from the heater, L? Note that $t_C = (L/a\ M_S)$ and solve equation (G.4) for M_S to get:

$$M_S = \frac{1+\alpha}{4} \pm \frac{1}{4}\sqrt{\alpha^2 - 6\alpha + 1} \qquad \text{for } M_S > 1 \qquad (G.5)$$

where $\alpha \equiv \frac{L}{a\Delta t}$

This solution is plotted as Figure G.2. It is remarkable that for a dimensionless distance $\alpha < 3 + 2\sqrt{2} \simeq 5.828$, the expansion wave never catches up to a front steepened shock. When α exceeds this limit there are two solutions. For example suppose $\alpha = 10$ and arriving shock pulses of increasing amplitude are observed. For very weak pulses the nonlinearity is small and the shock pulse propagates without modifying its shape appreciably. As M_S increases the expansion wave gradually overtakes the shock front until they coincide at $M_S = 1.15$. The observed waveform is now triangular which persists as the amplitude of the shock pulse increases until $M_S = 4.35$ which is the strong shock coincidence solution. Increasing the amplitude further results in a trapezoidal waveform since the shock front is again ahead of expansion wave by the time the shock pulse propagates the distance L. It should be noted that the strong shock branch of the coincidence diagram is only qualitatively correct since the weak shock assumptions, used in the derivation, are invalid.

Many shock-expansion coincidences were observed on the weak shock branch. For example, at $T_0 = 1.65^{o}K$ a family of front steepened shock pulses experienced a shock-expansion coincidence at the sensor station when the shock Mach number reached $M_S = 1.023 \pm .001$ (experiment A10). Knowing the station location, L = 10.04 cm and the heat pulse duration, $\Delta t = 100$ μsec, the distance parameter can be calculated as $\alpha = 49.2$. The theoretical coincidence Mach number is 1.022, easily within the experimental error (the greatest error is in the heat pulse duration). The fact that shock-expansion coincidences can be accurately calculated by this simple theory means that the following relation between the

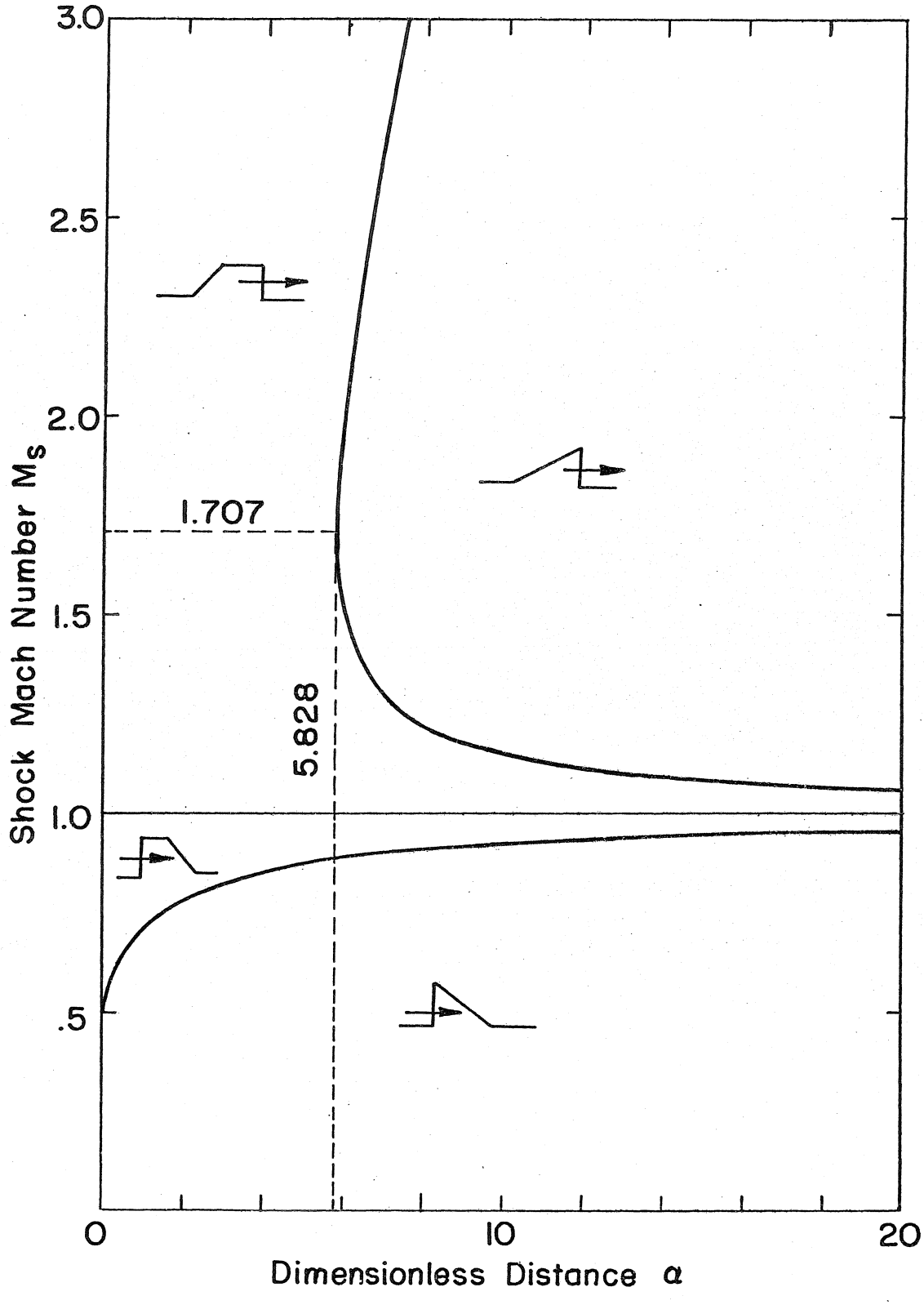

Figure G.2 MACH NUMBER OF THE SHOCK - EXPANSION COINCIDENCE

shock velocity and characteristic velocities is valid within present experimental precision:

$$U_S = \tfrac{1}{2}(u_0 + u_1)$$

To conclude this section, the coincidence Mach number of a back steepened shock will be presented. Similar calculations yield:

$$M_S = \frac{1 - \alpha}{4} + \frac{1}{4}\sqrt{\alpha^2 + 6\alpha + 1} \qquad \text{for } M_S < 1 \qquad \text{(G.6)}$$

This solution, which is plotted in Figure G.2, is the weak shock branch. The strong shock branch always has Mach number less than zero. That is, the shock is so strong that it would propagate back into the heater.

Appendix H. PROPAGATION OF A TRIANGULAR SHOCK PULSE

Consider a front steepened shock pulse having a triangular profile at time $t = 0$: the shock front is located at $x = 0$, the shock strength is $\Delta\theta_F$, and the physical length of the triangular tail is ΔX_F (see Figure H.1). As the shock pulse propagates, the temperature lowering expansion will move into the shock front and reduce its amplitude. This in turn causes the shock velocity to steadily decrease with time.

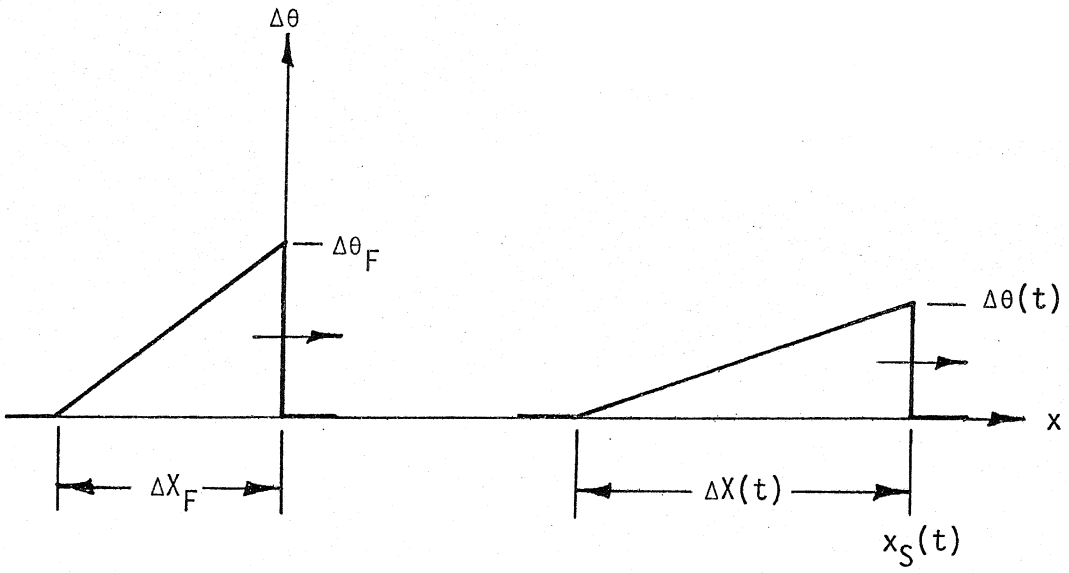

Figure H.1. PROPAGATION OF A TRIANGULAR SHOCK PULSE

In order to analyze the trajectory of such a shock pulse the concept of profile-area invariance will be utilized. This means that as the shock pulse evolves its temperature-area will remain constant:

$$\text{Area} = \tfrac{1}{2}\,\Delta X_F \Delta\theta_F = \tfrac{1}{2}\,\Delta X\ \Delta\theta \qquad \text{(H.1)}$$

To deduce how ΔX or $\Delta\theta$ changes with time it is useful to calculate how the slope of the expansion profile changes with time. At $t = 0$ the slope is simply $(\Delta\theta_F/\Delta X_F)$. At a later time t, this profile, which expands at a rate proportional to the characteristic velocity jump, Δu, will have the following slope:

$$\left(\frac{\partial\theta}{\partial x}\right)_t = \frac{\Delta\theta_F}{\Delta X_F + ab\Delta\theta_F t} \tag{H.2}$$

which is also equal to:

$$\left(\frac{\partial\theta}{\partial x}\right)_t = \frac{\Delta\theta(t)}{\Delta X(t)} \tag{H.3}$$

These three results allows one to calculate the change in shock strength with time, which turns out to be:

$$\frac{\Delta\theta_F}{\Delta\theta(t)} = \frac{\Delta X(t)}{\Delta X_F} = \sqrt{1 + (\Delta\theta_F)^2 \frac{t}{\tau}} \tag{H.4}$$

where $$\tau \equiv \frac{\Delta X \Delta\theta}{ab} = \frac{\Delta X_F \Delta\theta_F}{ab} \tag{H.5}$$

The time constant, τ, is a measure of the decay time of the shock pulse, and it is an invariant quantity.

Since the trailing edge of the expansion fan propagates at the undisturbed second-sound velocity, a, the trajectory of the shock front can easily be deduced as:

$$x_S(t) = at + \Delta X - \Delta X_F$$

or substituting in Equation (H.4):

$$x_S(t) = at + \Delta X_F\left[\sqrt{1 + (\Delta\theta_F)^2 \frac{t}{\tau}} - 1\right] \qquad (H.6)$$

Now, the shock Mach number is experimentally calculated by timing the shock front between two points. This always introduces some error since the shock front is continually slowing down, but the actual instantaneous Mach number can be calculated since its theoretical trajectory in the x-t plane is known. For example the average Mach number minus unity, $\langle M_S - 1\rangle$, normalized by the initial formation value, $(M_S - 1)_F = \frac{1}{2} b\Delta\theta_F$, is:

$$\frac{\langle M_S - 1\rangle}{(M_S - 1)_F} = \frac{\left(\frac{x_S}{at} - 1\right)}{\frac{1}{2}b\Delta\theta_F} = \frac{2\Delta\theta}{\Delta\theta_F + \Delta\theta} < 1 \qquad (H.7)$$

where the averaging was over the time interval beginning with $t = 0$ when $x_S = 0$. This ratio is always less than one since $\Delta\theta < \Delta\theta_F$ (except when $\tau \to \infty$ which is the infinite length, rectangle pulse profile limit).

REFERENCES

Atkins, K.R. 1959 Liquid Helium. University Press, Cambridge.

Bancroft, D., Peterson, E.L., and Minshall, S. 1956 Polymorphism of Iron at High Pressure. J. Appl. Phys. 27, 291.

Berman, R. 1976 Thermal Conduction in Solids. Clarendon Press, Oxford.

Brewer, D.F. and Edwards, D.O. 1959 The Heat Conductivity and Viscosity of Liquid Helium II. Proc. Roy. Soc. A251, 247.

Challis, L.J. 1961 The Kapitza Resistance. Proc. of 7th Inter. Conf. on Low Temp. Phys. LT7, 466.

Childers, R.K. and Tough, J.T. 1972 Superheating in He II. Proc. of 13th Inter. Conf. on Low Temp. Phys. LT13, 1, 359.

Clow, J.R. and Reppy, J.D. 1967 Temperature Dependence of Superfluid Critical Velocities Near T_λ. Phys. Rev. Lett. 19, 291.

Clow, J.R., Weaver, J.C., Depatie, D., and Reppy, J.D. 1964 Stability of Superfluid Flow Near the λ-Point. Proc. of 9th Inter. Conf. on Low Temp. Phys. LT9, 328.

Courant, R. and Friedrichs, K.O. 1948 Supersonic Flow and Shock Waves. Interscience Publishers, Inc.; New York.

Cummings, J.C., Schmidt, D.W., and Wagner, W.J. 1978 Experiments on Second-Sound Shock Waves in Superfluid Helium. Phys. Fluids 21, 713.

Dessler, A.J., and Fairbank, W.M. 1956 Amplitude Dependence of the Velocity of Second Sound. Phys. Rev. 104, 6.

Dimotakis, P.E. 1979 Personal communication.

Donnelly, R.J. and Penrose, O. 1956 Oscillations of Liquid Helium in a U-Tube. Phys. Rev. 103, 1137.

Fairbank, H.A. and Wilks, J. 1955 Heat Transfer in Liquid Helium Below 1^{o}K. Proc. Roy. Soc. A231, 545.

Feynman, R.P. 1955 Application of Quantum Mechanics to Liquid Helium. Prog. in Low Temp. Phys., 1, 17.

Ginzburg, V.L., and Pitaevskii, L.P. 1958 On the Theory of Superfluidity. Sov. Phys. -- JETP, 7, 858.

Goodman, S.E. 1971 Classical Model of the Roton-Quantized Vortex Interaction with an Application to Rotating Liquid He II. Phys. of Fluids 14, 1293.

Gorter, C.J., and Mellink, J.H. 1949 On the Irreversible Processes in Liquid Helium II. Physica 15, 285.

Gulyaev, A.I. 1970 Schlieren Photography of Thermal Pulses in Liquid He^4. Sov. Phys. -- JETP, 30, 34.

Hanson, W.B. and Pellam, I.R. 1954 Second Sound Attenuation in Liquid Helium, Phys. Rev. 95, 321.

Henkel, R.P., Smith, E.N. and Reppy, J.D. 1969 Temperature Dependence of the Superfluid Healing Length. Phys. Rev. Lett. 23, 1276.

Ivanov, A.G., Novikov, S.A., and Tarasov, Yu.I. 1962 Fragmentation Phenomena in Iron and Steel Caused by Explosive Shock Wave Interactions. Sov. Phys. -- Solid State, 4, 177.

Johnson, E.M. and Hildebrandt, A.F. 1969 Entrainment of Second Sound in Steady-State Counterflowing Normal and Superfluid Helium II. Phys. Rev. 178, 292.

Joynson, R.E. 1970 Superconductive Thin Films and Devices. in "Handbook of Thin Film Technology" (L.I. Maissel and R. Glang eds.) McGraw-Hill, New York.

Khalatnikov, I.M. 1952a Heat Exchange Between a Solid and Helium II. Zh. Eksperim. i Teor. Fiz. 22, 687 (In Russian) (See Khalatnikov, 1965, Chapter 23).

Khalatnikov, I.M. 1952b Discontinuities and Large Amplitude Sound Waves in Helium II. Zh. Eksperim. i Teor. Fiz. 23, 253 (In Russian) (See Khalatnikov, 1965, Chapter 13).

Khalatnikov, I.M. 1956 The Propagation of Sound in Moving Helium II and the Effect of a Thermal Current Upon the Propagation of Second Sound. Soviet Phys. -- JETP, 3, 649.

Khalatnikov, I.M. 1965 An Introduction to the Theory of Superfluidity. W.A. Benjamin, Inc., New York.

Khalatnikov, I.M. and Chernikova, D.M. 1966a Relaxation Phenomena in Superfluid Helium. Sov. Phys. -- JETP, 22, 1336.

Khalatnikov, I.M. and Chernikova, D.M. 1966b Dispersion of First and Second Sound in Superfluid Helium. Sov. Phys. -- JETP, 23, 274.

Kittel, C. 1971 Introduction to Solid State Physics. John Wiley & Sons, New York.

Laguna, G.A. 1975 Second Sound Attenuation in a Liquid Helium Counterflow Jet. Ph.D. Thesis, Calif. Inst. of Tech.

Laguna, G.A. 1976 Photolithographic Fabrication of High Frequency Second Sound Detectors. Cryogenics 16, 241.

Landau, L.D. 1941 The Theory of Superfluidity of Helium II. J. Phys. USSR 5, 71 (In Russian) (See Khalatnikov, 1965, Part V).

Landau, L.D., and Lifshitz, E.M. 1959 Fluid Mechanics. Pergamon Press, Oxford.

Landau, L.D., and Lifshitz, E.M. 1977 Quantum Mechanics (Non-Relativistic Theory). 3rd Edition. Pergamon Press, Oxford.

Langer, J.S. and Fisher, M.E. 1967 Intrinsic Critical Velocity of a Superfluid. Phys. Rev. Lett. 19, 560.

Little, W.A. 1959 The Transport of Heat Between Dissimilar Solids at Low Temperatures. Can. J. Phys. 37, 334.

Mamaladze, Yu.G. 1967 Parameters of Phenomenological Superfluidity Theory and the λ-point Shift. Soviet Phys. -- JETP, 25, 479.

Meyer, L. and Reif, F. 1961 Ion Motion in Superfluid Liquid Helium Under Pressure. Phys. Rev., 123, 727.

Notarys, H.A. 1964 Megacycle Frequency Second Sound. Ph.D. Thesis, Calif. Inst. of Tech.

Notarys, H.A. 1969 Pressure Driven Superfluid Helium Flow. Phys. Rev. Lett. 22, 1240.

Osborne, D.V. 1951 Second Sound in Liquid Helium II. Proc. Phys. Soc. (London) 64, 114.

Putterman, S.J. 1974 Superfluid Hydrodynamics. North-Holland Publishing Co., Amsterdam.

Rayfield, G.W. and Reif, F. 1963 Evidence for the Creation and Motion of Quantized Vortex Rings in Superfluid Helium. Phys. Rev. Lett. 11, 305.

Rayfield, G.W. and Reif, F. 1964 Quantized Vortex Rings in Superfluid Helium. Phys. Rev. 136A, 1194.

Reif, F. and Meyer, L. 1960 Study of Superfluidity in Liquid He by Ion Motion. Phys. Rev. 119, 1164.

Staas, F.A., Taconis, K.W., Van Alphen, W.M. 1962 Laminar and Turbulent Flow of He II in Wide Capillaries. Proc. of 8th Inter. Conf. on Low Temp. Phys. LT8, 93.

Temperley, H.N.V. 1951 The Theory of the Propagation in Liquid Helium II of Temperature-Waves of Finite Amplitude. Proc. Phys. Soc. 64, 105.

Van Alphen, W.M., Van Haasteren, G.J., Ouboter, R. de Bruyn and Taconis, K.W. 1966 The Dependence of the Critical Velocity of the Superfluid on the Channel Diameter and Film Thickness. Phys. Lett. 20, 474.

Vinen, W.F. 1961 The Detection of a Single Quanta of Circulation in Liquid Helium II. Proc. Roy. Soc. (London), A260, 218.

Whitham, G.B. 1974 Linear and Nonlinear Waves. John Wiley & Sons, New York.

Whitmore, S.C. and Zimmermann, W. Jr. 1965 Observation of Stable Superfluid Circulation in Liquid Helium II at the Level of One, Two, and Three Quantum Units. Phys. Rev. Lett. 15, 389.

Whitmore, S.C. and Zimmermann, W. Jr. 1968 Observation of Quantized Circulation in Superfluid Helium. Phys. Rev. 166, 181.

Wilks, J. 1967 The Properties of Liquid and Solid Helium, Clarendon Press, Oxford.

Wise, J.L. 1979 Experimental Investigation of First and Second Sound Shock Waves in Liquid Helium II. Ph.D. Thesis, Calif. Inst. of Tech.

Wolfmeyer, M.W., Fox, G.T., and Dillinger, J.R. 1970 An Electron Contribution to the Thermal Conduction Across a Metal-Solid Dielectric Interface. Phys. Lett. 31A, 401.

Zel'dovich, Ya.B., and Raizer, Yu.P. 1966 Physics of Shock Waves and High-Temperature Hydrodynamic Phenomena. Academic Press, New York.